Dissertation

Molecular Pathogenesis of Chronic Degenerative Liver Diseases: Role of Protein p62 and Keratins

Submitted by

M.Sc

Vineet Mahajan

for the Academic Degree of

Doctor of Philosophy

(Ph.D.)

at the

Medical University of Graz

Institute of Pathology

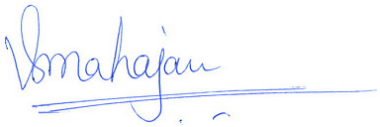
under Supervision of

Univ. Prof. Dr. Kurt Zatloukal

2011

Declaration

I hereby declare that this thesis is my own original work and that I have fully acknowledged by name all of those individuals and organizations that have contributed to the research for this thesis. Due acknowledgement has been made in the text to all other material used. Throughout this thesis and in all related publications I followed the guidelines of "Good Scientific Practice".



Graz, [27-10-11]

Dedicated to

To all my teachers, my mother and family

Inspiration



असाध्य ते साध्य। करिता सायास ॥
कारण अभ्यास। तुका म्हणे ॥

Impossible becomes possible by concerted efforts!
and due to continuous studies, says “Tuka” !!

Saint Tukaram (1608–1650)

Acknowledgment

I wish to express my sincerest gratitude towards my supervisor Univ. Prof. Dr. Kurt Zatloukal and Dr. Peter Abuja, Institute of Pathology, Medical University of Graz, Austria for accepting me as PhD student and providing all of their unconditional support that I needed to complete my studies.

I am grateful to my supervisor Prof. Kurt Zatloukal for giving me this golden opportunity of working in his research group as well as for his invaluable guidance and continuous encouragement throughout the period of my work. I also thank both of them to put their sincere efforts to develop a new era scientist by "throwing the tons of dirt to get an ounce of gold" in me. I wish to express my sincerest thanks to my co-supervisors, especially Dr. Karl Kashofer and Associate Professor PD. Dr. Johannes Haybaeck for their invaluable technical guidance in the research laboratory, moreover, step-by-step guidance as well as helping hands to solve all difficulties throughout this research. I also appreciate the kind support from Associate Professor Johannes Haybaeck for correcting my thesis several times and to complete my studies till date.

Relocation and livelihood in Graz would have been extremely difficult if Dr. Karin Osibow would not have helped me till date. I have absolutely no words to describe the kindness and grace of Dr. Karin Osibow

I would like to thank Prof. Dr. Andreas Tiran and Dr. Christian Gully, Core facility of Center for Biomedical Research, Medical University of Graz for providing all advanced facilities. I must acknowledge Mr. Markus Absenger for his assistance and great help every time in solving the bigger challenges in live cell imaging and confocal microscopy. I also appreciate great service from Mrs. Karin Meister and Ms. Nicole Stündl for DNA sequencing at Center for Biomedical research, Graz.

I am grateful to the colleagues from animal facility Hahnhof, Austria for providing the required mouse strains whenever an order was placed. Very special thanks go to Assistant Prof. Andelko Hrzenjak, Andrea Thüringer and Iris Kuffrath for being very friendly at all the way and of course for all the tremendous technical support and excellent suggestions when needed. I am highly overwhelmed for the cooperation from Rosa Steiner, Irmgard Kicker for providing me the innumerable number of histological sections for my studies. I am also grateful to Mrs. Sylvia Schauer, Ms. Elisabeth Schoeck, Ms. Nicole Kurzmann, Ms. Marie-Luise Kremser and Ms. Gintare Siaulyte for their constant help when needed and being kind to notorious PhD students like me.

I extend my special thanks to Mrs. Bettina Siebenhandl, Ms. Monica Moser, and Ms. Claudia Smole. I cannot forget their kindness and efforts for keeping friendly working environment.

I would like to thank specifically to Mrs. Therese Klingstedt, Prof. Dr. Peter Nilsson and other colleagues working with them in Department of Chemistry, Linkoping University for providing us novel chemical polymers as without their help a new direction in diagnostic methodology and research could not have been possible.

I provide my sincerest gratitude to Univ. Prof. Berthold Huppertz and his post-doctoral associate Dr. Martin Gauster from Institute of Histology and Embryology at Medical University of Graz for providing live cell imaging facilities, also time to time reviewing my work progress. I also thank Prof. Kai Uwe Froehlich, Institute of Molecular Biosciences, and Karl Franzes University for reviewing my work progress. I highly appreciate assistance of Prof. Thomas Magin, University of Bonn for providing Keratin 18-/- mouse strains in the past. I also sincerely acknowledge the timely help of Mr. Anton Ibovnik and Prof. Dr. Dagmar Kratky for providing us apparatus of ion-exchange chromatography.

I am grateful to Prof. Roger Davis (Department of Biochemistry and Molecular Pharmacology, University of Massachusetts, USA) for his communication on Jun Kinase (JNK1a) plasmid. I would like to officially acknowledge Prof. Dr. J.C. Tapia (Cell transformation laboratory, Faculty of Medicine, University of Chile) for providing *Xenopus lavis* GFP-CK2 plasmid; Prof. David W. Litchfield and Prof. Laszlo Gyenis, Ph.D. (Department of Biochemistry, The University of Western Ontario, Canada) for Wild type Human HA-CK2$_{\alpha}$pRc/CMV plasmid; Prof. Dr. Jae- Won Soh (Department of Chemistry, Inha University, Korea) for pEGFP3-PKCζ, pEGFP-PKCι, pHACE-PKCζ, pHACE-PKCι plasmid constructs; Prof. Tamotsu Yoshimory (Department of Cellular Regulation, Osaka University, Japan) for GFP-LC3 plasmid and Addgene for providing pCDNA3-FLAG-JNK1a plasmid construct. These studies would not have been successful without these generous gifts.

I appreciate Dr. Peter M Abuja also for helping in statistical analysis and correcting my thesis several times. I would like to express my deep gratitude to Dr. Shripad Joshi, Dr. Prakash Chandak, Dr. Tej Pratap Singh, Chandran Nagraj, Dr. Sonia Phillipose, Dr. Emina Halilbasic, Pooja Kumari Jha, Lada Brkic for helping me to recover from difficult circumstances –"the skiing disaster" of my life. These all friends became my priceless possessions.

I am grateful to Univ. Prof. Dr. Helmut Denk, Univ. Prof. Gerald Hoefler for allowing me to utilize all the facilities from Institute of Pathology. I am also grateful to Univ. Prof. Beham, Univ. Prof. Helmut Popper Associate Prof. Maria Waldhoer and Dr. Leopold Froehlich for their guidance in respective course work. It was a great experience to earn wisdom from their thorough experience.

I have absolutely no words for the greatest co-operation for the human tissues from Biobank, Graz, Austria under the kind co-ordination with Dr. Christian Viertler and his amazing colleagues.

I appreciate Aniket Nikam, for his help in statistical analysis and keratin isolation. I appreciate Pooja Chowdhury, Anita Kuldeep Mehta, Andrija Matak and all other colleagues for keeping a cordial atmosphere in the labs. Of course I am thankful to all my friends in Graz, Karin Kollar, Upeka Senanayake, Dr. Andreas Reinisch, Dr. Martin Asslaber, Dr. Ariane Aigelsreiter, Dr. Christian Kogler, Dr. Julia Pfeiffer and Dr. Andreas Reinisch. I also take this opportunity to thank my best friends from Vienna Dr. Sudarshan Patil, Dr. Yogesh Aher and Dr. Vinay Vishwanath. They all made my work much easier than it would ever have been. Nonetheless, I feel extremely sorry for the mouse strains I had to sacrifice for this study.

Most of all I offer my deepest sense of gratitude towards my parents and my elder brother for their constant emotional and moral support throughout my studies.

I would like to dedicate this thesis to all my teachers as well as to my mother and family.

INDEX

1 Introduction: 1

1.1 Protein aggregation diseases 1

1.2 Association of cytoplasmic MDBs and IHBs with ASH and NASH 1

1.3 Toxic Memory and MDB re-induction 2

1.4 Components of MDBs and IHBs 3

1.5 Disturbance in normal cellular protein degradation pathways 4

1.6 Ubiquitous association of p62 in liver and other degenerative diseases 5

1.7 Role of p62 in signaling cascades 6

1.8 Role of p62 in innate immunity, p62 as coordinator of ubiquitin mediated immune responses in activated macrophages 7

1.9 Role of p62 in tumourigenesis; p62 - the missing link between Ras and IKK activation. 9

1.10 Role of p62 in maintaining cellular homeostasis 9

1.11 Interaction partners of p62 10

1.12 Structural organization of protein p62: the possible mechanistic link between autophagy and ubiquitin-proteasome pathway 11

1.13 Aims and Hypothesis 15

2 Apparatus, materials and method 17

2.1. Technical equipments 17

2.1.1. Cell culture S2 laboratory 17

2.1.2. Microscopes and photodocumentation 18

2.1.3. Plasticware 18

2.1.4. Chemicals, buffer solutions and reagents 18

2.1.5. Antibiotic Stock Solutions 19

2.1.6. Electrophoresis buffer 50X TAE Stock 19

2.2. Buffers for isolation of Keratin 8 /18 Cytoskeleton. 20

2.3. Recombinant DNA 21

2.3.1. Restriction enzymes: 21

2.3.2. Polymerase Chain Reaction (PCR) 21

2.3.3. Ligases and buffers 22

2.3.4. Expression Vectors 22
2.3.5. Cloning and sub-cloning 22
2.3.6. Expression Plasmids used in Study. 23
2.4. Bacterial Strains and Microbiology 26
2.4.1. Bacterial culture conditions 26
2.4.2. Transformation 26
2.5. Site directed mutagenesis 26
2.6. DNA sequencing 27
2.7. Cell culture 27
2.8. Transfection 27
2.9. Luminescent Conjugated Oligothiophenes (LCOs) synthesis. 27
2.10. Synthesis of h-HTAA 27
2.11. Induction of MDBs in mice 28
2.12. Immunostaining (double Immunofluorescence) on cells 31
2.13. Immunoelectron microscopy 32
2.14. Human Tissue Samples 32
2.15. Immunofluorescence on tissue sections 32
2.16. Fluorescence Microscopy 33
2.17. Generation and detection of oxidative stress 33
2.18. Flow cytometry 34
2.18.1. Sample preparation for flow cytometry 34
2.19. Live cell imaging 34
2.20. Immunoblotting 35
2.21. Preparation of cell lysate 35
2.22. Preparation of proteins 35
2.23. Bradford's Assay and SDS PAGE 35
2.23.1. Isolation of keratin 8/18 pellet from mice liver 36
2.23.2. Separation of keratin 8 and 18 polypeptides 36
2.23.3. Protein measurement of isolated and purified keratins in urea containing buffers 37

2.24. In vitro assembly of keratin filaments 37

2.25. Circular dichroism spectroscopy 37

2.26. Oxidative modification of isolated keratin 8 and 18 polypeptides 'in vitro' 37

2.27. Dephosphorylation of keratin 8/18 'in vitro' 38

2.28. Immunoprecipitation 38

2.29. Statistical evaluation 38

3. Results 41

3.1. LCO profiling of inclusion bodies in human liver tissue: conformational discrimination between MDBs, IHBs and α-1 AT inclusions 41

3.2. LCOs bind to human and murine MDBs. 42

3.3. Cross β-sheet conformation is a primary feature of MDBs and not a consequence of a "maturation" process 45

3.4. MDBs in krt18-/- mice are rich in cross β-sheet structure 46

3.5. K8 and K18 reveal different propensities to acquire ß-sheet conformation in vitro 47

3.6. K8 is conformationally less stable than K18 53

3.7. *In vitro* dephosphorylation and oxidative modification of isolated and purified keratin polypeptides 55

3.8. Live-cell imaging reveals instantaneous acquisition of cross β-sheet conformation of overexpressed K8 in vitro 56

3.9. Role of p62 in autophagy 60

3.9.1. Misfolded keratins themselves, alone cannot induce autophagic response through LC3 60

3.9.2. Ubiquitinated misfolded K8/18 co-localize with LC3 62

3.9.3. p62 interacts with LC3/ATG 8 62

3.9.4. Molecular basis of p62-LC3 interaction 62

3.10. Misfolded keratins themselves do not trigger apoptosis 65

3.11. Live cell imaging and dynamics of hk8 aggregates, p62 and LC3 67

3.12. Dynamics of GFP-LC3 and GFP-p62 68

3.13. Influence of GFP-LC3 and p62 on hk8dsred aggregates 68

3.14. Kinases involved in MDB and IHB pathogenesis 72

3.14.1. Presence of Jun Kinase 1 (JNK1a/ MAPK8) in the aggregates 72

3.14.2. JNK1a associates with MDBs and IHBs ‘in vitro’ 73

3.14.3. JNK1a interacts with K8 and p62 74

3.14.4. Predicted phosphorylation sites of p62 74

3.14.5. Determination of phosphorylation sites by Mass-spectrometry 77

3.14.6. Site directed mutation at key phosphorylation sites S24 and S152 of p62 77

3.14.7. Interaction studies with JNK 1a/ MAPK-8: Molecular basis of p62- JNK1a interaction 78

3.14.8. JNK1 overexpression induces cell death 80

3.15. Interaction studies with PKCζ 81

3.15.1. p62 interacts with PKCζ 81

3.15.2. Molecular basis of p62-PKCζ interaction 83

3.15.3. Interaction studies of p62 with CK2α and molecular basis of p62-CK2α interaction 83

3.15.4. Dynamics of CK2 alpha by live cell imaging 85

3.16. Role of functional domains and phosphorylation sites in governing ultrastructure and morphology of the aggregates 88

3.16.1. Role of phosphorylation sites in governing cellular distribution of p62 88

3.16.2. Functional significance of p62 domains in determination of ultrastructure and cellular distribution 89

3.16.3. Impact of p62 domains and phosphorylation sites in determining cellular distribution patterns of p62 with K8 92

3.16.4. Influence of ubiquitin (Ubi) on the interaction with p62 with K8 95

3.16.5. Deletion of SH_2 domain induces cross β-sheet structure of p62 100

3.16.6. Additional oxidative stress does not have inhibitory effect on p62, Ubi, K8 interaction 101

4. General Discussion: 105

4.1. Structural characterization of the MDBs and predominant components p62 and K8 105

4.2. Multiple facets of interaction of p62 with misfolded K8/18 106

4.3. Ubiquitination and phosphorylation involved in MDB pathogenesis with reference to p62 106

4.4. p62 at the intersection of autophagy and apoptosis 110

5. References 111

Hintergrund und Ziele: Falsch gefaltete Proteine, welche in Einschlusskörpern wie Mallory-Denk Körpern (MDBs) und Intrazellulären Hyalinen Körpern (IHBs) gefunden werden können, stellen die zellulären Hauptmerkmale alkoholischer und nichtalkoholischer Steatohepatitis, hepatozellulärem Karzinom (HCC) und einiger anderer Lebererkrankungen dar. MDBs sind Aggresomen, welche aus fehlgefaltetem Keratin 8 /18, Ubiquitin und p62 zusammengesetzt sind und als Folge eines eingeschränkten Ubiquitin-abhängigen proteasomalen Abbaus gebildet werden. Trotz zahlreicher mechanistischer Erkenntnisse und der Kenntnis der Bindungspartner von p62 ist der mögliche Einfluss von Konformationsänderungen und post-translationalen Modifikationen auch weiterhin unbekannt. Sequestosome 1/p62, Ubiquitin, Keratin 8 (K8) und Keratin 18 (K18) sind die wichtigsten Bestandteile von MDBs. Einerseits war es eines der wichtigsten Ziele aufzuklären, ob die Interaktion von p62 mit K8/18 von a) Konformationsänderungen, b) strukturellen Domänen, c) Phosphorylierung und/oder d) Ubiquitinierung von p62 abhängig ist. In dieser Studie wurde die neue Technologie "lumineszierender konjugierter Oligothiophene (luminescent conjugated oligothiophenes, LCOs)" verwendet, um Unterschiede in der molekularen Struktur der Komponenten in verschiedenen Arten von Leber-Einschlüssen zu untersuchen, um neue Einblicke in die Natur und die Entstehung von Proteinaggregaten in Lebererkrankungen zu erhalten und dadurch die Rolle dieser Proteine bei der Krankheitsentstehung aufzeigen. Andererseits sollte die Rolle von p62 in Wechselwirkung mit K8/K18 bei der MDB-Bildung untersucht werden. Auch die Regulierung der Interaktionen zwischen p62 und LC3 oder p62 und K8/K18 an wichtigen Phosphorylierungsstellen, die Fähigkeit von K8/18-Aggregaten eine apoptotische Reaktion zu aktivieren und die Bedeutung von p62 in Autophagie von K8/18-Aggregaten waren bislang noch ungeklärt. Darüberhinaus wurde der Beitrag der strukturellen Domänen von p62 an der Bildung von MDBs und IHBs untersucht.

Methoden: Unter Verwendung der neuartigen molekularen LCOs h-HTAA und p-FTAA, fluoreszierender Amyloid-Liganden, welche spezifisch an Proteine mit β-Faltblatt-Konformation binden, wurden die strukturellen Eigenschaften von p62 und K8/18 untersucht. LCOS wurden verwendet, um Konformationsänderungen in MDBs *in situ* in humanen und murinen Lebern sowie in Transfektionsstudien nachzuweisen. Protein-Protein-Interaktionen von p62 mit seinen Partnern wurden anhand der

Überexpression von p62 in Leberpathologie-imitierenden Zellmodellen mittels Immunfluoreszenz-Methoden untersucht.

Ergebnisse: β-Faltblatt-Konformationen konnten mittels LCO-basierter Analyse in MDBs von Patienten mit alkoholischer und nicht-alkoholischer Steatohepatitis und hepatozellulärem Karzinom, aber nicht in intrazellulären hyalinen Körpern, alpha-1-Antitrypsin- oder Milchglas-Einschlüssen nachgewiesen werden. LCOs banden an MDBs, welche durch 5-Diethoxycarbonyl-1, 4-dihydrocollidine-Fütterung von Mäusen induziert worden waren, zu allen Zeitpunkten in deren Entwicklung. CHO-K1 Zellen, welche mit unterschiedlichen Kombinationen von SQSTM1/p62, Ubi und Krt8/Krt18 transfiziert worden waren, zeigten, dass K8 wesentlich haufiger in einer β-Faltblatt-Konformation vorkommt als K18, während p62 nie β-Faltblatt-Konformation annimmt. Die unterschiedlichen konformativen Eigenschaften von K8 und K18 wurden zusätzlich mittels einer Circulardichroismus-Analyse nachgewiesen.
Darüber hinaus wurden weiterführende Experimente zur Charakterisierung der Rolle von p62 im Zusammenhang mit ubiquitinierten Keratin-Aggregaten und LC3 sowie deren Interaktion mit Kinasen (JNK, PKCζ und CK2α) durchgeführt. Diese Experimente zeigten die Interaktion von p62 mit mehreren wichtigen Proteinen in Zusammenhang mit Keratin-Aggregation in der menschlichen Leber auf. Die SH2, ZIP und UBA-Domänen von p62 spielen eine entscheidende Rolle bei der Regulation dieser Interaktionen. Deletionen dieser Domänen führen zur spezifischen Entstehung unterschiedlicher zellulärer Ultrastrukturen von p62. Die Interaktion von p62 mit JNK, PKCζ und CK2α deutet auf eine zentrale Rolle von p62 bei der Initiierung mehrerer Signalkaskaden hin. Diese Studie zeigt auch, dass die erhöhte Expression von p62 unter Stressbedingungen zur Interaktion mit falsch gefalteten Keratinen und LC3 führt, die wahrscheinlich zum Abbau der Ubiquitin-Aggregate im Rahmen der Autophagie dient. Dies unterstreicht die Funktion von p62 in der MDB- und IHB-Pathogenese bei verschiedenen Lebererkrankungen.

Schlussfolgerung: Die LCO-basierenden Studien zeigten, dass K8 seine Konformation von überwiegend α -Helix- zu ß-Faltblatt-Struktur ändern kann, was es K8 ermöglicht MDBs auszubilden. Diese Erkenntnisse könnten die Beobachtung erklären, dass KRT8 -/- Mäuse keine MDBs bilden, während K8-Überschuss die MDB-Bildung erleichtert. LCOs könnten bei der Diagnose von Lebererkrankungen eingesetzt werden, da sie

sowohl auf Gefrierschnittmaterial als auch auf Formalin-fixiertem, in Paraffin eingebettetem Gewebe angewandt werden können, um Protein-Aggregate in Leberzellen zu charakterisieren. Da fehlgefaltete Keratine selbst nicht Autophagie oder Apoptose initiieren können, ist die Rolle von p62 von entscheidender Bedeutung bei der Aufrechterhaltung der Proteinhomöostase. p62 scheint durch die Interaktion mit LC3 unverzichtbar für die Aufrechterhaltung der Stabilität von Proteinaggregaten. Außerdem können einige der Phosphorylierungsstellen von p62 die Interaktion mit LC3 regulieren. Diese Studie deutet auch darauf hin, dass Konformationsänderungen und Ubquitinierung von p62 nicht nur die Interaktionsmuster von p62 mit K8/18, sondern auch zelluläre Verteilungsmuster, die Morphologie und Topologie der Aggregate regulieren könnte.

Background and Aims: Misfolded proteins found in inclusion bodies such as Mallory Denk bodies (MDBs) and Intracellular Hyaline bodies (IHBs) are cellular hallmarks of alcoholic and non-alcoholic steatohepatitis (ASH and NASH), hepatocellular carcinoma (HCC) and several other liver diseases. MDBs are aggresomes composed of misfolded keratin 8/18, ubiquitin and p62. They are formed as a result of impaired ubiquitin dependent proteasomal (UPS) degradation. Despite of some of the mechanistic insights and known binding partners of p62, the potential influence of conformational alterations and post-translational modifications continue to be undefined. Sequestosome 1/p62, ubiquitin, Keratin 8 (K8) and Keratin 18 (K18) are the major constituents of MDBs. On one hand, one of the major goals of this study was to elucidate whether the interaction of p62 with K8/18 is dependent on a) conformational alterations b) phosphorylation or c) structural domains of p62 and d) ubiquitination. In this study new tools of Luminescent Conjugated Oligothiophenes (LCOs) were used to investigate differences in the molecular structure of the components present in the various types of hepatic inclusions that can help obtaining new insight into nature and genesis of protein aggregates in liver diseases. This would highlight the role of these proteins in investigating their formation and role in disease pathogenesis. On the other hand it was an additional aim to investigate role of p62 in correlation with K8/K18 aggregates during MDB formation. Additionally, how key phosphorylation sites of p62 regulate the interaction between p62 and LC3 or p62 and K8/K18 is not clear. The ability of K8/18 aggregates to activate an apoptotic response or the requirement of p62 in autophagic clearance of the K8/18 aggregates still remains to be clarified. The contribution of structural domains of p62 involved in MDB and IHB formation was also investigated.

Methods: Structural properties of p62 and K8/18 were investigated by using novel molecular probes-Luminescent conjugated oligothiophenes (LCOs), h-HTAA and p-FTAA that are fluorescent ligands to amyloid which specifically bind proteins with cross β-sheet conformation. LCOs were used to detect conformational changes in MDBs *in situ* in human and murine livers as well as in transfection studies. Studies on protein-protein interaction were carried out by over-expression of p62 and detected by immunofluorescence methodologies in 'liver pathology mimicking' cellular models.

Results: LCO-based analysis demonstrated cross β-sheet conformation in MDBs from patients with ASH and NASH or hepatocellular carcinoma, but not in intracellular hyaline bodies, alpha-1-antitrypsin or ground glass inclusions. LCOs bound to MDBs

induced by 3, 5-diethoxycarbonyl-1, 4-dihydrocollidine-feeding of mice at all developmental stages. CHO-K1 cells transfected with various combinations of p62, Ubi and Krt8/Krt18 demonstrated that K8 was more likely to have cross β-sheet conformation than K18 while p62 never displayed any cross β-sheet conformation. The different conformational properties of K8 and K18 were also shown by circular dichroism analysis.

In addition present series of the experiments further characterization of the role of p62 in context with 'ubiquitinated' keratin aggregates and LC3 as well as its interacting kinases (JNK, PKCζ and CK2α) was carried out. They showed interaction of p62 with several key proteins in context with keratin aggregation in human liver. SH_2, ZIP, and UBA domains of p62 play a crucial role in regulating these interactions. Their deletion exhibited distinct different types of cellular ultrastructure of p62. Interaction of p62 with JNK, PKC and CK2α indicated involvement of p62 in several signaling cascades. This study also demonstrates during stressed signals, up-regulation of p62 induces association with misfolded keratins and LC3, probably for autophagic clearance of the ubiquitinated aggregates. This highlights the function of p62 in MDB and IHB pathogenesis observed in several liver diseases.

Conclusions: From these studies, LCO based characterization revealed that K8 can undergo conformational changes from predominantly α-helical to cross ß-sheet which would allow it to form MDBs. These findings might account for the observation that *krt8*$^{-/-}$ mice do not form MDBs whereas its excess facilitates MDB formation. LCOs might be used in diagnosis of liver disorders to characterize protein aggregates in liver cells as they can be applied to cryosections as well as formalin-fixed, paraffin-embedded tissues.

Misfolded keratins themselves cannot activate autophagy or apoptosis. Therefore the role of p62 may be crucial in maintaining protein homeostasis. p62 may be indispensible for influencing the stability of the aggregates by interacting with LC3. Also, some of the phosphorylation sites of p62 may regulate the interaction with LC3. This study also indicates that conformational alterations and ubquitination of p62 appears to regulate not only the interaction pattern of p62 with K8/18 but also cellular distribution patterns as well as morphology and topology of the aggregates.

Interaction of p62 with JNK, PKC and CK2α indicates involvement of p62 in several cellular signaling pathways in MDB and IHB pathogenesis.

Abbreviations

MDBs – Mallory Denk Bodies

IHBs – Intracellular Hyaline Bodies

HCC- Hepatocellular carcinoma

CHO-K1 – Chinese Hamster Ovary cell line K1

p62 - Protein p62/ Sequestosome 1

p62ΔSH$_2$ - SH$_2$ domain deleted p62

p62ΔZIP - Protein Kinase C interacting ZIP domain deleted p62

p62ΔUBA - UBA domain deleted p62

***Krt8*-** Human keratin 8 gene

***Krt18*-** Human keratin 18 gene

***krt8*-** Mouse keatin 8 gene

***krt18*-** Mouse keratin 18 gene

K8 – keratin 8 protein

K18 – keratin 18 protein

JNK1a – Jun kinase 1 isoform a

PKCζ – Protein Kinase C zeta

CK2α - Casein Kinase 2 alpha

LC3- Microtubule associated Light Chain 3

NF- κb- nuclear factor kappa-light-chain-enhancer of activated B cells

α-1AT- Alpha 1 anti-trypsin deficiency

UPS – Ubiquitin Proteasome Pathway

FACS – Fluorescent Activated Cell Sorting

CHAPTER 1
INTRODUCTION

1 Introduction:

1.1 Protein aggregation diseases

Protein aggregation due to misfolded proteins is defined as 'cellular hallmark' of chronic degenerative diseases. The most common examples of protein aggregation include Mallory Denk bodies (MDBs) in alcoholic and non-alcoholic steatohepatitis (ASH and NASH), neurofibrillary tangles in Alzheimer's and Lewi bodies in Parkinson's disease (Denk *et al.*, 1981; Denk *et al.*, 1979; Zatloukal *et al.*, 2007). Exposure of the cells to oxidative stress leads to protein misfolding and failure to dispose these proteins result in protein aggregation (Janig *et al.*, 2005; Strnad *et al.*, 2008a; Wu *et al.*, 2009). In ASH and NASH as well as in hepatocellular carcinoma (HCC) alteration of hepatocyte cytoskeleton is one of the most common findings (Strnad *et al.*, 2008a; Zatloukal *et al.*, 2004b) . These diseases are often characterized by misfolded keratins or even a loss of keratins, cytoplasmic inclusions like MDBs, steatosis, hepatocyte ballooning, pericellular fibrosis and ultimately inflammation (Zatloukal *et al.*, 2004b). Hepatocytes normally express specifically type I keratin 8 (K8) and type II keratin 18 (K18). K8 and K18 assemble into equimolar ratios (1:1) to form a filamentous network of hepatocytes (Zatloukal *et al.*, 2000).

1.2 Association of cytoplasmic MDBs and IHBs with ASH and NASH

MDBs were first described by Frank B Mallory as cytoplasmic hyaline inclusion bodies in hepatocytes of patients with ASH in 1911 (Mallory, 1911). Helmut Denk and colleagues have established the first non-transgenic animal model of MDB formation by feeding griseofulvin to mice (Denk *et al.*, 1975; Zatloukal *et al.*, 1990). Another non transgenic mouse model was later generated by feeding 3, 5-diethoxycarbonyl-1, 4-dihydrocollidine (DDC) (Yokoo *et al.*, 1982). Since then established non transgenic and transgenic mouse models which include $K8^{-/-}$, $K18^{-/-}$, K8 overexpression have played key role in elucidating the underlying pathogenesis of MDB formation as shown in figure 1 (Baribault *et al.*, 1994; Magin, 1998; Nakamichi *et al.*, 2005).

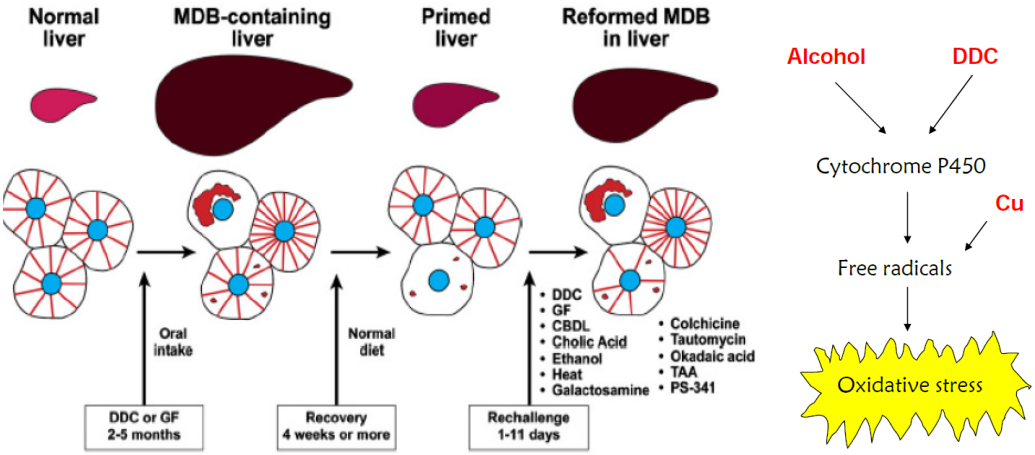


Figure 1: Mouse models of MDB formation and re-intoxication. Mice fed with DDC or GF for 2–5months readily form MDBs in association with liver damage and loss of the hepatocyte keratin network in MDB-containing hepatocytes. Upon drug withdrawal for 4 weeks, livers revert morphologically back to near normal, MDBs disappear and most hepatocytes regain their keratin networks. The drug-primed mice have, intriguingly, a "molecular memory" by which they can be induced to re-form MDBs within a very short time (1–11 days, typically 7 days) if rechallenged with DDC, GF, or several other drugs and conditions. TAA- thioacetamide; CBDL- common bile duct ligation. (Figure and figure legends are taken from Zatloukal *et al* 2002, Experimental and Cell Research 2007)

1.3 Toxic Memory and MDB re-induction

Strnad et al. observed structural changes in the proteins are retained after DDC priming which ultimately contribute to the reaction of rapid MDB reappearance and linked with MDB formation (Strnad *et al.*, 2008b). Altered chaperone expression and function, post-translational modifications in molecular chaperones, in addition with protein cross-linking may participate to the "toxic memory" of the DDC re-intoxicated mice (Figure 2). This indicates that similar mechanisms are important mediators to inclusion body formation in several other diseases such as Alzheimer's disease, Parkinson's disease and Alpha 1 antitrypsin deficiency (Strnad *et al.*, 2008a).

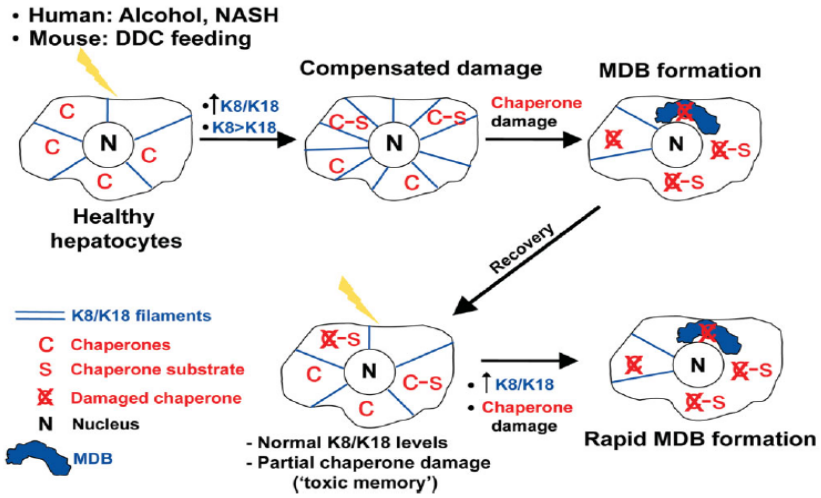


Figure 2: Persistent chaperone dysfunction associates with rapid MDB reformation upon DDC refeeding. The schematic highlights the major molecular events that occur during MDB formation, recovery, and rapid MDB reformation (Figure and figure legends are taken from Strnad *et al*. Hepatology, vol. 48, no.3, 2008).

1.4 Components of MDBs and IHBs

The major protein constituents of MDBs are keratin 8 and 18 (K8/K18), ubiquitin, heat shock proteins (HSP) and p62. (Denk *et al.*, 1981; Denk *et al.*, 1989; Stumptner *et al.*, 2002; Stumptner *et al.*, 1999; Zatloukal *et al.*, 2002) MDBs are accredited as very important histological and progression liver markers not only in ASH and NASH but also in Alpha-1 antitrypsin deficiency and several other liver diseases such as HCC. IHBs are the other type of protein inclusions lacking keratins. (Stumptner *et al.*, 2007; Stumptner *et al.*, 1999; Zatloukal *et al.*, 2007) They predominantly consist of p62 and ubiquitin as shown in Figure 3.

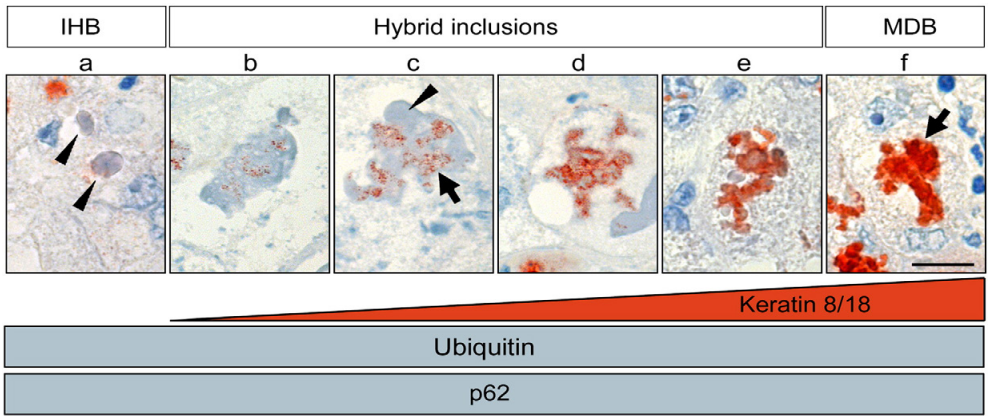


Figure 3: Immunohistological profiles of hepatocyte MDB, IHB and hybrid inclusions. In a–f, different transitional stages (hybrid inclusions) between IHBs (exemplified by arrowheads in **a** and **c**) and MDBs (arrows in **c** and **f**) are shown as seen by staining of the fixed liver tissue from a child with idiopathic copper toxicosis using antibodies to K8/18 (red) and hematoxylin as counterstain (light blue). Note that the transition from IHB to MDB is characterized by increased presence of keratin whereas ubiquitin and p62 are present (this staining is not shown but represented schematically) and relatively constant constituents of IHBs and MDBs. Scale bar =10 μm (Figure and figure legends: Zatloukal *et al.* Experimental cell research, 2007).

1.5 Disturbance in normal cellular protein degradation pathways

Protein misfolding is an ensemble of signal transduction pathways that corresponds to perturbations in the oxidative, folding environment of the endoplasmic reticulum (ER). During the last decade, ongoing research entailed these mechanisms in maintaining cellular homeostasis and organism integrity when exposed to various types of stresses.

A eukaryotic cell has designated pathways for disposal of misfolded proteins which accumulate during the course of protein synthesis under physiological conditions (Toivola *et al.*, 2010; Tyedmers *et al.*, 2010). The accumulation of misfolded proteins increases when the cells are exposed to additional stress (Janig *et al.*, 2005). Misfolded proteins generally interfere with normal cellular functions and therefore need to be efficiently eliminated. The molecular chaperones HSP 27, 70 and 90 were shown to be involved in refolding of the misfolded proteins (Janig *et al.*, 2005; Stumptner *et al.*, 2001).

The ubiquitin proteasome pathway is blocked due to its limited capacity of protein disposal hence misfolded proteins require different pathways for their degradation such as autophagy. Misfolded proteins often aggregate using their hydrophobic core in cytoplasm at microtubule organizing center via retrograde transport mechanisms (Bence *et al.*, 2001; Kopito *et al.*, 2000).

Loss of cytoskeleton and resulting cell death are common pathological features in neurodegenerative and chronic degenerative liver diseases (Omary, 2009; Strnad *et al.*, 2008a). They also point towards possible common fundamental mechanisms which are responsible for causing cell death. The molecular pathogenesis of misfolded proteins in chronic degenerative conditions still remains unclear (Omary, 2009). It remains a mystery whether protein aggregation appears to be the third line of immunological defense or it triggers the cell damage aggravating the hazardous effects.

It is still unclear in case of ASH and NASH if fibrillar or non fibrillar assemblies of misfolded proteins formed due to aberrant conformational changes exert toxicity causing cellular damage (Strnad *et al.*, 2008b).

1.6 Ubiquitous association of p62 in liver and other degenerative diseases

In order to reveal the underlying molecular pathogenesis responsible for inclusion bodies to be formed and cellular consequences elicited by protein aggregation, it is important to identify the key proteins involved in regulating this phenomenon. The emerging research thus directs towards investigating protein-protein interactions involved in inclusion body formation.

Already mentioned earlier, it was observed that key proteins involved in MDB formation were keratins (K8 and K18), HSPs, and Ubiquitin (Ubi). Thereafter a protein termed p62 was found to be associated with MDBs and IHBs in liver diseases (Stumptner *et al.*, 2002; Stumptner *et al.*, 2007; Zatloukal *et al.*, 2002). In addition, p62 was identified to be a prominent member of MDBs in all developmental stages evident from transgenic and non-transgenic mouse models (Stumptner *et al.*, 2002).

The gene that encodes p62 is comprised of 8 exons and 7 introns. p62 is an ~62 kD cytosolic protein that constitutes 440 amino acids. The amino acid sequence is indicative of several functional domains and motifs, based on homology modeling, described later in this chapter. p62 also known as ZIP, A170 or Sequestosome 1(SQSTM 1). It was first identified as a tyrosine kinase $p56^{LCK}$ ligand in the process of mitogenic signaling (Park *et al.*, 1995). Thereafter association of p62 with ubiquitin positive aggregates and Lewi bodies in Alzheimer's and Parkinson's disease, respectively as well as in spino-cerebral ataxia was revealed (Babu *et al.*, 2005; Donaldson *et al.*, 2003; Hoozemans *et al.*, 2009; Seidel *et al.*, 2009; Zheng *et al.*, 2009). The overexpression of p62 in these diseases proposed possible common mechanistic role of p62 also in MDB formation. p62 was also demonstrated to be one of the key proteins involved in maintaining cellular homeostasis. Interaction of p62 with atypical protein kinase C (aPKC) (one of the prominent binding partners) designated the regulation of nuclear (transcription) factor NF-κB mediated signaling cascades (Duran *et al.*, 2008; Sanz *et al.*, 2000; Sanz *et al.*, 1999).

1.7 Role of p62 in signaling cascades

From these recent studies though it appears that p62 is having protective function. However Komatsu et al. showed for the first time that disruption of p62 remedied the deleterious effects on liver hypertrophy and reversed the expression of oxidative stress induced enzymes (Komatsu *et al.*, 2010). This indicated that p62 aggregation has a role in regulating a stress response to liver (Komatsu *et al.*, 2007). It was further demonstrated that up-regulation of p62 also induces overexpression of Nuclear factor 2 (erythroid like 2) (Nrf-2) regulated genes (Lau *et al.*, 2010). Removal of p62 decreased the Nrf-2 translocation to the nucleus but addition of anti-oxidants did not decrease nuclear accumulation of Nrf-2. This highlighted a positive regulation of Nrf-2 regulated genes by p62 irrespective of oxidative stress status of the cell (Jain *et al.*, 2010). Further research recently reported that Nrf-2 regulates p62 and p62 regulates Nrf-2 by interacting with keap-1(Kelch like ECH-associated protein-1), the transcriptional controller of Nrf-2 (figure 4) (Komatsu *et al.*, 2010).

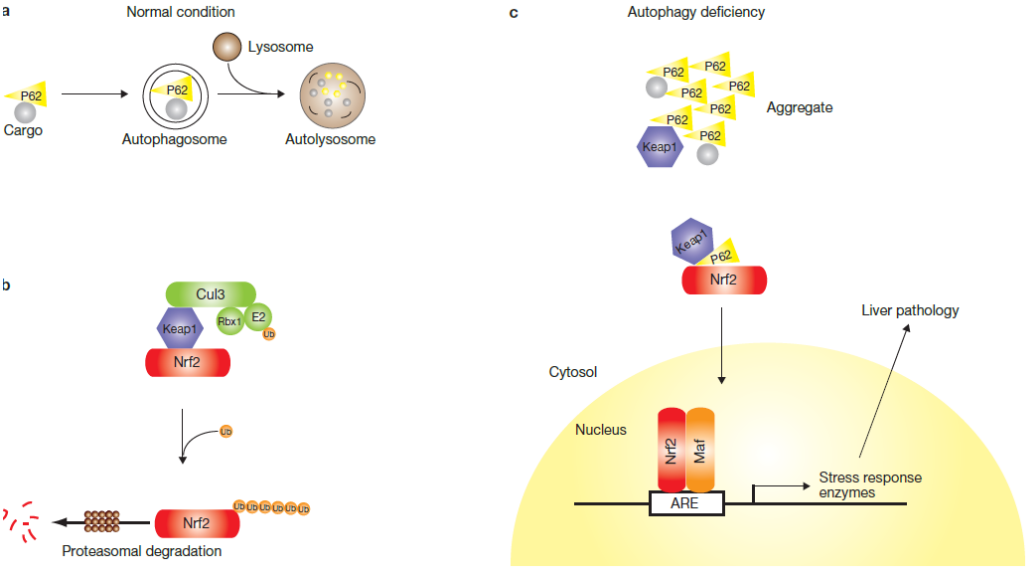


Figure 4: Control of Nrf2 activity by the autophagy substrate p62 (**a**) under normal conditions, basal autophagy continuously clears p62 and associated cargo (such as toxic aggregate-prone proteins) from the cytoplasm. (**b**) Nrf2 is ubiquitylated by the Cul3–Rbx1 ubiquitin ligase complex through the adaptor Keap1 and degraded by the proteasome. (**c**) Under conditions of autophagy deficiency, p62 and associated cargo accumulates in the cytoplasm. Excess p62 binds Keap1, disrupting ubiquitylation and ensures the degradation of Nrf2. This causes cytoplasmic Nrf2 levels to increase, allowing Nrf2 to enter the nucleus, heterodimerise with the transcription factor Maf and activate transcription from antioxidant response element (ARE) containing promoters. Increased Nrf2 activity is

the main contributor to pathology observed in livers with defective autophagy. (Figure and figure legends are taken from Rusten *et al*. Nature Cell Biology, Vol.12, no.3, 2010)

Komatsu *et al*. proposed that lack of autophagy might be responsible for accumulation of p62, which in turn causes up-regulation of stress induced pathways. Accumulation of p62 led to increase in nrf-2 activity that led ultimately to pathological consequences (Komatsu *et al.*, 2007, Komatsu *et al.*, 2010). With single and double mutants and knocking down autophagic pathways it was demonstrated that keap-1 deficient mice livers showed comparatively less hypertrophy but increase in expression levels of nrf-2 genes. This explained that keap-nrf-2 interaction is one of the mechanisms of pathogenesis as observed in autophagy deficient mice.

Any hepatocyte lethality was not observed because of overexpression of p62 (Komatsu *et al.*, 2010; Komatsu *et al.*, 2007; Lau *et al.*, 2010). White and colleagues showed the mechanistic link to this perplex (Mathew *et al.*, 2009).

Their experiments with the heterozygous mice for autophagy regulator beclin1 and p62 revealed spontaneous tumor formation because of partial disruption of autophagy. As p62 accumulates, NF-κB is suppressed which leads to up-regulation of the canonical TNF-alpha pathway responsible for inflammation. The authors also indicated an inverse relationship between p62 and NF-κB signaling (Mathew *et al.*, 2009). Though not conclusive but these experiments highlight cytokine mediated hypertrophy induced by p62-NF-κB regulation. As p62 is found to be involved in regulation of wide number of cellular processes, it may appear to play a positive role in regulating some processes whereas negative in others (Rusten *et al.*, 2010).

1.8 Role of p62 in innate immunity, p62 as coordinator of ubiquitin mediated immune responses in activated macrophages

Kim et al. elucidated role of p62 for the first time in innate immunological response. It was reported that IFN-γ and Toll like receptor (TLR) signaling stimulated late expression of p62 in murine macrophages. Overexpression of p62 resulted down regulation of multiple numbers of cytokines IL-12 p40, TNF-beta, IL-1, IL-6, and IFN-γ. RNA silencing of p62 resulted in up-regulation of above mentioned cytokines. This indicated negative regulation of cytokine expression by p62 in macrophages. It was proposed that interaction of IFN regulatory factor-8 (IRF8) and Ro52, transcription factor and ubiquitin E3 ligase collectively responsible for IL-12p40 expression. When macrophages are stimulated, p62 interacted with TNF receptor associated factor

(TRAF6), another E3 ligase important for activation of NF-κB signaling. Later recruitment of the de-ubiquitinating enzyme cylindromatosis, an inhibitor of NF-κB activity replaced this interaction. Therefore reduction of TRAF6 was linked with lowering NF-κB signaling pathway. These data clearly showed role of p62 in regulation of ubiquitination in macrophages to reduce post transcriptional activation of cytokines. Additionally interaction of p62 with TRAF6 and CYLD may also involve post translation modifications of p62 in such schematic regulation of cytokine expression (Kim *et al.*, 2009).Hence p62 provides a mechanism that is responsible for controlling excessive inflammatory responses after activating macrophages. A two-step model has been described in figure 5. However, these changes may also be relevant in high fat fed or DDC intoxicated mice so the regulation of inflammation can be elucidated in the context of liver injury.

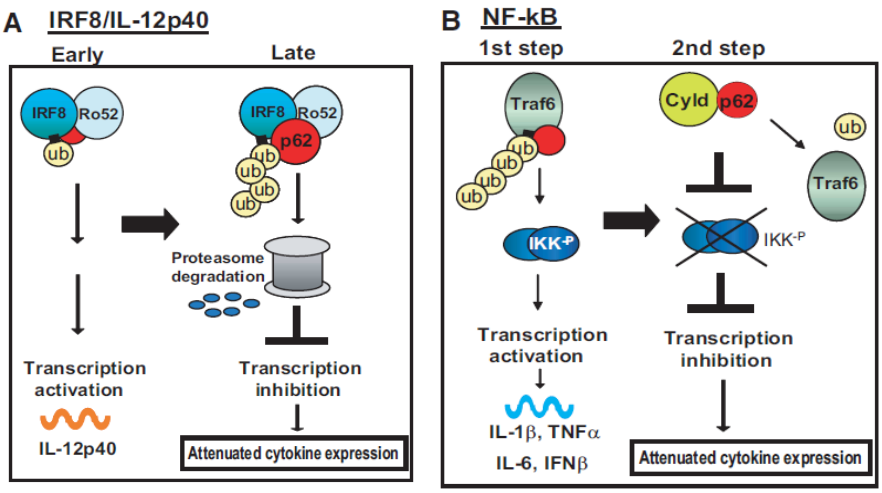


Figure 5: Models for a dual mode of p62 action *A*, IRF8 and Ro52, transcription factors important for IL-12p40 expression, are induced by IFN-γ /TLR early, whereas p62 is induced later in macrophages. In an early stage, Ro52-mediated ubiquitination of IRF8 enhances IL-12p40 transcription. In a later stage as the p62 expression increases, the p62-Ro52 interaction increases, facilitating polyubiquitination of IRF8 and the subsequent degradation. **B**, p62 interacts with another E3 ubiquitin ligase, TRAF6, upon IFN-γ/TLR stimulation, causing TRAF6 auto-ubiquitination and NF-κB activation, leading to the induction of proinflammatory cytokines (the first step). Subsequently, the interaction of p62 with TRAF6 is replaced by that with CYLD to reduce TRAF6 auto-ubiquitination, weakening NF-κB activation (the second step). In this model, p62 orchestrates timely attenuation of cytokine expression by coordinating ubiquitin modification of signaling molecules and transcription factors. (Figure and figure legends: Kim *et al*. Journal of Immunology 4049, 2131-2141)

1.9 Role of p62 in tumourigenesis; p62 - the missing link between Ras and IKK activation.

The basis of tumor formation depends upon the balance of cell survival and cell death. Imbalance in the regulation of cell survival and cell death is crucial for tumor progression. Regulation of these vital cellular processes depends upon NF-κB pathway. Previous studies have pointed out towards activation of NF-κB by a family of important oncogenes 'Ras'. This oncogenic family includes 3 protein members H-ras, K-Ras and N-Ras. Activation of these members triggers a myriad of signaling pathways as shown previously (Downward, 2003). It has been proposed that selective knock down of NF-κB pathway in case of colonic epithelial cells helps to prevent progression of tumor whereas inhibition of NF-κB pathway does not prevent but enhances tumorigenesis in DEN-induced liver cancer (Greten *et al.*, 2004). The cell death in case of hepatocytes activates inflammatory reactions directed by liver macrophages which secrete proliferative cytokines. This ultimately results in growth and development of surviving hepatocytes and thus supporting tumorigenesis in liver. The NF-κB signaling is essential and central to pro-survival function of Ras (Maeda *et al.*, 2005). Duran *et al*. show that Ras induces p62. Ras mediates the survival and transformation through p62. p62 appears to be involved in multiple signaling cascades. These signaling cascades are also part of activation of IKK through TRAF6. Ras induces up-regulation of p62 and it is proposed that up-regulation of p62 is observed in all tumors suggesting enhanced levels of p62 is significant if not in tumor initiation but at least in tumor progression. Duran et al. also show that lack of p62 significantly diminishes the potential of Ras to up-regulate IKKα/β phosphorylation and inhibits polyubiquitination of TRAF6. Duran and coworkers also showed that $p62^{-/-}$ mice did not develop lung adenocarcinomas (Duran *et al.*, 2008). p62 appears to be mandatory for Ras to induce Iκβ kinase through polyubiquitination of TRAF-6. Lack of p62 induces increased reactive Oxygen Species (ROS) which are responsible for enhanced cell death and reduction in tumorigenecity. Therefore p62 is shown to be a mechanistic link between IKK and Ras for the up-regulation of NF-κB pathway. It was also proposed p62 as one of the drug targets to reduce tumorigenesis in human cancer (Duran *et al.*, 2008).

1.10 Role of p62 in maintaining cellular homeostasis

Komatsu et al. studied p62 in detail with special reference to inclusion bodies in brain and liver injury. Role of p62 was investigated in $p62^{-/-}$ and $LC3/Atg7^{-/-}$ as well as in

p62/LC3$^{-/-}$ mouse models. The study demonstrated excision of p62 resulted in reduced ubiquitin positive inclusion bodies which otherwise are present voluminously in Atg7$^{-/-}$ hepatocytes (Komatsu *et al.*, 2010; Komatsu *et al.*, 2007). This may provide a hint that overexpression of p62 hindered autophagy which led to the formation of inclusion bodies. It seems plausible that ubiquitinated proteins interact with p62 initially and thereafter the protein complex form inclusion bodies in p62 dependent manner. Wooten *et al.* also demonstrated inhibition of proteasome results in significantly lesser ubiquitin positive inclusions in p62 deficient cells. This also indicates p62 as common mediator in inclusion body formation. It was observed that Atg7 ablated liver showed marked pathological features assumed to be the result of excessive presence of p62 and resulted oxidative stress. It is proposed that p62 may segregate the ubiquitin positive inclusions in cells in order to get them degraded by autophagic pathway. The study also proposes the formation of cytotoxic protofibrillar oligomeric intermediate earlier than the harmless aggregates. The cytotoxic oligomers then generate the reactive oxygen. Therefore autophagy deficient liver demonstrated combined symptoms of cytotoxic response and protective consequences. Hence, authors proposed that continuous loss of p62 on the background of autophagy deficiency reduces the formation of harmful cytotoxic oligomers leading to formation of harmless inclusions resulting in smoothening of liver injury (Komatsu *et al.*, 2010; Komatsu *et al.*, 2007).

Komatsu *et al*. also demonstrated nuclear translocation of nrf-2 on the background of oxidative stress generated by cytotoxic oligomers (Komatsu *et al.*, 2010). These observations highlight expression levels of p62 that are responsible for maintaining homeostasis through autophagy by controlling the intracellular inclusion body formation (Komatsu *et al.*, 2010; Komatsu *et al.*, 2007).

1.11 Interaction partners of p62

Table 1: Interacting partner of p62 with mechanistic insights

Signaling pathway	**Binding partner**	**Effect**
T cell signaling	p56lck	?
TNF-signaling	RIP-aPKC	NF-κB activation
NF-κB	RIP-TRAF6 aPKC-ζ	Cell Survial

MAP-kinase	P38, MEKK-3	Signal transduction
Cell cycle	Cyclin dependent kinase (Cdk)	Controls the timely transit of cells through mitosis and tumor cell proliferation.
UPS	Polyubiquitin	Degradation of aggregates
Autophagy	LC3/ATG 8	Autophagic degradation
Apoptosis	Keap-1,	Apoptosis NRF-2/Keap1 Pathway
Protein aggregation	polyubiquitin	?
Transcription	?	?

1.12 Structural organization of protein p62: the possible mechanistic link between autophagy and ubiquitin-proteasome pathway

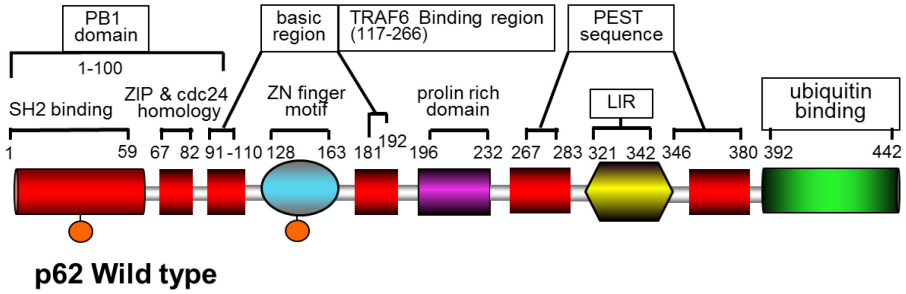


Figure 6: Schematic representation of domain organization of protein p62.

p62 has a N-terminal PB1 domain, which constitutes SH_2 domain and ZIP domain followed by Zinc finger, LCR and ultimately C-terminal UBA domain.

As shown in figure 6, p62 is an adaptor protein that consists of a number of functional domains. p62 has a characteristic Phox and Bem I (PB1) domain (AA 1-100) at its N terminus which consist of typical OPCA motif(Moscat *et al.*, 2006). p62 also contains Zinc finger domain (ZZ), Microtubule light chain binding protein (LC3) Interacting Region LIR (Ichimura *et al.*, 2008) and a classical polyubiquitin binding domain (UBA) at its C-terminal end.

Table 2: Structural domains of p62 and their functional characterization

Amino acid sequence	Domain	Function
1-59	SH_2	N-terminal peptide sequence still remains to be characterized in context of specific binding partner.
67-82	PKC-ζ interacting region /ZIP	A region required for binding with all the PKC isoforms.
1-100	PB1	N-terminal well characterized peptide sequence responsible for mediating interaction with PKC-ζ, PKC-ι, LC3, IκB kinase (IKK),Extracellular signal-regulated kinases (ERK-1). PB1 domain is also responsible for polymerization of p62.
128-163	Zinc Finger (ZZ)	A binding site for ring finger protein TNF-α Receptor Associated Factor (TRAF6) and for Receptor Interacting Protein (RIP-1)
117-266	TRAF6	TNF-α Receptor Associated Factor (TRAF6) interacting region responsible for upregulation of NF-κB pathway.
196-232	Prolin rich domain	Not well characterized till date.
267-283 346-380	PEST	Proline (P), glutamic acid (E), serine (S) and threonine (T), sequence acts a signal peptide for its degradation. This sequence generally is found in proteins with short intracellular half-life.
321-342	LIR	LC3 binding peptide sequence, involved in autophagy
392-442	UBA	C-terminal Ubiquitin binding region, interacts with polyubiquitin

Classical PB1 domains were found to be important in several of the cytoplasmic proteins as they mediate a wide range of protein- protein interaction. PB1 domain are found to be present in scaffold and adaptor proteins as it provides a specific platform for interaction with other PB1 containing proteins during cellular signaling (Moscat *et al.*, 2006). PB1 domain is also responsible of dimerization and/or oligomerization of the protein. (Wilson *et al.*, 2003) Previously it was reported that AA 1-100 are considered to be not one but two structural motifs, one of them was designated as **SH_2 domain (AA**

1-50) because of its homology and second domain was referred to as **ZIP (PKC-ζ interacting region AA 67-82)**.

The ZZ domain still remains to be characterized and protein partners that interact with p62 based on this domain are not yet discovered. ZZ domain containing proteins are known to interact with DNA, however in case of p62 it is not yet investigated.

Previously PEST [proline(**P**),glutamic acid(**E**), serine(**S**), and threonine(**T**)] sequence was assumed to be responsible for degradation of p62 by UPS however it is now speculated that p62 aggregates might be degraded by autophagic pathway whereas short lived p62 speckles might be degraded by UPS (Zheng *et al.*, 2009).

For interaction with LC3, LCR and PB1 domains are necessary. Deletion of any of the both domains disrupts the interaction. Recently interaction of p62 with LC3 is revealed for inducing autophagic clearance of the aggregates in Huntington's disease (Bjorkoy *et al.*, 2005; Pankiv *et al.*, 2007).

The UBA domain (AA 392-440) is well characterized, highly important structural motif that enables p62 for interaction with ubiquitin. Deletion of this structural domain leads to loss of the interaction with ubiquitin (Stumptner *et al.*, 2007).

The proteins that are aggregation prone can be degraded by both of the pathways, the UPS and autophagy driven ones. There is evidence that UPS can be initial response for proteinopathic diseases for removal of misfolded protein and changes in UPS are primary indicators of pathology in these diseases. Recent studies also indicate that tau, α synucleins, mutated superoxide dismutase; poly Q aggregates are largely dependent on autophagy for their removal. Hence current research also focuses in direction of 'co-ordination between autophagy and UPS in removal of misfolded/unfolded proteins' (Zheng *et al.*, 2009).

p62 appears to have a role in the co-ordination between autophagy and UPS because of its structural motifs. p62, polymerizing itself via PB1 domain and might interact with proteasomal subunits using its N-terminal ubiquitin like (UBL) domain. Recent studies indicate a role of p62 as a key linker between UPS and autophagy because of its ability to guide 'ubiquitinated' proteins towards autophagic removal. It was also shown that by using proteasomal inhibitors, p62 expression is induced. In addition accumulation of p62 is an indication of autophagic malfunction. It was also reported that presence of p62 is mandatory for removal of polyubiquitin positive inclusion bodies by autophagic degradation as a response to stress (Zheng *et al.*, 2009).

Depletion of p62 reduces formation of ubiquitin positive inclusions and the autophagosomes, in addition induces a rapid increase in apoptosis. This clearly points out towards protective function of p62 (Zheng *et al.*, 2009).

Despite of recently discovered mechanisms such as failure of ubiquitin proteasome pathway in processing the aggregates and involvement of autophagy, wide cleft remains in solving the functional relevance of cytoplasmic inclusion bodies in '*in-vitro*' tissue culture models, animal models and facts observed in diseased human liver.

1.13 Aims and Hypothesis

Interaction of p62 with K8/18 and effect of conformational alterations, autophagy, phosphorylation and ubiquitination on this interaction

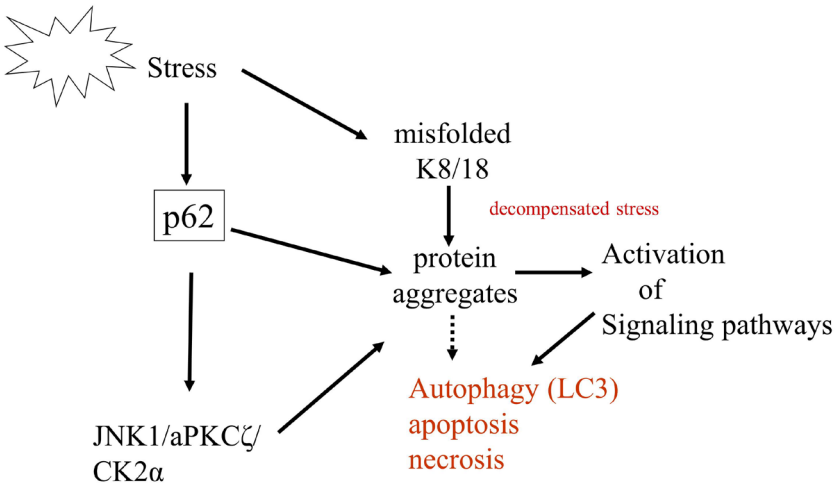
Despite of some of the mechanistic insights and known binding partners of p62, the potential influence of conformational alterations and post-translational modifications i.e. phosphorylation on the interaction of p62 with misfolded keratins continue to be undefined. Sequestosome 1/p62, ubiquitin, Keratin 8 (K8) and Keratin 18 (K18) are the major constituents of MDBs. The major focus of this thesis is to investigate, in 'liver pathology mimicking' cell models, whether interaction of p62 with K8/18 in MDB and IHB pathogenesis is influenced by

1. conformational alterations (Chapter 3 part I)
2. autophagic initiator molecule LC3 (Chapter 3 part II)
3. phosphorylation and interaction with various kinases (Chapter 3 part III) and
4. structural domains of p62 and ubiquitination (Chapter 3 part IV)

In this study new tools of Luminescent Conjugated Oligothiophenes (LCOs) were used to investigate differences in the molecular structure of the components present in the various types of hepatic inclusions that can help obtaining new insight into nature and genesis of protein aggregates in liver diseases *in vivo* and *in vitro*.

Furthermore the role of structural domains of p62 in influencing cellular distribution and ultrastructural pattern of MDBs and IHBs was investigated.

The ability of K8/18 aggregates to activate an apoptotic response or the requirement of p62 in autophagic clearance of the K8/18 aggregates still remains to be clarified. In present series of the experiments, characterization of the role of p62 in context with 'ubiquitinated' keratins and LC3 as well as impact of its phosphorylation sites on this interaction is carried out. It was also hypothesized that, stress induced protein p62 gets associated with misfolded keratins and interacts with various proteins partners such as LC3 which ultimately leads to induction of various signaling pathways. These signaling pathways may culminate into either autophagy or apoptosis. Also phosphorylation sites of p62, S24 and S152 may regulate the interaction with LC3 and other protein partners of p62.Additionally these phosphorylation sites may act as a regulator also on interactions of p62 with kinases such as PKC-ζ and PKC-ι, CK2-α. Moreover SH_2, ZIP, and UBA (structural) domains of p62 may play a crucial role in regulating these interactions.



Proposed modified scheme from personal communication of Zatloukal *et al*: Role of p62 in determining cellular fate towards autophagy or apoptosis

CHAPTER 2

Materials and Methods

2 Apparatus, materials and method

2.1.Technical equipments

Centrifuges:

- Biofuge fresco; (Heraeus, Buckinghamshire, United Kingdom)
- Megafuge 2.0R; Heraeus
- Sorvall RC-5B; refrigerated superspeed centrifuge; (Sorvall, Vienna, Austria)

PCR-machine: Gene Amp PCR System 9700 PE; (Applied Biosystems, Foster city, CA, USA)

Gel electrophoresis instruments

- Sub-cell GT; (BIO-Rad, Vienna, Austria)

Photodocumentation of Gel: Herolab UVT-28 MP; (Herolab, Wiesloch, Germany)

Spectrophotometer: Smart spec 3000; Biorad

Shaker: Certomat H and U;B.Braun

Incubators: at 37^0C, 50^0C and 60^0C; Heraeus

Thermo block: Thermomixer comfort; (Eppendorf, Hamburg, Germany)

Vortex: (Vortex- Genie 2, USA)

Waterbath for ligation: mgw; Lauda RMS

UV-Cross linker: Stratalinker 2400 Stratagene

2.1.1. Cell culture S2 laboratory

- CO_2 incubator: Forma Scientific Steri –cult 200
- Waterbath:-Julabo SW-20^0C; water sterilised with Prothermal; Lucerna ChemAG
- Sterile Workbench :Prettl; Laminar flow + Prozesstechnik GmBH
- Haemocytometer -Counting chamber: 0.200 mm depth; 0.0625mm^2; (Fuchs-Rosenthal, Assistant Germany)

- Square coverslips, 22mm diameter (Assistant, Germany)

2.1.2. Microscopes and photodocumentation.

- Light optical microscope: Nikon, Eclipse E 600 with 10x, 20x, 40x, 60x objectives; Nikon JAPAN

- Digital Camera : Canon S3 Canon

- Immunofluorescence microscope: with 25x, 40x oil, 63x oil and 100x oil objectives; (Carl Zeiss, Jena, Germany)

- Confocal Laser Scanning Microscope: Zeiss LSM 510; Zeiss

2.1.3. Plasticware

- 1.5 mL to 15 ml tubes were purchased from Corning, Eppendorf and Sarstedt

- PCR-softstrips (0.2ml);Biozym

- 6 well plates and 75 cm^2 vented culture flasks; Costar

2.1.4. Chemicals, buffer solutions and reagents

- PBS pH 7.2-7.3

$Na_2HPO_4.2\ H_2O$	1.4625 g
KH_2PO_4	0.2450 g
NaCl	8.0 g
H_2O demineralised	ad100 mL

PBS was sterile filtered for cell culture.

50% Glycerol: diluted from 87% glycerol (Merck) with ddH_2O to 50%; Sterile filtered.

Sodium Acetate (3M, pH 5.2)

51.0g sodium acetate*3 H_2O was dissolved in 95 mL ddH_2O. pH was adjusted to 5.2 with hydrochloric acid (few drops). The volume was adjusted to 100 ml with ddH_2O.

2.1.5. Antibiotic Stock Solutions

Kanamycin (Km or Kan; Sigma)

Stock : 50 mg/ml

Final concentration in the medium 50µg/ml.

Ampicillin

Stock:100 mg/ml

Final concentration in the medium 100 µg/ml

All antibiotic solutions were dissolved in ddH_2O and stored at -20^{0}C.

Agarose gel electrophoresis of DNA

For analytical or preparative gel electrophoretic separation of DNA fragments agarose gels were prepared as follows

0.8% agarose gel

SeaKem ME Agarose for gel electrophoresis, Cambrex	0.8g
Prediluted TAE (0.5x)	49.2ml

2.1.6. Electrophoresis buffer 50X TAE Stock (Current protocols in molecular biology)

Tris base	242g
Glacial Acetic Acid	57.1ml
0.5M EDTA pH-8.0	100ml
Distilled water	1000ml
pH	self adjusted.

5x Gel loading buffer (Fermentas, Graz, Austria)

DNA reference standard: DNA ladder (Middle range DNA ladder – 500bp-5kb) was obtained from (Fermentas). 20µl of DNA molecular weight marker was applied in every agarose gel. Electrophoresis was carried out in 0.5x-1x TAE at voltage of 70-100.

2.2. Buffers for isolation of Keratin 8 /18 Cytoskeleton.

Dithiothreitol (DTT)

0.7715g dissolved in 5ml distilled water.

Phenylmethanesulfonylfluoride (PMSF)

0.348g dissolved in 50 ml Methanol.

Rinsing Buffer

0.15M NaCl	8.766g
10mM Tris HCl	10ml (1M stock)
0.02% Sodium Azide	0.2g
Distilled water	1000ml
pH	7.4

Medium A

96 mM NaCl	5.61g
8mM KH_2PO_4	1.08g
5.6mM Na_2HPO_4	0.996g
1.5mM KCL	0.1118g
10mM Na_2EDTA	3.722g
Distilled water	1000ml
pH	6.8
DTT	1 ml
PMSF	10ml

Column Buffer

8M Urea	480.48g
30 mM Tris	30 ml (1M stock)
5mM DTT*	0.77g
Distilled water	1000ml
pH	8

Extraction Medium I

2M KCL	149.1g
200 mM NaCl	11.69
10mM Tris-HCl	10ml
Distilled water	1000ml
pH	7.4
DTT	1ml
PMSF	10ml

Extraction Medium II

1.5M KCL	111.8g
1% Triton X100	10ml
150mM NaCl	8.77g
Distilled water	1000ml
pH	7.4
DTT	1ml
PMSF	10ml

Reconstitution Buffer I (RB I)

4M Urea	240.48g
30 mM Tris	30 ml (1M stock)
5mM DTT	0.77g
Distilled water	1000ml
pH	7.2

Reconstitution Buffer II (RB II)

5mM DTT	0.77g
30 mM Tris	60 ml (1M stock)
0.1mM $MgCl_2$	40.66mg
Distilled water	2000ml
pH	7.0 -7.3

Sample Buffer

9.5M Urea	5.7g
2.5mM DTT	0.00385
5mM Tris	50µl (1M stock)
Distilled water	10ml
pH	8

*To make the column buffer charged, 2 table spoons of amberlite MB-1(Serva) added to the column buffer and stirred for 30 minutes. The column buffer was filtered and then DTT was incorporated. Thereafter pH was adjusted to 8.

Transfection Reagent

Lipofectamine 2000; (Invitrogen) for high efficiency transfection, cationic lipid based reagent.

Mounting medium

DAKO cytomation mounting medium (DAKO) was used on mounting coverslips onto slides for immunocytochemistry and immunohistochemistry.

2.3. Recombinant DNA

2.3.1. Restriction enzymes:

DNA digests were performed according to manufacturer's instructions.10 units (=1µl) of enzymes were used per reaction (30 or 50µl total volume). A digestion was set up usually for 2 hours at 37^0C. For double digestions, either favourable buffer was selected or digestion was sequentially performed. All the enzymes were purchased from Fermentas or Roche (Roche Diganostics, Boehringer Manheim) or New England Biolabs (NEB)

2.3.2. Polymerase Chain Reaction (PCR)

ABI gold Taq DNA Polymerase with PCR buffer and $MgCl_2$ (Applied Biosystems)

Platinum high fidelity Taq DNA Polymerase PCR buffer and $MgSO_4$ (Invitrogen)

Pfu Taq DNA polymerase PCR buffer and $MgSO_4$ (Fermentas)

Deoxyribonucelotide phosphate (DNTP) mixture (10 mM) (NEB)

2.3.3. Ligases and buffers

Quick ligation kit (NEB)

All ligations were performed in 20 µl reaction total volume using 1 µl of Quick T4 DNA ligase. Ligations were carried out at room temperature for 25 to 30 minutes.

2.3.4. Expression Vectors

Following expression vectors served as cloning vectors. Design of all vectors promotes constitutive high level expression of protein due to strong CMV enhancer promoter in mammalian cell lines. Kanamycin or Ampicillin resistance was used to select and maintain the plasmid in *E.coli.*

1. pCDNA3.1
2. pcDNA4his
3. pcDNA4myc His
4. pEGFP-N1
5. pDsRed2-N1
6. pECFP-C1

2.3.5. Cloning and sub-cloning

The coding region of full length human keratin 8 (K8) (accession number BC000654) was amplified and cloned into the pEGFP-vector between the Eco-RI and Bam-H1 sites.(Janig *et al.*, 2005) To create the fusion protein pDsRed2N1 (Clontech, Vienna Austria), human k8 cDNA from pEGFP-hk8 was amplified using Ampli Taq Gold polymerase (Applied Biosystems, Foster City, CA) with hk8-EcoRI-fw 5'-tcg aat tct atg tcc atc agg gtg acc cag a-3' and hk8-BamH1 rv 5'-gtg gat ccc gct tgg gca gga cgt cag a-3' introducing a restriction site downstream of the termination codon. The resulting amplicon lacked the termination codon for the C-terminus DsRed, cloned into PCR 2.1 vector using the TOPO-TA Cloning kit (Invitrogen, Groningen, Netherlands). The cDNA fragment of human K8 was isolated by digesting PCR2.1-k8 with Eco-RI and Bam-HI (Roche diagnostics, Manheim, Germany) and purified using Qiagen reaction cleanup kit (Qiagen). The ligation was performed at room temperature, 1:3 molar ratio, 25 min. using quick ligation kit (NEB, MA, USA). The sequence of the expression construct hk8-dsRed2N1 was confirmed by DNA sequencing. All the enzymes and reagents were stored at -20^{0}C as per manufacturer's instructions.

1. To construct fluorescently tagged proteins for live cell imaging

- Jun kinase cDNA from pCDNA3-FLAG-Hygro-JunKinase (Addgene organization) (NCBI accession:NM_002750) was subcloned in pEGFP-C1 vector between *Hind III* and *EcoRI*
- Human keratin 8 c-DNA(NCBI accession number: BC000654) from pEGFP-C1-k8 was sub-cloned into pECFP-C1 between *Bam HI* and *EcoRI* sites
- Human keratin 18 c-DNA from pEGFP-C1-K18 (NCBI: accession: BC020982) was sub-cloned into pECFP-C1 between *Hind III* & *Eco-RI* sites.
- Human p62 c-DNA (NCBI accession: NM_00390) from pEGFP-C1-p62 was subcloned into pECFP-C1 between *XhoI* and *Hind III* sites.

2.3.6. Expression Plasmids used in Study.

No	Plasmid	Description	Reference
1	pcDNA4HisMAx-p62wt	Human p62 cDNA with poly-Histidine tag (6x) at N terminal of p62 under CMV promoter	Stumptner *et al.* 2002
2	pcDNA4HisMAx-p62S24A	p62 cDNA that contains mutation at Serine 24 to Alanine and His tag	Mahajan *et al.* (Unpublished data)
3	pcDNA4HisMAx-p62S152A	p62 cDNA that contains mutation at Serine 152 to Alanine and His tag	Mahajan *et al.* (Unpublished data)
4	pEGFP-C1-hk8	Human cyto-keratin 8 fused with GFP at N' terminus of K8	Janig *et al.*, 2005
5	Hk8-dsRed2N1	Human cytokeratin 8 expression plasmid with CMV promoter to GFP at C' of PKCι.	Mahajan *et al.*, 2011
6	pCMV-ßGal	ß-galactosidase (Clontech)	Clontech
7	pcDNA3-hk8	Human cytokeratin-8 (K8) under CMV promoter at N terminal of K8	Stumptner *et al.*, 2002
8	pcDNA3-hk18	Human cytokeratin 18 (K18) under CMV promoter	Stumptner *et al.*, 2002

9	pcDNA4/His-MAX_p62PKCΔzip	Deletion mutant: PKC interacting region of p62 (amino acids 66-82) deleted, Polyhistidine tag under CMV promoter at its N' terminus	Stumptner *et al.* (unpublished data)
10	pcDNA4/His-MAX_p62 ΔSH_2	Deletion mutant: Deletion of SH_2 domain(Amino acid 1-50: domain at N terminal end), CMV promoter at N' with Poly histidine tag	Stumptner *et al.* (unpublished data)
11	pcDNA4His-MAX_p62 ΔUBA	Deletion mutant :Deletion of UBA domain (Amino acid 386-439: domain at C terminal end) ,CMV promoter at N' with Poly histidine tag	Stumptner *et al.*, 2007
12	pcDNA4/HisMAXC hubi	Human ubiquitin with polyhistidine tag at C' under CMV promoter at N' end	Stumptner *et al.*, 2007
13	pcDNA3-hubi	Human ubiquitin under CMV promoter and His Tag at N terminus	Stumptner *et al.*, 2007
14	pcW7 yeast ubiquitin	Yeast Ubiquitin	Stumptner *et al.*, 2007
15	hubi-pcDNA4MycHisC	Human ubiquitin myc His at C terminus	Stumptner *et al.*, 2007
16	pHACE-PKCζ	Human Protein Kinase C Zeta under CMV promoter.	Soh *et al.*, 1999
17	pHACE-PKCι	Human Protein Kinase C iota expression plasmid under CMV promoter.	Soh *et al.*, 1999
18	GFP3-PKCζ	Protein kinase C Zeta (PKCζ) under CMV promoter fused to GFP at C' terminus.	Soh *et al.*, 2003
19	GFP3-PKCι	Protein kinase C iota (PKCι) under CMV promoter; fused to	Soh *et al.*, 2003

		GFP at its C' terminus.	
20	pCDNA3-FLAG-Hygro-JunKinase	Human Jun kinase a1 under CMV promoter and Flag tag at its N' terminus.	Addgene; Roger Davis (MIT-USA)
21	pEGFP-JNK-a1	Human Jun kinase a1 under CMV promoter fused to GFP at its N terminus	Mahajan *et al.* (Unpublished data)
22	pEGFP-CK2α	*Xenopus laevis* Casein kinase 2 alpha (CK2) fused to GFP at N terminus under CMV promoter.	Tapia *et al.*, 2006
23	pEGFP-CK2β	Chicken Casein kinase 2 beta (CK2) fused to GFP at N terminus. under CMV promoter	Dr. Odile Filhol-Cochet Theis-Febvre *et al.*, 2005
24	pEGFP-CK2α	Chicken Casein kinase 2 alpha (CK2) under CMV promoter, fused to GFP at N terminus	Dr. Odile Filhol-Cochet Theis-Febvre *et al.*, 2005
25	pRC/CMV-CK2- α HA	Chicken Casein kinase 2 alpha (CK2) under CMV promoter, fused to HA tag at its 'C' terminus.	Dr. Laszlo Gyenis Duncan *et al.*, 2008
26	pECFP-C1-p62	Human p62 fused to cyan fluorescent protein (CFP) under CMV promoter	Mahajan *et al.* (Unpublished)
27	pECFP-C1-hk8	Human cytokeratin 8 fused with CFP at N' terminus.	Mahajan *et al.* (Unpublished)
28	pECFP-C1-hk18	Human cytokeratin 18 fused with CFP at N' terminus	Mahajan *et al.* (Unpublished)

2.4. Bacterial Strains and Microbiology

For site directed mutagenesis E-coli XL-1 blue (Stratagene) was used in the experiment. For transformation and amplification of the plasmid *E-coli* DH-5-α was used. For sub-cloning experiments E-coli Match1^{TM}T1^{R} was used.

2.4.1. Bacterial culture conditions

- E. coli cells were grown at 37°C with shaking at 200 rpm in Luria Bertani (LB) broth and maintained on LB plates with 1.5% agar (Sambrook *et al.* 1989).
- For plasmid DNA preparation recombinant *E. coli* were grown in LB media supplemented with ampicillin or kanamycin.

2.4.2. Transformation

1. The competent *E. coli* DH-5α cells (Invitrogen) were prepared according to Sambrook *et al.* (1989). DNA (~50 ng in a volume of 10 μL or less) was added to competent *E. coli* cells, mixed and kept on ice for 30 min.

2. The cells were then incubated at 42°C for 1 min. (heat shock treatment)

3. To each tube 800 μL of LB broth was added and further incubated at 37°C for 1 h.

4. About 100 μL of the transformed competent cells was spread onto LB plates containing appropriate antibiotic [and/ or IPTG + X-gal in case of cloning] (Sambrook *et al.* 1989).

2.5.Site directed mutagenesis

The p62S24A and p62S152A mutants were created by Alanine-scanning mutagenesis. To create separate point mutations at Serine 24 (S24) and Serine 152 (S152) Quick change site directed mutagenesis kit (Stratagene) was used. The p62 c-DNA (from expression construct pcDNA4-p62) with was amplified using following primers as per manufacturer's instructions. {S24A Long F-5'GAG ATT CGC CGC TTC GCC TTC TGC TGC AGC CC -3' S24Long R -5' GGG CTG CAG AAG GCG AAG CGG CGA ATC TC- 3'}{ S152A Long F- 5'TGC CCA GAC TAC GAC TTG TGT GCC GTC TGC GAG -3' S152A Long R- 5' CCT CGC AGA CGG CAC ACA AGT CGT AGT CTG GGC A- 3'} to introduce point mutations in resulting amplicons. After PCR amplification PCR products were digested using *Dpn I* provided in the kit to remove parental DNA strands. The 10 μl Dpn *I* digested PCR product was then transformed into *E.coli XL-1 blue*.

2.6. DNA sequencing

Resulting clones were sequenced using ABI big dye chemistry 3.1 (Applied Biosystems) with ABI-DNA Sequencing analyzer 3700. [Center for Medical Research (ZMF), Graz, Austria]

2.7. Cell culture

Chinese Hamster Ovary Cells (CHO-K1 -CCL-61 ATCC Manassas VA) cells were maintained in HAM's F12 medium supplemented with 10% fetal blood serum (FBS) (Sigma Aldrich) and 2.2 gm $NaHCO_3$ (Merk) in incubator with 5% CO_2 in 75cm^2 vented culture flask. HeLa (ATCC #CCL2), HEK and Hep-G2 (CCL-61 ATCC Manassas VA) cells were maintained in DMEM medium supplemented with 10% FBS and (Sigma Aldrich) and 2.2 g $NaHCO_3$ (Merk) in hydrogenated incubator with 5% CO_2 in 75cm^2 vented culture flask.

2.8.Transfection

400,000 CHO-K1 cells were seeded on glass coverslips in 6 well plates (Costar) 24 hours before transfection and allowed to grow to 80% confluency. Transfection was performed using 6µg of DNA with 9µl lipofectamine 2000 (Invitrogen) (>3 independent experiments). For control, cells were transfected with empty pCDNA4 myc-his expression vector (Invitrogen). Transfection efficiency was determined in 3 independent experiments by counting GFP-positive cells vs. the total number of cells in 30 vision fields at 250 x magnification

2.9. Luminescent Conjugated Oligothiophenes (LCOs) synthesis.

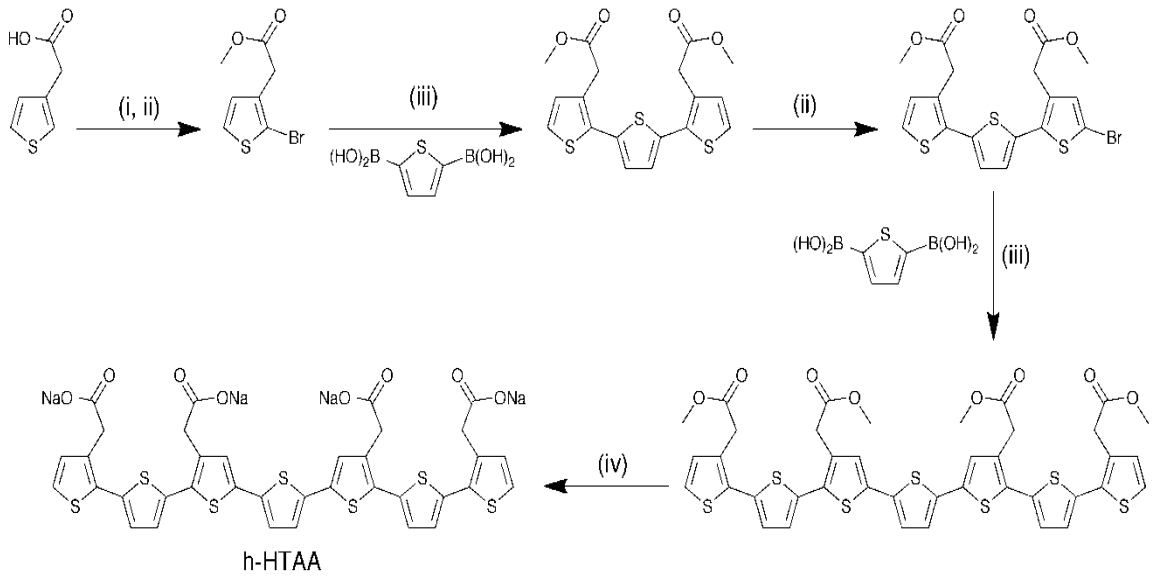
Synthesis of all the conjugated oligothiophenes was carried out at the Department of Chemistry, Linkoping University, Sweden. The synthesis of p-FTAA was reported previously. (Aslund *et al.*, 2009), (Nilsson *et al.*, 2010),

2.10. Synthesis of h-HTAA

The conditions for each reaction are shown in Scheme 1 and the detailed synthesis will be published elsewhere (Klingstedt *et al*. submitted to *Organic and Biomolecular Chemistry*).

Scheme: Schematic representation of the synthesis of h-HTAA. In brief, (3,3"-bismethoxycarbonylmethyl-[2,2';5',2"]terthiophen-3-yl)-acetic acid methyl ester (compound 1)[16] was monobrominated to achieve compound (**2**). Compound (**2**) was

mixed with one equivalent of 2, 5-thiophene diboronic acid (compound **3**) and through a similar Suzuki coupling reaction, compound (**4)** was achieved. Deprotection of the carboxyl groups in NaOH and dioxane yielded the final product h-HTAA. The conditions for each reaction are shown in Supplemental Figure 1 and the detailed synthesis will be published elsewhere (Klingstedt *et al*. submitted to *Organic and Biomolecular Chemistry*) *(*Acknowledgement: Dr. K.P.R Nilsson, Department of Chemistry, Linkoping University, Sweden).



2.11. Induction of MDBs in mice

Animal experiments were performed in accordance with national regulations under animal experimentation licence. MDB formation was induced in male Swiss Albino mice (strain Him-OF1, Institute of Laboratory Animal Research, Medical University of Vienna, Himberg, Austria) by feeding a 3,5-diethoxycarbonyl-1,4-dihydrocollidine (DDC, 0.1% w/w) containing diet as described previously.(Stumptner *et al.*, 2001) Three groups of mice (6 animals each) were kept 8-10 weeks on DDC-diet, two groups of these were left to recover from intoxication for four weeks, of which one group was re-intoxicated with DDC for three days (Denk *et al.*, 2000, Stumptner *et al.*, 2001). Heterozygous *krt8*$^{+/-}$ FVB/N mice were backcrossed for 10 generations with 129/Ola mice to obtain homozygous *krt8*$^{-/-}$ 129/Ola mice (Baribault *et al.*, 1994, Denk *et al.*, 2000). *krt18*$^{-/-}$ mice of 129/Ola genetic background were used(Kachi *et al.*, 1993; Magin, 1998). MDBs were induced in 12 week-old *krt8*$^{-/-}$ and *krt18*$^{-/-}$ mice (both of 129/Ola background), weighing 25 to 30 g, by DDC-feeding for 12 weeks.

Table 3: Primary Antibodies:

IIF – Indirect immunofluorescence on cells**; IHC –** Immunohistochemistry

Sr.No	Name of the antibody	Company	Raised in	Nature	Target	Dilution
1.	Anti p62 lck ligand	BD transduction laboratories	Mouse	Monoclonal	Human p62	1:100 IIF
2.	Anti p62 CT	Zatloukal *et al*. 2002	Guinea pig	Polyclonal	p62	1:100 IIF 1:100 IHC
3	Ks 8.7	Progen	Mouse	Monoclonal	Cytokeratin 8	1:30 IIF 1:30 IHC
4	Ks18.4	Progen	Mouse	Monoclonal	Cytokeratin 18	1:30 IIF 1:30 IHC
5	Troma I	Developmental Studies Hybridoma Bank, Department of Biology, University of Iowa, USA	Rat	Monoclonal	Cytokeratin 8	1:100 IIF 1:100 IHC
6	Keratin 8 and 18	Leica (Novocastra, Vienna, Austria)	Mouse	Monoclonal	Cytokeratin 8 and 18	1:50 IIF on Paraffin embedded tissue section.
7	Anti-alpha1 antitrypsin deficiency	Biogenex Laboratories (Sant Ramon, CA, USA)	Rabbit	Polyclonal	α1-antitrypsin	Ready to use
8	Anti-ubiquitin	DAKO (Glostrup, Denmark)	Rabbit	Polyclonal	Ubiquitin	1:50 IIF 1:200 IHC
9	Anti –his_6	Roche Diganostics	Mouse	Monoclonal	Histidine tag	1:20 IIF
10	Anti- HSP 27	Chemicon International	Mouse	Monoclonal	Heat Shock Protein 27	1:50 IIF
11	Anti-Myc	Abcam	Rabbit	Polyclonal	Myc Tag	1:50 IIF

12	Anti– Protein Kinase Cζ	Santacruz (Vienna, Austria)	Goat	Polyclonal	PKCζ	1:50 IIF
13	Anti-Casein Kinase 2α	Santacruz	Goat	Polyclonal	CK2 α	1:100 IIF 1:100 IHC
14	Anti α-1 Antitrypsin	DAKO	Rabbit	Polyclonal	Anti α-1 Antitrypsin	Ready to use. No dilution needed

Table 4: Secondary Antibodies:

IIF – Indirect immunofluorescence on cells**; IHC –** Immunohistochemistry

Sr. No	**Name of the antibody**	**Company**	**Raised in ... against target**	**Emitted colour**	**Excitation max in nm / Emission max in nm**	**Dilution**
1.	Alexa 488	Molecular probes (Invitrogen)	Goat anti-mouse immunoglobulin	Green	495/ 519	1:250 IIF
2.	Alexa 488	Molecular probes (Invitrogen)	Goat anti-rabbit immunoglobulin	Green	495/ 519	1:250 IIF
3	Alexa 488	Molecular probes (Invitrogen)	Chicken anti-goat immunoglobulin	Green	495/ 519	1:250 IIF
3	Alexa 594	Molecular probes (Invitrogen)	Goat anti-mouse immunoglobulin	Green	590/617	1:250 IIF
4	Alexa 594	Molecular probes (Invitrogen)	Goat anti-rabbit immunoglobulin	Red	590/617	1:250 IIF

5	FITC*	DAKO	Swine anti-rabbit immunoglobulin	Green	460-500/510-560	1:100 IIF
6	TRITC**	DAKO	Swine anti-rabbit immunoglobulin	Red	530-550/570-590	1:100 IIF
7	Rhodamine/ TRITC**	Jackson Laboratories (Westgrove, PA)	Goat anti-guinea pig immunoglobulin	Red	550-570/580-590	1:100 IIF 1:100 IHC
8	Rhodamine/ TRITC**	Jackson Laboratories	Guinea pig anti-rat	Red	530-550/570-590	1:100
9	Cy3	GE healthcare (USA)	Goat anti-mouse immunoglobulin	Far red	530-560/590-650	1:2000 IIF 1:2000 IHC
10	Cy 5	Molecular probes (Invitrogen)	Goat anti-mouse immunoglobulin	Far red	590-640/660-740	Pre-diluted 1:100

*Fluorescein isothiocyanate **Tetramethylrhodamine isothiocyanate

The secondary antibodies were diluted in PBS and centrifuged briefly to remove antibody precipitates.

2.12. Immunostaining (double Immunofluorescence) on cells

Cells were fixed in absolute methanol for 5 minutes at -20^{0}C and for 30 seconds in acetone. Cover slips were washed for 5 mins in PBS buffer. Anti p62 antibody (BD biosciences) or anti-keratin 8 (Troma I) were diluted in PBS 1:100 and incubated for 30 minutes at room temperature. Coverslips were washed in PBS for 10 minutes and put the secondary antibody (Alexa /Alexa 594) (Molecular Probes,) used in 1:200 and 1:300 dilution with incubation time for 30 minutes at room temperature. The LCOs h-HTAA and p-FTAA were used at PBS at 1:500 dilution and incubation time of 20 minutes Cover slips were washed with PBS for 30 minutes. Residual PBS buffer on the cover slip was removed and 30µl of fluorescent mounting medium (Dako cytomation) containing DAPI was used. For negative control, respective secondary antibodies were

used on non-transfected CHO-K1 cells. Also only secondary antibody was used on un-transfected CHO-K1 cells to check the specificity of the secondary antibody.

2.13. Immunoelectron microscopy

For immunoelectron microscopy, frozen sections (5µm thick) were fixed in cold acetone (-20°C) for 10 minutes. For double labeling, p62CT and a pool of Ks 8.7 and Ks 18.04 antibodies were used as primary antibodies, and 10 nm gold-conjugated goat anti–guinea pig Ig (Bio-Cell Research Laboratories, Cardiff, United Kingdom) and 18 nm gold-conjugated goat anti-mouse IgG (Dianova), respectively, were used as secondary antibodies. After immunolabeling, sections were fixed in 2.5% glutaraldehyde (in 0.1 mol/L sodium cacodylate, pH 7.3), treated with 1% OsO4, and embedded in agar 100 resin (Agar Scientific Ltd., Essex, United Kingdom). Ultrathin sections (50 nm thick) were prepared with an ultramicrotome (Ultracut; Reichert-Jung, Nussloch, Germany), stained with uranyl acetate and lead citrate, and examined with a CM 100 electron microscope (Philips Electronic Instruments Co., Eindhoven, The Netherlands) at 80 kV (Stumptner *et al.*, 2007). (Acknowledgement-Andrea Fuchsbichler/ Thüringer)

2.14. Human Tissue Samples

Cryosections, formaldehyde-fixed and paraffin-embedded human tissue samples were acquired from the Biobank of the Medical University of the Graz.

Diganosis	**Organ**	**Number**
Steatohepatitis	Liver (biopsy)	Steatohepatitis 1-22
Hepatocellular carcinoma (HCC)	Liver (biopsy)	HCC case 1-17
Liver cirrhosis	Liver (biopsy)	Liver cirrhosis case 1-10
α-1 antitrypsin deficiency	Liver (biopsy)	α-1AT case 1 -10
Hepatitis B (HBV)	Liver (biopsy)	Case 1-14

2.15. Immunofluorescence on tissue sections

The tissue sections were fixed with and without acetone. The liver sections were stained with anti p62 (p62 CT - Progen) and anti K8 antibody (Troma-I) and LCOs. For anti K8, Rhodamine was used as secondary antibody. For anti p62 antibody, cy5 was used

which has an emission spectrum above 631nm so emission and excitation mixing with spectra of LCOs was compensated.Sections were cut onto charged slides and dried. Slides were fixed with cold acetone (-20 degrees) for 10 minutes and dried. Rat-anti Troma-I (K8) was applied in dilution 1:200 in PBS for 60 min. The slides were washed in PBS 3 times. Secondary antibody anti-rat Rhodamine was applied in dilution 1:100 in PBS for 30 min and slides were incubated in the dark. Slides were washed in PBS 3 times. The LCOs h-HTAA and p-FTAA were used at 1:500 dilutions and allowed to incubate for 30 minutes. Slides were washed in PBS 3 times. Slides were mounted with fluorescent mounting medium Mowiol or DAKO fluorescent mounting medium. Immunofluorescence was analyzed with a LSM 510 laser-scanning confocal microscope (Carl Zeiss) or LSM 510 Meta laser-scanning confocal microscope (Carl Zeiss) (ZMF).

2.16. Fluorescence Microscopy

The spectra were collected with following setup. For cryosections, we recorded spectra with a LSM 510 META (Zeiss) confocal laser scanning microscope with a Plan-Neofluar 63/0.75 objective. The sample was excited with a laser tuned to 488 nm or 458 nm and the emitted fluorescence was detected in steps of 10 nm by a photomultiplier tube array detector with 32 elements (META detector accessory). Accompanying software Zeiss Image Browser 4.2 and ZEN were used for the presentation of images and selection of spectral regions. Spectra were collected from 10 individual spots within 3–5 MDBs from 3 groups of mice intoxicated with 8 week DDC, 3 mice with DDC recovery, and three mice with DDC re-intoxicated for 3 days and 3 *krt* 8-/-, *krt*18 -/- and *p62*-/- mice.

2.17. Generation and detection of oxidative stress

Buthionine Sulphoximine (BSO), tertiary butyl hydroperoxide (TBHP), (Sigma Aldrich) were used for generating oxidative stress. CHO-k1 cells were grown to 80% confluency when seeded in 6 well plates (costar). After 24 hours medium was changed to HAM's F12 without antibiotic and cells were transfected using Lipofectamine 2000 (Invitrogen) as per manufacturer's instructions. CHO-K1 cells were then treated - overnight with 50μM-BSO followed by 100 μM, 250 μM, and 500 μM t-BHP for 15 to 20 minutes. Cells were then washed and incubated with 5 μM 2', 7'-dichlorodihydrofluorescein diacetate (H_2DCFDA) (Invitrogen) for 15 to 30 minutes.

Production of reactive oxygen species as indicated by fluorescence was detected by flow cytometry. (Beckman Coulter FC 500), (480 nm/495-529nm, ex/em)

For a certain series of experiments CHO-K1 cells were then treated - overnight with 50μM, 100 μM, 250 μM, and 500 μM –BSO and UV induced stress was generated by exposing the cells with 100 J and 500 J wavelengths in UV cross linker chamber (Stratagene).

2.18. Flow cytometry

CHO-K1 cells were seeded into 6-well plate (4×10^6 per well) 1 day before stress treatment. On the next day, cells were transfected with Lipofectamine 2000 and respective expression constructs. Six hours post transfection the cells were treated overnight with BSO. On day 3, cells were stressed with (TBHP) followed by incubation with H_2DCFDA. Control cells were incubated in same growth medium. After incubation, both control and treated cells were harvested (0.25% trypsin-EDTA), fixed with 5 mL ice-cold methanol stored at -20°C; resuspended in 500 μL PBS (pH 7.4). Propidium iodide (PI) (Invitrogen) [50 μg/mL] staining was performed by using DNA-Prep stain according to the manufacturer's instructions. Finally, the cells were analyzed on flow cytometer: Coulter EPICS XL-MCL using System II3.0 data analyzing software Flowjo was provided by the manufacturer (Beckman Coulter Fullerton, CA).

2.18.1. Sample preparation for flow cytometry

CHO-K1 cells (in 6 well plates) were trypsinised and were collected in 1.5 mL microcentrifuge tubes (Eppendorf) and centrifuged at 2000 rpm for 5 minutes. The supernatant was discarded and cells were re-suspended in PBS containing 7-Aminoactinomycin D (7-AAD 2-5 μg/ml) or PI (5-10 μg/ml).

2.19. Live cell imaging

Live cell imaging was performed using a Cell Observer Axiovert 200M (Zeiss) phase contrast microscope with black and white camera Axiocam HRM. The sample was excited at 488 and 546 nm using filter set LP 09 FITC (Zeiss) and FS 20 Rhodamine with 40 x objective. Emission was collected between 500-615 nm and 575 -640 using filter set LP 515 (Zeiss) and BP 575-640. The images were recorded every 30 minutes for 24 to 48 hours with exposure of 100ms for FITC and 800ms for pDsRed2n1. The live cell imaging started post transfection 4-6 hours. The live cell movies were made

using Image J, an open source software for processing images. The live cell movies are displayed at the rate of 2 frames per second.

2.20. Immunoblotting

The following antibodies and concentrations/dilutions were used: Mouse anti-p62 (1 μg/ml); Goat anti-p62CT (1 μg/ml); rat anti-keratin8 (9 μg/ml); Mouse anti-keratin18 (3 μg/ml); mouse anti-p21 (0.5 μg/ ml); rabbit anti-JNK (1: 2000); and goat anti-Casein Kinase 2 (Ck2) α-(1: 500), Rabbit anti-Jun kinase (JNK).

2.21. Preparation of cell lysate

The cells were trypsinized, collected and centrifuged at 800 rpm for 2 minutes. The cells were resuspended in 1mL PBS and centrifuged for 2000 rpm for 2 minutes. The supernatant was discarded.

2.22. Preparation of proteins

The cell pellet was resuspended in 50 μL RIPA buffer (25 mM Tris-HCl pH 7.6, 150 mM NaCl, 1% NP-40, 1% sodium deoxycholate, 0.1% SDS). The Ripa buffer is previously mixed with protease inhibitor cocktail (Sigma) and phenylmethyl-sulfonylfluoride (PMSF) (Sigma) diluted 1:1000). The cell pellet was incubated with RIPA buffer for 30 minutes and vortexed every 5 minutes. The samples were then centrifuged at 15000 RPM /min in LE-80 Ultracentrifuge, Beckman, NVT 65 rotor for 30 minutes at 4°C. The supernatant from the centrifugation was collected into precooled microcentrifuge tube.

2.23. Bradford's Assay and SDS PAGE

The total protein concentration was determined by Bio-Rad D_C Protein Assay using photometry at 750 nm with a Bradford Kit (Bio-Rad Laboratories, Hercules, CA). (Bradford, 1976). After the Bradford assay, all the protein samples were adjusted to make a final total concentration of protein 20 μg. The samples were denatured at 65^0C for 15 min and loaded onto 7.5% or 12.5 % (based on the resolution of the bands to be separated) SDS Gel. The proteins were separated by Biorad Gel electrophoresis system and transferred to PVDF or nitrocellulose membrane (Bio-Rad). All blots were incubated overnight at 4°C with all primary antibodies, followed by washing with TBST buffer and minimum 2-hours incubation at room tempratature with secondary antibodies. We used secondary antibodies as follows- rabbit anti-mouse and swine anti-rabbit HRP-coupled antibodies at a final concentration of 1 μg/ml (DAKO,

Copenhagen, Denmark). Specific protein bands were detected by enhanced chemiluminescence assay (ECL plus; Amersham Biosciences, Buckinghamshire, England). As an internal control all the protein samples for all western blots were probed either for β-tubulin or for β-actin.

2.23.1. Isolation of keratin 8/18 pellet from mice liver

Keratin 8/18 cytoskeleton of liver tissue from mouse liver homogenates was isolated as filamentous residues using high ionic strength buffer and triton X-100. (Zatloukal *et al.*, 1989b) Mice were sacrificed and isolated livers were rinsed in ice-cold rinsing buffer. After mincing the liver with scissors 10% homogenate was prepared with glass homogenizers equipped with Teflon pestle in medium A. 1 volume of this homogenate was mixed with 3 volumes of extraction medium I. The resulting suspension was stirred for 30 minutes at 4^0C. The suspension was then centrifuged at 10,000 x g in SS-34 (Sorvall RC5B centrifuge) tubes for 20 minutes at 4^0C. The resulting pellet was dissolved in 9 volumes of extraction medium II. For further extraction the suspension was stirred for 90 minutes at 4^0C. The keratin filaments were recovered by repeated centrifugation for 20 minutes at 10,000 x g. The resulting pellet was then washed with PBS (pH 7.4, DTT- 0.1mM, 0.4 mM PMSF) 3 times at 4000 x g for 20 minutes.

2.23.2. Separation of keratin 8 and 18 polypeptides

The isolated cytoskeleton in the form of pellet was dissolved in sample buffer. To separate the dissolved cytokeratin polypeptides 8 and 18, the solubilized cytoskeletal components were dialyzed against column buffer. The solution containing keratins in column buffer thereafter loaded on a DEAE cellulose column pre-equilibrated with column buffer. The proteins were eluted with linear gradient ranging from 0 to125 mM guanidine hydrochloride in column buffer. The fractions containing separated cytokeratin 8 and 18 were pooled after examination of chloroform-methanol precipitated aliquots by running them on SDS- PAGE. For precipitation of protein, 200 µl of the sample, 400 µl methanol, 100 µl chloroform and 300 µl distilled water were mixed and centrifuged at 11,000 x g for 1 minute. After removal of upper phase, 300 µl methanol were added to the lower and interphase and centrifuged for 1 min at 11,000 x g. The pellet was allowed to dry under vacuum. The dried pellet was then directly re-dissolved using 4x sample buffer containing β-mercapto-ethanol and heated in water bath at 60^0C for 10 minutes. The samples thereafter examined for appropriate bands of

particular molar masses by SDS -PAGE and Comassie blue staining. (Zatloukal *et al.*, 1989b)

2.23.3. Protein measurement of isolated and purified keratins in urea containing buffers

The purified keratins in column buffer and later in RBI was measured using 2D Quant kit (GE healthcare, Vienna, Austria).

2.24. In vitro assembly of keratin filaments

The concentrations of isolated keratin 8 and 18 polypeptides were adjusted to 0.4mg/ml proteins and both were mixed in equimolar ratios for (intermediate filaments) also treated separately as individual K8 and K18 fractions. Two step dialysis procedures was used to reassemble the intermediate filament- at first using reconstitution buffer I (RB-1) containing at room temperature for 3 hours. This results in formation of hetero-tetramers. At second step the two keratin components are dialyzed against reconstitution buffer II (RB-II) for 10 hours at 4^0C. Reconstitution of intermediate filaments was examined by electron microscopy using negatively stained samples.

2.25. Circular dichroism spectroscopy

CD measurements on mouse K8 and K18 were performed at 20°C on a Chirascan CD spectrometer (Applied Photophysics Ltd., Surrey, United Kingdom) in the far-UV region using a 0.4 cm path-length cuvette. The protein concentrations were 1.0 μM for both K8 and K18. The full spectra between 190 nm and 260 nm were recorded every 0.5 nm with 10 repeats for each protein. The buffer spectrum was subtracted from the protein spectra. CD spectroscopy was carried out at Department of Chemistry, Linkoping University, Sweden.

2.26. Oxidative modification of isolated keratin 8 and 18 polypeptides 'in vitro'

Isolated K8 and K18 were adjusted to concentration of 0.5 mg/mL, dialysed into Tris-HCl buffer devoid of urea. 2′-azobis (2-amidinopropane) dihydrochloride (AAPH) was dissolved into the keratin solution at 125 mM and incubated at 37° for a total of 3 hrs. During this period Trp-fluorescence was monitored at 280/340 nm (ex/em). At the end of the modification, samples were extensively dialyzed against RB-I at 4°C, to stop the reaction, remove AAPH and suspend the keratins in 4M urea (Acknowledgement: Dr. Peter Abuja).

2.27. Dephosphorylation of keratin 8/18 'in vitro'

Dephosphorylation of keratins was carried out using 'phosphatase enzyme' (NEB). 40μg purified K8, K18 and reassembled K8+K18 filaments were treated by 2.5 units of dephosphoylase in 1x buffer provided with and incubated at room temperature for 1 hour at 37^0C. Thereafter 15μM h-HTAA was added to the samples and fluorescence was monitored at 280/340 nm (ex/em).

2.28. Immunoprecipitation

For immunoprecipitation, cell lysates were collected at 24 hrs post-transfection in Cytobuster protein extraction reagent (Novagen, Darmstadt, Germany), Phosphosafe protein extraction reagent (Novagen) or (RIPA) buffer containing 10 mM sodium phosphate buffer (25 mM Tris-HCl pH 7.6, 150 mM NaCl, 1% NP-40, 1% sodium deoxycholate, 0.1% SDS). 1mM dithiothreitol (DTT), 1 mM phenylmethylsulfonyl fluoride (PMSF), and a protease inhibitor cocktail (PIC) (Sigma) were always added to the RIPA buffer prior to use. Dynabeads Protein A or Protein G (Invitrogen) 20 to 50 μl were incubated with 2.5 μg of antibody diluted in PBS or 0.5M citrate buffer with rotation at room temperature for 10 minutes. The cell lysates were then incubated with Dynabead –antibody complex overnight at 4^0C with rotation. The immunoprecipitated complexes were washed with PBS or 0.5 M citrate buffer three times and eluted in sample buffer by boiling for 10 minutes at 65^0C. To detect protein expression in the total cell lysates, 20 μl of the cell lysates in RIPA buffer was mixed with 10 μl of diluted 1X NuPage LDS sample buffer (Invitrogen) and boiled for 10 minutes at 65^0C. Samples were then resolved by SDS-polyacrylamide gels (PAGE) and transferred onto PVDF or nitrocellulose membranes for western blot analysis.

2.29. Statistical evaluation

Results are expressed as mean +/- standard error of the mean (SEM) or standard deviation (SD), as indicated. Statistical significance between samples was assessed using a two-sample Welch t-Test for distributions with unequal variance. (Acknowledgement – Mr. Aniket Nikam for his assistance in LCO based characterization of K8/18 aggregates in tissue culture)

Gastroenterology Sep;141(3):1080-1090

CHAPTER 3

Results

Structural characterization of misfolded keratins

Adopted from 1st author publication in '*Gastroenterology*'

Cross β-sheet conformation of keratin 8 is a specific feature of Mallory-Denk bodies in liver diseases

Vineet Mahajan*, Therése Klingstedt‡, Rozalyn Simon‡, K. Peter. R. Nilsson‡, Andrea Thueringer*, Karl Kashofer*, Johannes Haybaeck*, Helmut Denk*, Peter M Abuja*, Kurt Zatloukal

Introduction

Protein aggregates consisting of misfolded proteins are hallmarks of several chronic diseases, such as neurofibrillary tangles and amyloid plaques in Alzheimer's disease, (Clavaguera *et al.*, 2009) Lewy bodies in Parkinson's disease, (Brooks, 2009) and Mallory-Denk bodies (MDBs) in steatohepatitis (Zatloukal *et al.*, 2007). Alterations of hepatocytic keratin intermediate filaments (IFs) with MDB formation are characteristic features of alcoholic (ASH) and non-alcoholic steatohepatitis (NASH) (Stumptner *et al.*, 2007, Zatloukal *et al.*, 2004b). MDB formation also results from drug intoxication and chronic cholestasis, particularly in primary biliary cirrhosis. Furthermore, MDBs might be present in Wilson´s disease, idiopathic copper toxicosis, Indian childhood cirrhosis, after intestinal bypass surgery, α1-antitrypsin (α1-AT) deficiency and hepatocellular neoplasms (Stumptner *et al.*, 2007, Zatloukal *et al.*, 2004b, Zatloukal *et al.*, 2004a).

The biological role of MDBs in steatohepatitis is still largely unknown, but they are generally associated with severity of the disease. While there is detailed information about the primary composition of MDBs, little is known about their molecular structure, and whether a specific molecular structure would have functional implications. The filaments of MDBs differ from "classical" IFs in that they have diameters ranging from 3 to 24 nm (versus the typically 10 nm-sized IFs) and are coated with amorphous material (Yokoo *et al.*, 1982; Zatloukal *et al.*, 2007; Franke *et al.*, 1979). The difference was further demonstrated by monoclonal antibodies recognizing conformation-dependent epitopes on keratins in MDBs (Hazan *et al.*, 1986). Moreover, pressure-tuning infrared spectroscopy revealed that the typical α-helical signature of native keratin was reduced whereas ß-sheet structure increased in the cytoskeleton enriched fraction of MDB-containing hepatocytes of griseofulvin-treated mice (Cadrin *et al.*, 1991). Furthermore, Kachi and coworkers reported an increase in the relative amounts of ß-sheet in isolated mouse and human MDBs, using infrared spectroscopy (Kachi *et al.*, 1993). Although the method applied in these studies did not allow *in situ* investigation of protein aggregates it was the first evidence that MDBs differ from IFs on the molecular structural level.

Recently, a relationship between MDBs and intracellular hyaline bodies (IHBs) was reported. IHBs, like MDBs, contain ubiquitin and p62, but keratin is not detectable (Denk *et al.*, 2000). MDBs and IHBs can be present simultaneously in both neoplastically transformed (HCC) and non-neoplastic hepatocytes, e.g. in idiopathic

copper toxicosis (Denk *et al.*, 2006). So-called "hybrid" inclusions consist of both types, (Stumptner *et al.*, 2007) suggesting similarities or even a direct relationship of their pathogeneses. It is thought that hybrid inclusions are formed whenever overexpression of p62 in combination with ubiquitin prevails over keratin. IHBs are probably generated by aggregation of overexpressed p62 and ubiquitin in the absence of abnormal keratins, whereas keratin and p62 are present at similar proportions in MDBs (Stumptner *et al.*, 2007, Denk *et al.*, 2006). These findings suggest a yet unknown specific role for keratins in the formation of MDBs.

Using new tools to investigate differences in the molecular structure of the components present in the various types of inclusions can help obtaining new insight into nature and genesis of protein aggregates in liver diseases. Luminescent conjugated poly- and oligothiophenes (LCPs and LCOs) have a swivelling thiophene backbone and were described as fluorescent ligands for amyloids. The non-covalent binding to amyloid proteins constrains the rotational freedom of the flexible thiophene backbone and thereby alters the spectral properties of the LCP or LCO depending on the conformation of the bound protein.(Herland *et al.*, 2005, Nilsson *et al.*, 2004) LCPs and LCOs were reported to be sensitive tools for detecting conformational variability in various amyloidogenic protein aggregates (Almstedt *et al.*, 2009; Aslund *et al.*, 2009; Herland *et al.*, 2005; Nilsson, 2009; Nilsson *et al.*, 2007; Nilsson *et al.*, 2010; Sigurdson *et al.*, 2007). These luminescent ligands have also been used as conformation-sensitive optical probes for prion strain differentiation(Sigurdson *et al.*, 2007, Almstedt *et al.*, 2009), and were recently applied for the characterisation of amyloid-beta aggregates as well as neurofibrillary tangles, the two pathological hallmarks of Alzheimer's disease (Aslund *et al.*, 2009). Here we used LCOs to investigate changes in the molecular structure of MDB-components in steatohepatitis and related *in vivo* and *in vitro* models and compared MDBs with other types of protein aggregates occurring in a variety of liver diseases.

3. Results

3.1. LCO profiling of inclusion bodies in human liver tissue: conformational discrimination between MDBs, IHBs and α-1 AT inclusions.

To investigate the applicability of LCOs in characterizing hepatocellular inclusions in liver disorders, we used them to stain human liver cryosections of patients suffering from steatohepatitis (8 ASH and 3 NASH cases), HCC (13 cases), α-1 AT deficiency (5 cases), and ground-glass inclusions from hepatitis B virus (HBV) infected liver (3 cases) (Figure 7).

LCOs specifically bound to MDBs and showed distinct co-localization with K8/18 antibodies. In addition, the characteristic spectral signatures corroborate their binding to protein with cross ß-sheet conformation: p-FTAA showed two distinct emission maxima (514 nm, 549 nm), while h-HTAA fluorescence was further red-shifted with emission maxima at 538 nm and 581 nm (Figure 7A, B). Similar well-resolved spectral signatures have previously been observed for LCOs bound to a wide range of amyloid deposits (Aslund et al., 2009; Herland et al., 2005). In human HCC containing both MDBs and IHBs we observed cross β-sheet conformation only in MDBs as LCOs co-localized with p62 or K8 in MDBs (Figure 7D) while IHBs were not stained by h-HTAA. Double-staining of h-HTAA with p62 or K8 antibodies revealed specific co-localization of LCOs with K8 in MDBs. Since IHBs consist mostly of p62 and do not contain keratins (Stumptner *et al.*, 2007), selective binding of h-HTAA to keratin but not to p62 is proposed. In addition, we investigated human liver sections with α-1 AT-deficiency. α-1 AT inclusions were negative for p-FTAA and h-HTAA (Figure 7F, 8D) whereas MDBs, which may also be present in α-1 AT deficiency, stained positive for LCOs (Figure 7E). To extend the observations in cryo-sections we adapted the protocol for FFPE-sections and validated it by comparative analysis of cryo- and FFPE-sections from the same case. Thereafter additional FFPE cases with ASH (14), NASH (17) and HCC (10), α-1 AT-deficiency (11 cases) and ground-glass inclusion from HBV-infected livers (16) were investigated. The results indicate that LCO-staining can be applied to FFPE-sections and that LCO-binding is specific for MDBs. Similar spectral signatures were observed for both cryo- and FFPE-sections stained with LCOs (Figure 16A). In particular, MDBs in ASH, NASH and HCC were constantly positive (Figure 8A, B, C). Furthermore, MDBs in ASH, NASH and HCC had similar emission spectra (Figure 16B, C), indicating similar molecular structure of MDBs in different types of liver diseases. However, other types of inclusions, such as IHBs (Figure 7D), α-1 AT

inclusions (Figure 7F, 8D), and ground-glass inclusions were not stained by LCOs (not shown).

3.2.LCOs bind to human and murine MDBs.

Both h-HTAA and p-FTAA bound to mouse MDBs (Figure 9A, B) and the respective emission spectra (Figure 9A, B) were comparable to human MDBs (Figure 7A, B, 16D). LCOs specifically co-localized with K8 in MDBs in all cases investigated (Figure 9). LCOs did neither bind to intact hepatocytic keratin IF cytoskeleton (Figure 9C) nor to cytoplasmic speckles containing p62 but no keratin.

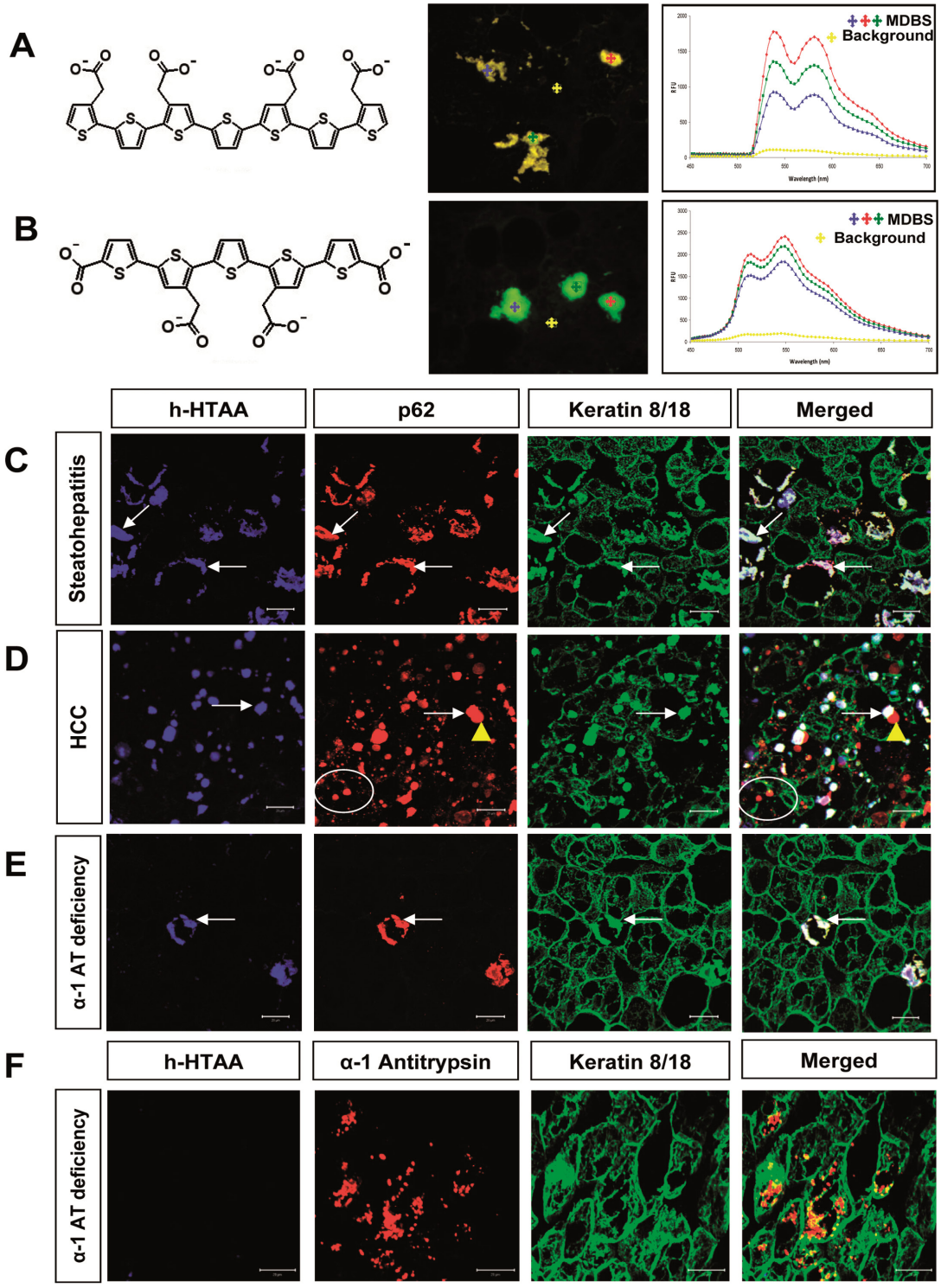


Figure 7: LCOs: structure, emission spectra and profiling of human liver diseases (cryo sections). (A) Structure of h-HTAA. Fluorescence image of MDBs in an h-HTAA-stained human liver section with steatohepatitis. h-HTAA bound to MDBs shows emission maxima at 538 nm and 581 nm. (B) Structure of p-FTAA. Fluorescence image of MDBs in a p-FTAA-stained human liver section with steatohepatitis. p-FTAA bound to MDBs shows emission maxima at 514 nm and 549 nm. (C) High-resolution pseudo-colour fluorescence imaging of human liver with steatohepatitis triple-stained [h-HTAA (blue), p62 (red), keratin 8/18 (K8/18) (green): MDBs stained with h-HTAA co-localizing with p62 and K8 (white arrow). (D) MDBs in human HCC exposed to h-HTAA: p62 and K8 are selectively

stained (white arrow) whereas IHBs (white circle, yellow arrowheads) remain unstained. (E) Human livers with α-1 AT deficiency stained with h-HTAA, anti-p62 and anti-K8 antibodies: MDBs are stained by h-HTAA. (White arrow) (F). Human liver with α-1-AT deficiency stained with h-HTAA and anti-α-1 AT antibody showed no colocalization of α-1 AT inclusions and h-HTAA. All scale bars 20 µm.

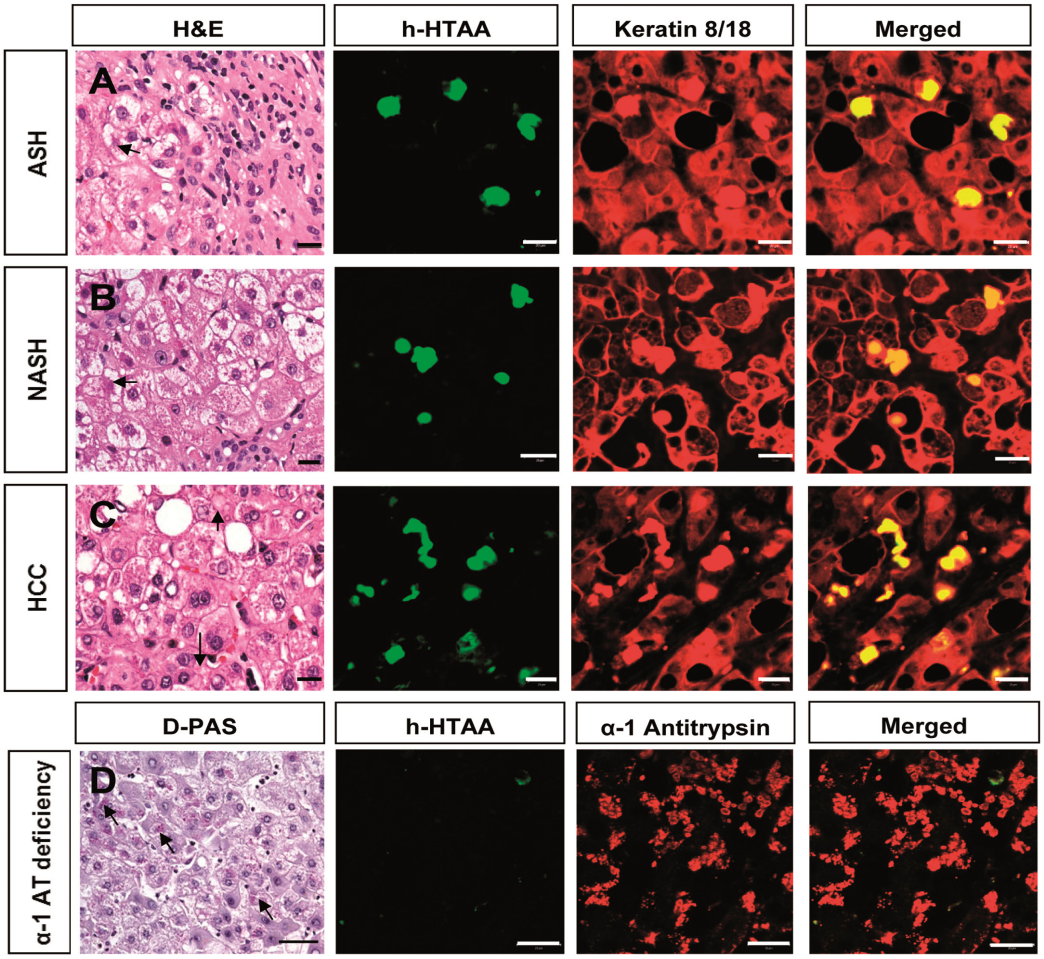
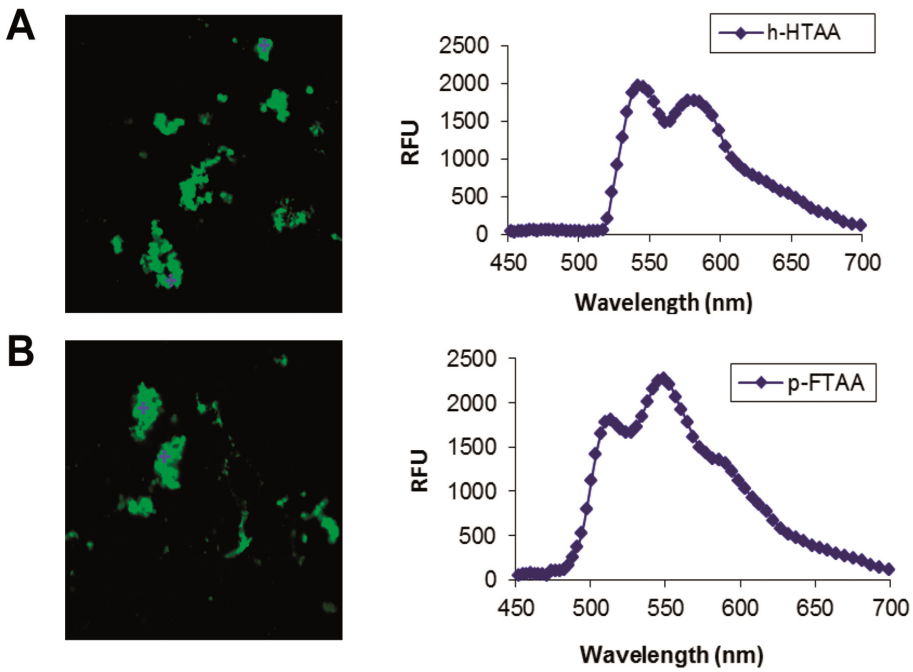


Figure 8: LCO-based structural characterization of MDBs in ASH, NASH and HCC (FFPE sections) (A) Hematoxylin-eosin (H&E) staining of FFPE human liver sections with ASH: enlarged and ballooned hepatocytes, presence of MDBs. High-resolution pseudo-color fluorescence imaging of the same tissue specimens double-stained with h-HTAA (green), keratin 8/18 (K8/18) (red) showing co-staining of MDBs. (B) H&E stained FFPE human liver section with NASH: rounded hepatocytes containing MDBs, enlarged nuclei and inflammation. The same human NASH liver specimen exposed to h-HTAA and anti-K8/18 antibodies show distinct co-localization. (C) H&E-stained FFPE human liver sections with HCC: enlarged hepatocytes, loss of regular cytoskeleton and MDBs surrounded by neutrophils in human HCC; fluorescence imaging of the same specimen stained with h-HTAA and antibody against K8/K18, revealing co-localization. (D) D-PAS staining of a FFPE human liver section with α-1 AT deficiency shows presence of many α-1 AT inclusion bodies. Scale bar 50 µm. The same human liver specimen stained with h-HTAA and anti-α-1-AT antibody: there is no colocalization of α-1-AT inclusions with h-HTAA. If not stated otherwise scale bars are 20 µm.

3.3. Cross β-sheet conformation is a primary feature of MDBs and not a consequence of a "maturation" process

To understand the dynamics of cross β-sheet formation we investigated MDBs in mice at different stages of their development. Livers of mice intoxicated for 8 weeks with DDC contained many MDBs. To better distinguish between old and newly formed MDBs, mice fed DDC for 8 weeks were allowed to recover for 4 weeks on standard diet. By then, most MDBs had disappeared but residual MDBs typically located at the cell periphery were stained by h-HTAA (Figure 3D). After re-intoxication of recovered mice for 3 days, several newly formed MDBs could be observed. In re-intoxicated mice even the very small MDBs formed during re-induction stained positively (Figure 3E) indicating that keratin acquires cross β-sheet structure instantaneously during MDB formation and not as a consequence of a "maturation" process.



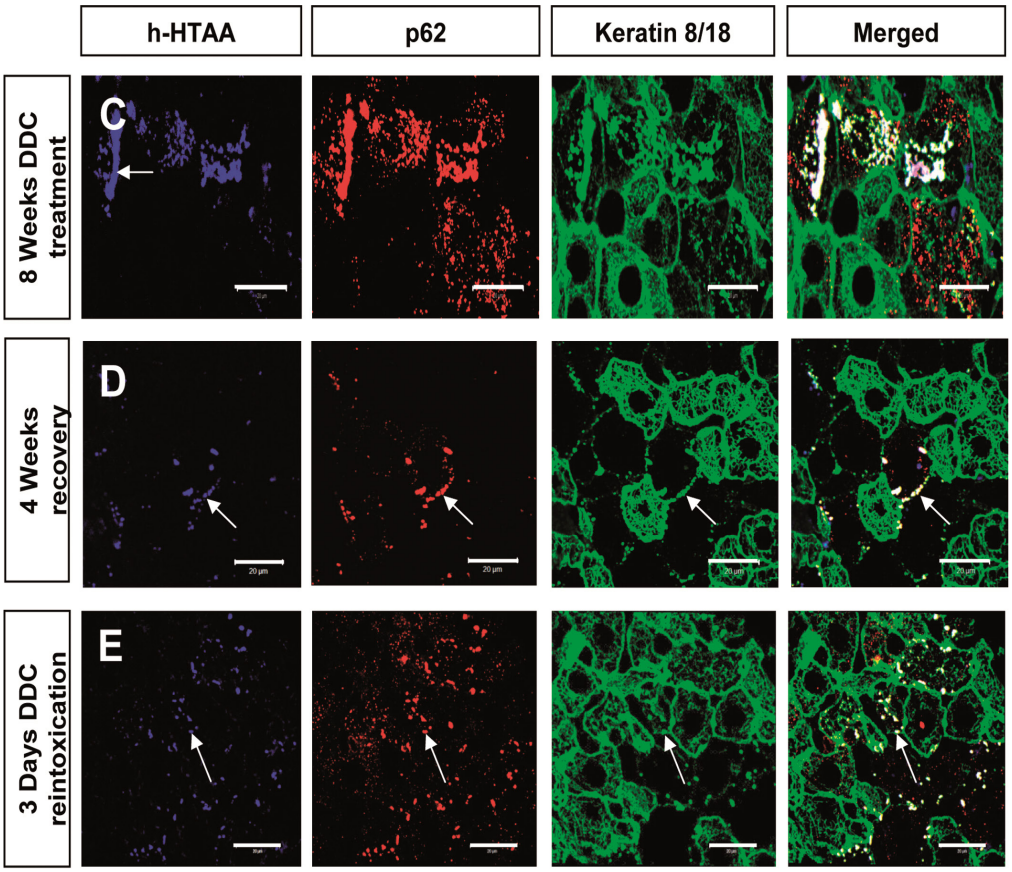


Figure 9: *In vivo* conformational dynamics of keratin aggregates with cross β-sheet assemblies in DDC-intoxicated mice (A) MDBs in a h-HTAA-stained liver section of a mouse intoxicated with DDC for 8 weeks. h-HTAA bound to MDBs showed two emission maxima at 542 nm and 581 nm. (B) MDBs in a p-FTAA-stained liver section of a mouse fed DDC for 8 weeks. p-FTAA bound to MDBs showed two emission maxima at 514 nm and 549 nm.

(C) Fluorescence images of liver sections of a mouse fed DDC for 8 weeks. Triple staining of p62 (red), K8/18 (green) and h-HTAA (blue). MDBs (white arrow) showed triple-positive staining. Scale bars: 10µm. (D) Liver sections of a mouse recovered for 4 weeks after DDC diet. Triple staining of p62 (red), K8/18 (green) and h-HTAA (blue). White arrow indicates residual triple-positive MDBs. Scale bars: 20µm. (E) Liver sections of a mouse recovered for 4 weeks from DDC diet and re-intoxicated with DDC for 3 days. Triple staining of p62 (red), K8/18 (green) and h-HTAA (blue). Newly formed MDBs (white arrow) showed cross β-sheet conformation within 3 days. Scale bars: 20µm.

3.4. MDBs in krt18-/- mice are rich in cross β-sheet structure

K8-overexpressing transgenic and *krt18*$^{-/-}$ mice are more susceptible to DDC-induced MDB formation than wild-type mice (Nakamichi *et al.*, 2005) (Haybaeck et al., unpublished). These studies highlight that excess of K8 over K18 facilitates the formation of MDBs (Nakamichi *et al.*, 2005), (Denk *et al.*, 2000). Furthermore, in *krt18*$^{-/-}$ mice the excess of K8 in the absence of its binding partner K18 even spontaneously led to MDB formation at high age (Kachi *et al.*, 1993). For comparison,

livers from wild-type, *krt18*$^{-/-}$, and *krt8*$^{-/-}$ mice were investigated (Figures 9C, 10A and 10B). In DDC-fed *krt8*$^{-/-}$ mice, no cross β-sheet-rich aggregates were observed (Fig 9A) although misfolding of K18 in the absence of its binding partner cannot be excluded. In contrast, DDC-fed *krt18*$^{-/-}$ mice revealed numerous cross β-sheet-rich K8 aggregates that previously had been characterized as MDBs based on immunohistochemical and ultrastructural features (Kachi *et al.*, 1993) (Figure 10B).

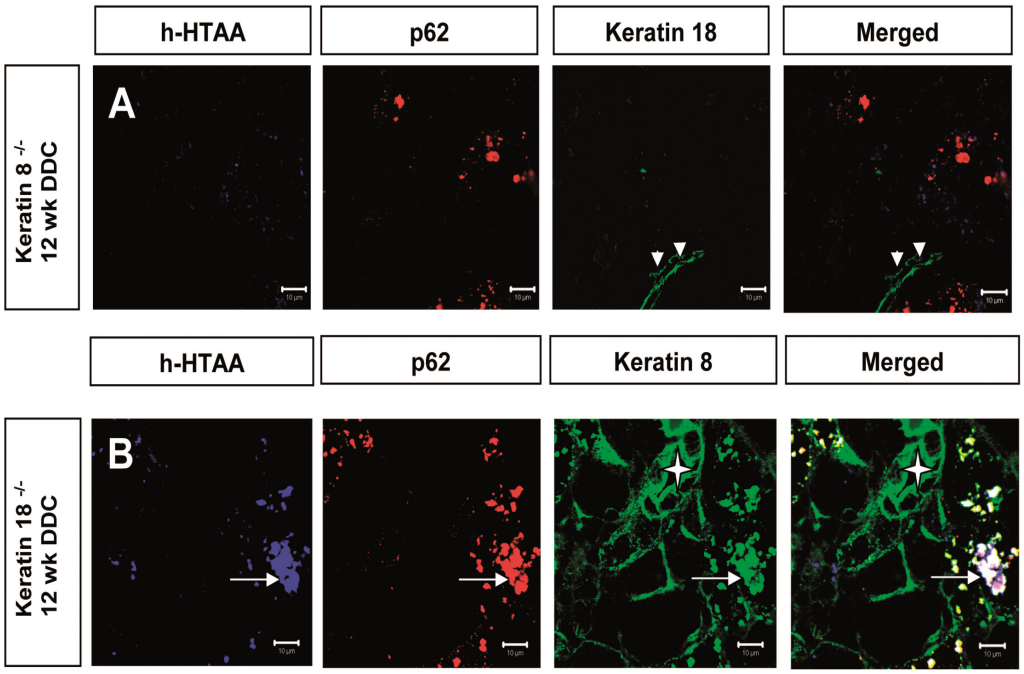


Figure 10: Only K8 forms cross β-sheet rich MDBs in absence of its binding partner K18. (A) Triple staining of a liver section of a krt8-/- mouse for p62 (red), K18 (green) and h-HTAA (blue) revealed absence of MDBs. The white arrow indicates K18 in bile duct epithelial cells. p62 inclusions not associated with K18 can be observed. (B) Triple staining of liver sections of a krt18-/- mouse for p62 (red), K8 (green) and h-HTAA (blue) revealed presence of MDBs (white arrow). The white asterisk highlights the presence of K8 in bile duct epithelium. Scale bars in (A) and (B): 10 µm.

3.5. K8 and K18 reveal different propensities to acquire ß-sheet conformation in vitro

To investigate whether keratin is the key protein contributing to cross β-sheet structure in MDBs, CHO-K1 cells were transfected with p62, *ubi*, *Krt8*, *Krt18* or combinations thereof. Transfection with *Krt8* or *Krt18* produced granular amorphous aggregates.(Stumptner *et al.*, 2007) Previous studies have shown that co-transfection with *p62* and *ubi* in addition to *Krt8/18* is necessary to produce type II-like MDBs(Stumptner *et al.*, 2007). To investigate the structure of such MDBs, *p62*, *ubi* and *Krt8* were co-transfected into CHO-K1 cells. *In vitro* generated MDB-like structures

were stained by LCOs like MDBs in mouse and human liver (Figure 14B). Spectra collected from h-HTAA-stained *in vitro* produced MDB-like inclusions showed two peaks at 532nm and 561nm (Figure 15A).

Neither p62- nor ubiquitin-transfected CHO-K1 cells formed inclusions with cross ß-sheet conformation. In contrast cytoplasmic aggregates in *Krt8*-transfected CHO-K1 were constantly stained with LCOs. Surprisingly, K18 aggregates only occasionally bound LCOs (Figure 14 A, C and E*).*

These differences of K8 and K18 in acquiring cross ß-sheet conformation prompted us to further investigate their structural properties. Various factors influence specific conformations in the misfolded state and we hypothesized that oxidative stress might be one of them. Thus, CHO-K1 cells transfected with either *Krt8* or *Krt18* were additionally stressed using BSO and t-BHP. Formation of reactive oxygen species was assessed using H_2DCFDA detected by flow cytometry (Figure 12). *Krt8*-transfected cells showed high numbers of h-HTAA-positive aggregates per total number of CHO-K1 cells [230 h-HTAA positive (~90%) of 259 *Krt8* transfected cells; 10 random microscopic fields] irrespective of non-stressed or stressed conditions. There was no difference in spectra collected from *Krt8*-transfected cells under stressed and non-stressed conditions (Figure 15B, D). In contrast, *Krt18*-transfected cells showed lower numbers of h-HTAA-positive aggregates per total number of CHO-K1 cells [14 h-HTAA positive (~13%) of 97 *Krt18*-transfected cells; 10 random microscopic fields] under non-stressed conditions. However, when *Krt18*-transfected cells were exposed to additional oxidative stress, markedly increased numbers of h-HTAA aggregates per total number of CHO-K1 cells [158 h-HTAA positive (60%) of 264 *Krt18*-transfected cells; 10 random microscopic fields] were found. The differences in cross ß-sheet conformation between *Krt8*-transfected, unstressed CHO-K1 cells and *Krt18*-transfected, unstressed CHO-K1 cells was statistically significant ($p<0.05$) (Figure 13A, B). Spectra collected from *Krt18*-transfected CHO-K1 cells under stressed and non-stressed conditions are shown in Figure 9C and E. These results demonstrate that K8 is more prone to acquire cross ß-sheet structure than K18 (Figure 14C-F) independent of the interaction with p62. The structural differences of keratin aggregates have not been detected so far by classical electron microscopy underlining the more specific insights obtained by LCOs. At the ultrastructural level, CHO-K1 cells transfected with either *Krt8* or *Krt18* revealed indistinguishable keratin aggregates consisting of amorphous material, resembling to some extent type III MDBs (Figure 11A, B).

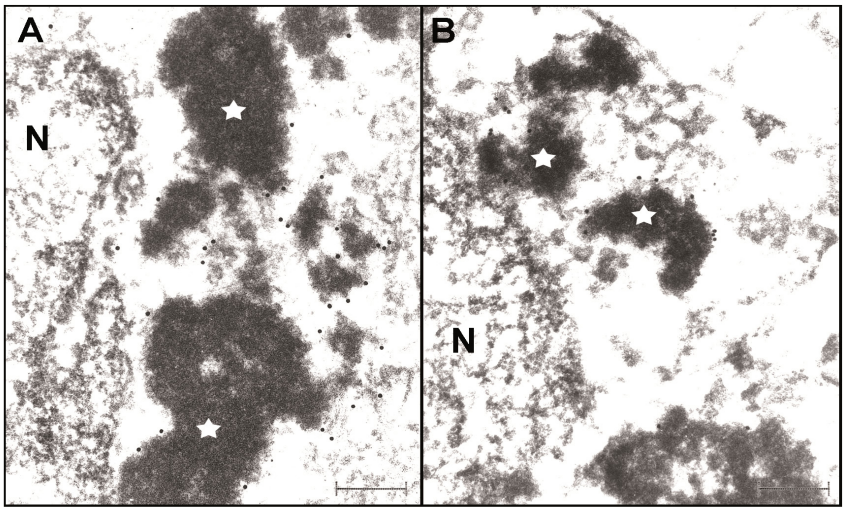


Figure 11: Electron microscopic characterisation of transfected K8 and K18

Immunoelectron micrographs of keratin aggregates in transfected cells stained with anti K8/K18 antibodies and secondary antibodies linked to 18 nm gold particles. (A) CHO-K1 cells transfected with Krt8; granular amorphous K8 aggregates (asterisk), nucleus (N). (B) CHO-K1 cells transfected with Krt18; granular amorphous K18 aggregates (asterisk), nucleus (N). Scale bars: 500 nm (Acknowledgement: Andrea Thüringer)

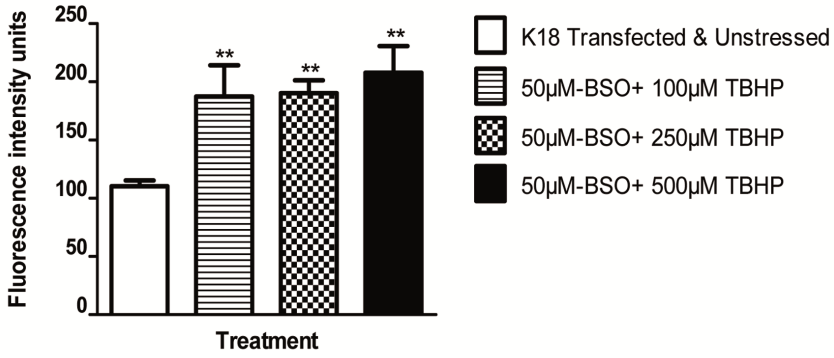


Figure 12: Generation and detection of oxidative stress.

Oxidative stress was generated in *Krt18*-transfected CHO-K1 cells using buthionine sulphoximine (BSO) and tertiary-butyl-hydroperoxide (t-BHP) at the concentrations indicated. Formation of reactive oxygen species (ROS) was detected using H_2DCFDA by flow cytometry. Stronger ROS production was observed at 500 μM t-BHP. Data are expressed as mean of fluorescence intensity ± SD. **P<0.01; compared to controls, using one-way ANOVA followed by Bonferroni's multiple comparison test. Viability of the CHO-K1 cells was between 75 to 95 %. Only living cells were analysed. 15000 independent events in each case were measured.

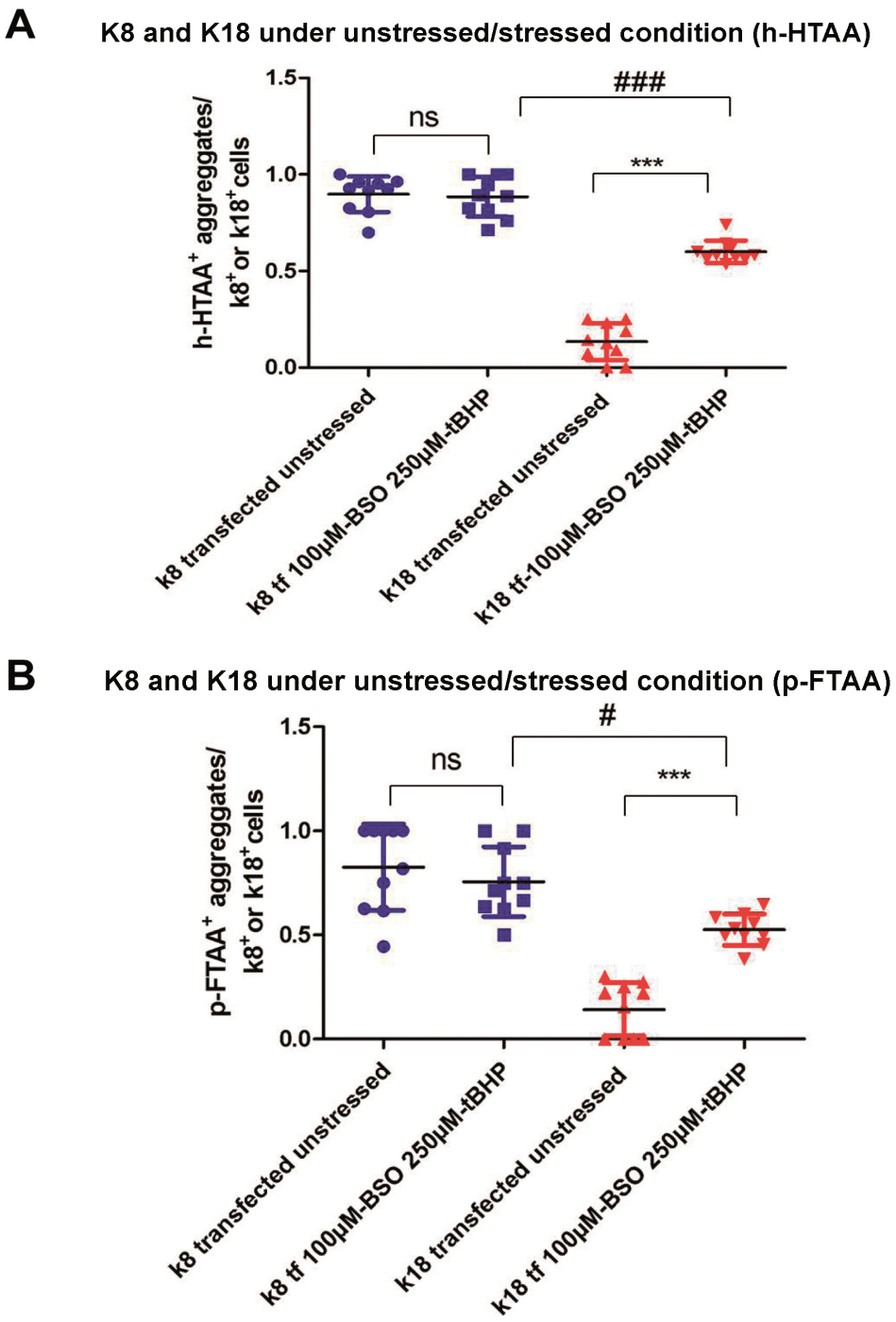


Figure 13: Different behaviour of K8 and K18 under stress: statistical analysis.

Dot plots indicate that aggregates in *Krt8*-transfected CHO-K1 cells do not show any difference under unstressed and stressed conditions whereas K18 in *Krt18*-transfected cells acquires cross β-sheet structure predominantly under stressed condition. All transfected cells formed aggregates. Data are expressed as the mean of the ratio of K8 and/or K18 detected by LCOs to *Krt8*$^{+}$ or *Krt18*$^{+}$ cells ± SD. ***P<0.001; unstressed K8 and K18 compared to stressed K8 and K18, $^{\#}$P<0.05, $^{\#\#\#}$P<0.001; stressed K8 compared to stressed K18 using one-way ANOVA followed by Bonferroni's multiple comparison test.

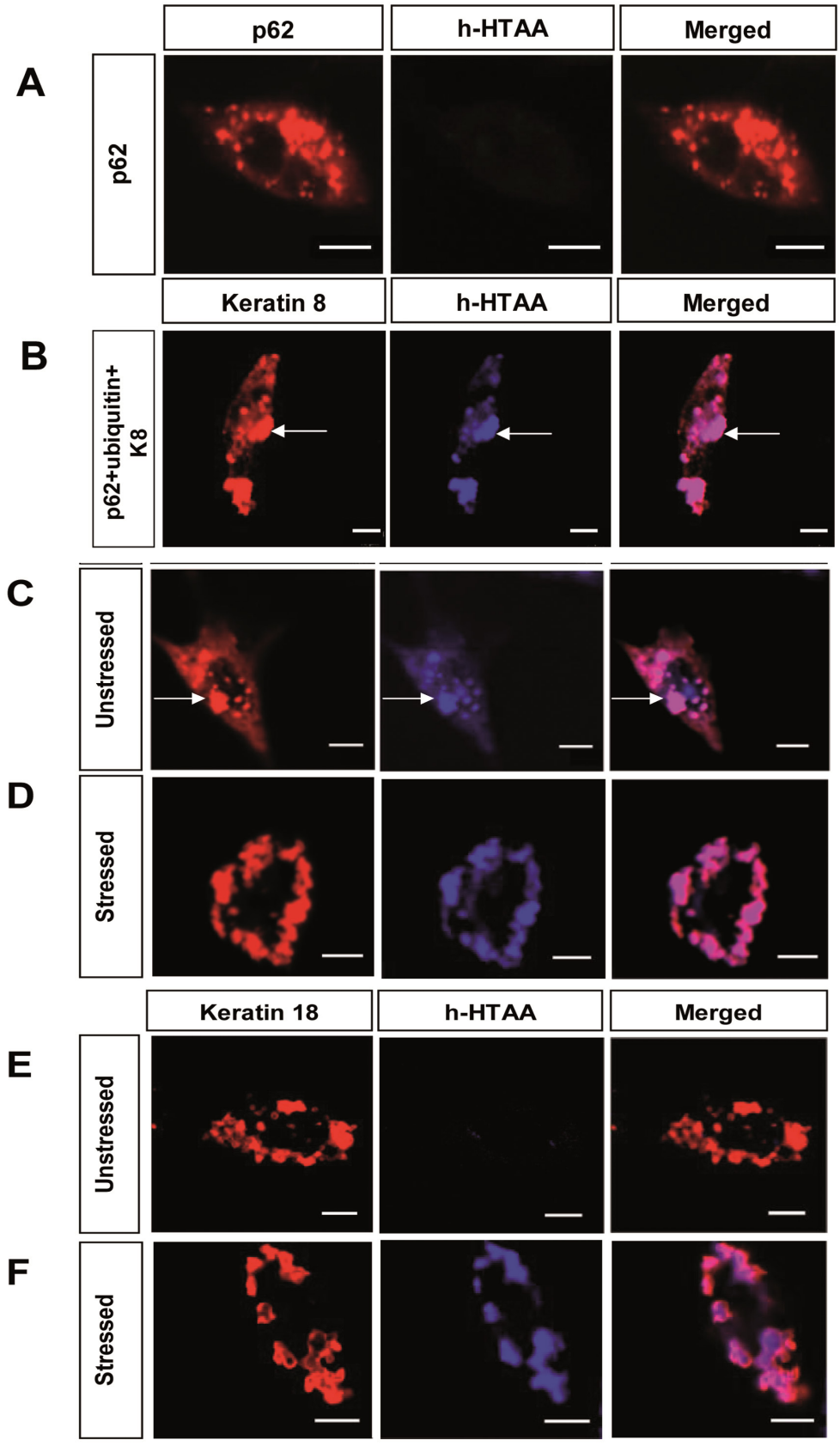


Figure 14: *In vitro* analysis of conformational behaviour of proteins involved in MDB formation (A) CHO-K1 cells transfected with human p62, stained with anti-p62 (red) and h-HTAA (blue). Absence of h-HTAA staining indicated no cross β-sheet structure of p62. (B) CHO-K1 cells co-transfected with equimolar ratios of p62, ubiquitin and *Krt8*, and stained with anti-p62 (not

shown), anti-K8 (red) and h-HTAA (blue). White arrow denotes co-localization of K8 and h-HTAA (C) CHO-K1 cells transfected with human Krt8 and stained with anti-K8 (red) and h-HTAA (blue) (white arrows: co-localization). (D) CHO-K1 cells transfected with *Krt8* and stressed with BSO and t-BHP, stained with anti-K8 (red) and h-HTAA (blue). (E) CHO-K1 cells transfected with human Krt18 stained with anti-K18 (red) and h-HTAA (blue) revealed no binding of h-HTAA to K18. (F) CHO-K1 cells transfected with *Krt18* and stressed with BSO and t-BHP were stained with anti-K18 (red) and with h-HTAA (blue). Note that under stressed condition h-HTAA bound to K18. All scale bars: 5 µm.

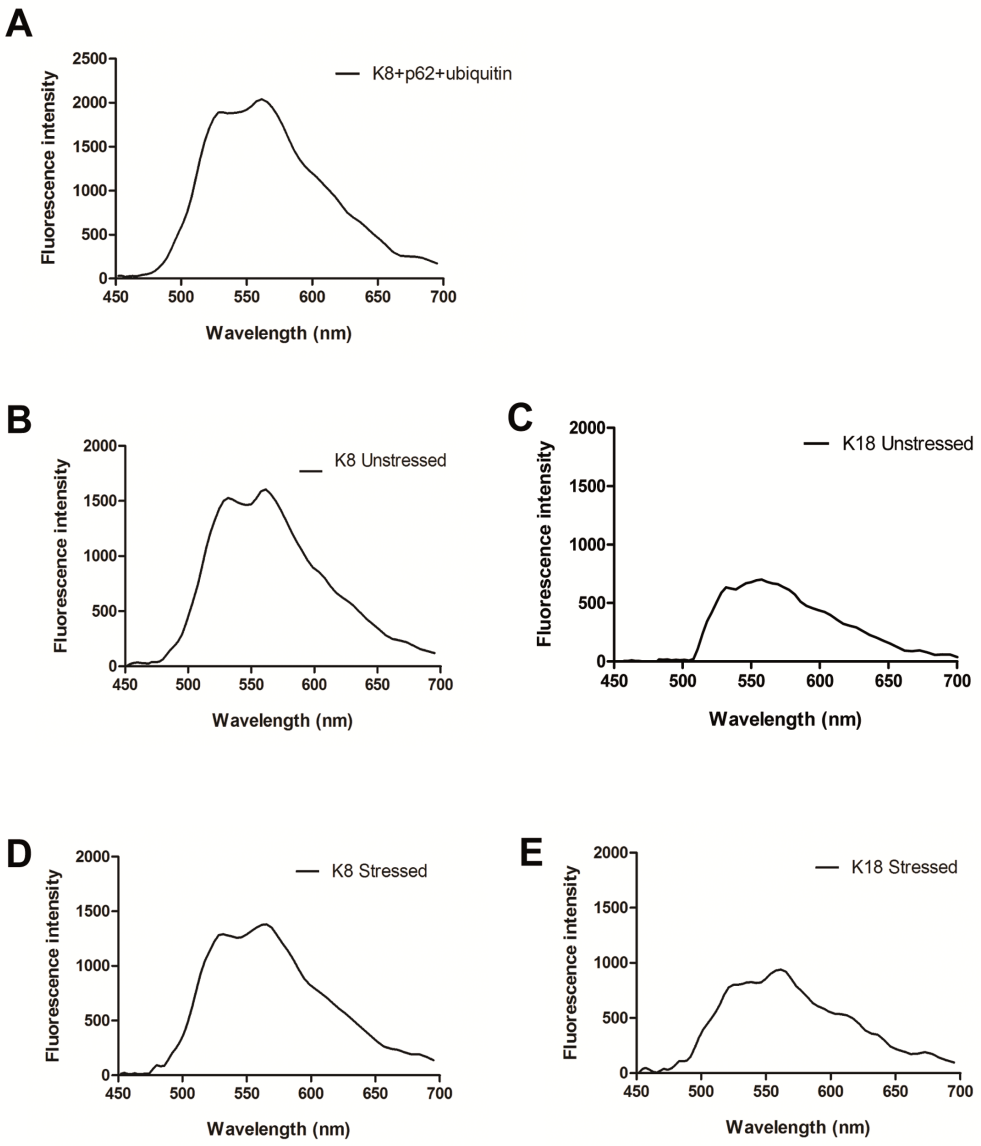


Figure 15: Emission spectra from keratin-containing inclusions in CHO-K1 cells. **(*A*)** The emission spectrum of h-HTAA bound to inclusion bodies formed in vitro after co-transfection of *p62, Ubi* and *Krt8* at equimolar ratios in CHO-K1 cells showed two distinct peaks at 532 nm and 561 nm (B) The emission spectrum of h-HTAA bound to inclusion bodies in Krt8-transfected, unstressed CHO-K1 cells showed two distinct peaks at 532 nm and 561 nm. (C) The emission spectrum of h-HTAA bound to inclusion bodies in Krt18-transfected unstressed CHO-K1 cells showed less well-resolved spectral peaks and lower fluorescence intensity. (D) The emission spectrum of h-HTAA bound to inclusion

bodies in Krt8 transfected stressed CHO-K1 cells was similar to that of h-HTAA bound to inclusion bodies in these cells under unstressed conditions. (E) The emission spectrum of h-HTAA bound to inclusion bodies in *Krt18*-transfected, stressed CHO-K1 cells showed two peaks at 532 nm and 561 nm similar to D.

3.6. K8 is conformationally less stable than K18

To understand the different propensity of K8 and K18 to form cross ß-sheets, they were isolated from normal mouse liver (Figure 16E) and analyzed by CD spectroscopy. Spectra were typical α-helical for both proteins (minima: 208/222 nm; maximum: 191 nm). However, the smaller amplitude of K8 spectrum indicated lower content of α-helices (with increased coiled-coil structure as indicated by increased $[\theta]_{222/208nm}$; Figure 16F). The difference in α-helical content might explain the different propensity of K8 and K18 to form aggregates.

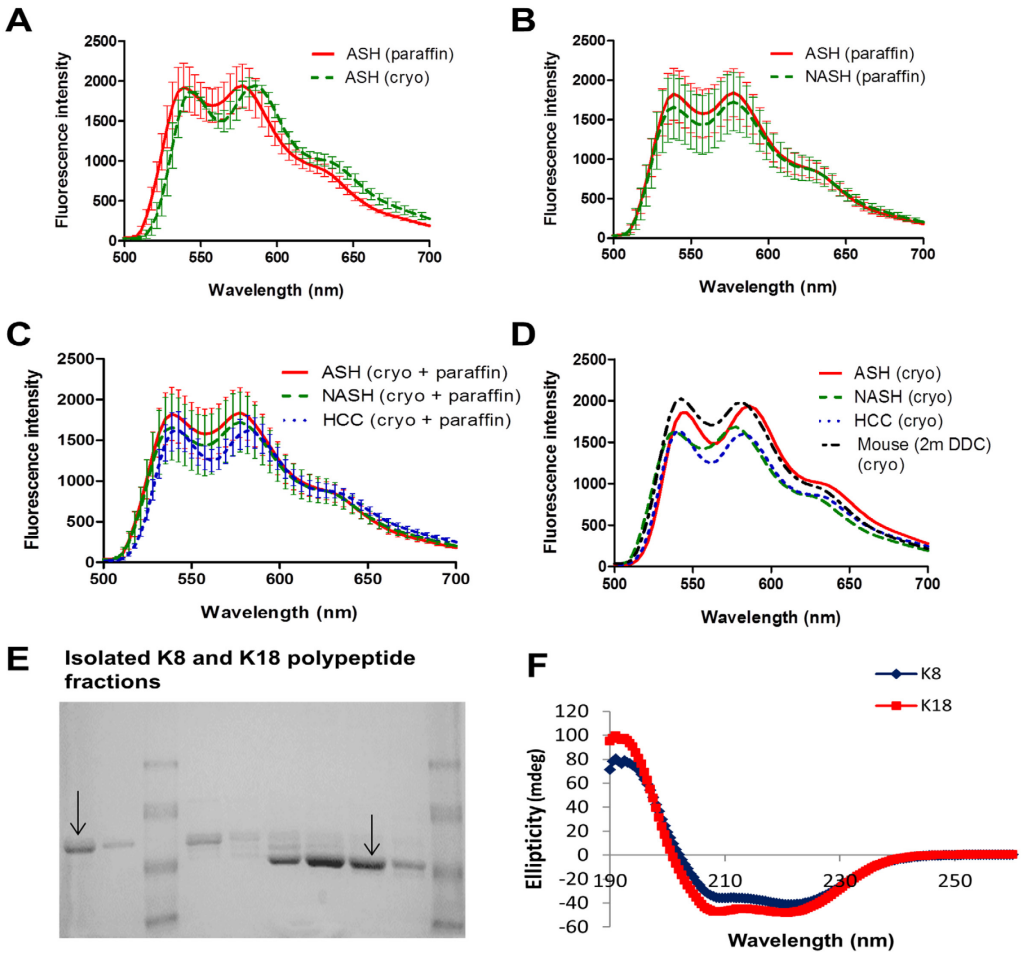


Figure 16: Comparison of h-HTAA emission spectra of MDBs in different liver diseases, and CD spectra of K8 and K18

(A) Comparison of h-HTAA emission spectra of MDBs from human liver cryo-sections and FFPE sections with ASH (emission maxima 539-546 nm and 578-586 nm). (B) Comparison of h-HTAA

emission spectra of MDBs from human liver sections with ASH and NASH (both FFPE) (emission maxima at 539-546 nm and 579-586 nm). (C) Comparison of h-HTAA emission spectra of MDBs from human livers with ASH, NASH and HCC (summary of results from cryo and FFPE sections). (D) Comparison of h-HTAA emission spectra from MDBs from human livers with ASH, NASH and HCC and murine livers with MDBs (all cryo sections). Data are shown as mean +/- SD (n=5). (E) SDS page gel showing isolated and column purified keratin8 and 18 fractions. (F) CD spectra of isolated K8 (blue line) and K18 (red line). The smaller amplitude of the spectrum for K8 indicates lower content of α-helices compared to K18. The increase in $[\theta]_{222/208nm}$ for K8 indicates coiled-coil helices. (Acknowledgement: Spectra measurements were performed at Department of Chemistry, Linkoping University Sweden)

3.7. *In vitro* dephosphorylation and oxidative modification of isolated and purified keratin polypeptides

To understand role of post translational modifications of keratins towards contribution of cross β-sheet conformation, the isolated and purified keratins were subjected to oxidative modification by 2′-azobis (2-amidinopropane) dihydrochloride (AAPH) h-HTAA-fluorescence was monitored to conclude for presence of cross β-sheet conformation. No significant difference was found as compared to controls (data not shown).

To investigate the impact of phosphorylation of K8/18 on their structural orientation, isolated K8/18 polypeptides were subjected to phosphatase treatment and incubated with h-HTAA. The fluorescence was monitored to determine the presence of cross cross β-sheet conformation however no statistically significant differences were observed in between modified and unmodified keratins (Figure 17)

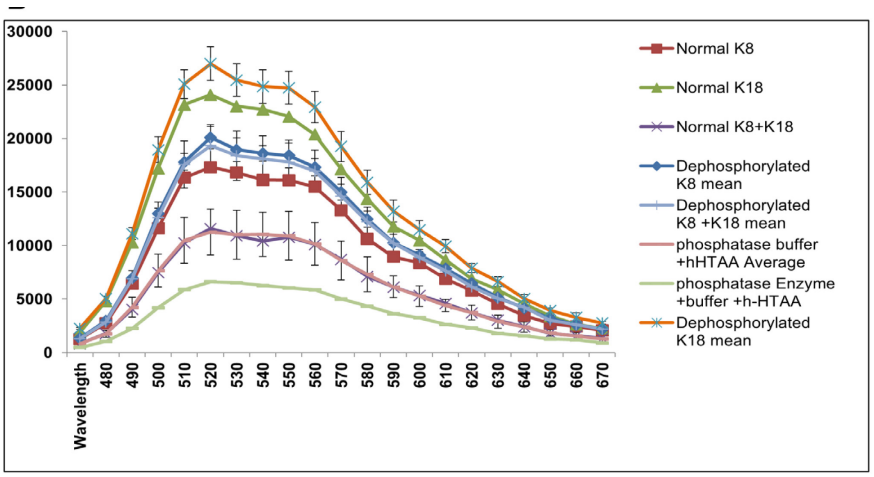


Figure 17: Dephosphorylation of isolated and purified keratin polypeptides

The graph indicates relative fluorescence units as a function of characteristic 531/580 nm wavelength always specific for h-HTAA.

3.8. Live-cell imaging reveals instantaneous acquisition of cross β-sheet conformation of overexpressed K8 in vitro

Conformational variation is inherent to many polypeptides and ranges from fluctuations of side chains to secondary structure changes and re-organization of the entire protein folding (Tokuriki *et al.*, 2009). To increase our understanding of the dynamics of conformational changes during accumulation of K8 aggregates, we performed live-cell imaging of *Krt8*-transfected CHO-K1 cells. h-HTAA or p-FTAA were found constantly bound to keratin aggregates appearing 4-6 hours post transfection and this conformation remained stable for 16-18 hours. Data are shown on following website "http://www.medunigraz.at/pathologie/images/content/file/p62/".

Video 1A/2A: p-FTAA.avi

Real time imaging of transiently transfected CHO-K1 cells with hk8dsRed2N1 stained with p-FTAA 4-6 hours post transfection in green (pseudo blue) channel. A total stack of 47 images was collected over 24 to 48 hours starting from 4-6 hours post transfection, with a time interval of 30 minutes. The video is displayed as 2 frames per second. p-FTAA positive K8-inclusions can be observed.

Video 1B/2B: hk8dsred.avi

Real time imaging of transiently transfected CHO-K1 cells with hk8dsRed2N1 in red channel. Accumulation of K8-positive inclusions can be observed over the period of 24-48 hours.

Video 1C/2C: p-FTAA+ hk8DsRed merged.avi

Real time imaging of transiently transfected CHO-K1 cells with hk8dsRed2N1 stained with p-FTAA in merged channel. Instant acquisition of cross β-sheet structure as indicated by p-FTAA bound to K8 inclusions can be seen. Co-localization of p-FTAA and hk8dsRed2N1 inclusions is shown as pink pseudo-colour. These video files are available on http://www.medunigraz.at/pathologie/images/content/file/p62/

Discussion

Investigation of the molecular structure of protein aggregates opens a new level of insight into disease pathogenesis. Until recently, no simple method for *in situ* detection of conformational variation in such aggregates was available. Spectroscopic or crystallographic methods are of limited use for aggregates of complex protein composition(Huiyuan Li FR, 2009). Furthermore, dyes used conventionally, such as Congo red and Thioflavin-T have sterically rigid structures, reducing specificity and sensitivity of their binding properties, and they fluoresce with a limited defined spectrum (Sigurdson *et al.*, 2007, Nilsson, 2009, Nilsson *et al.*, 2010). LCOs are advantageous since their rotationally flexible thiophene backbone leads to fluorescence in different colours depending on the geometry of their backbone. Since the latter depends on the conformation of the structures to which they are bound, the emission spectra of LCOs reflect protein conformation (Nilsson, 2009).

LCOs allowed for the first time to characterize *in situ* the molecular structure of different types of protein aggregates occurring in liver diseases. IHBs, α-1 AT and ground glass inclusions did not show cross ß-sheet structures whereas MDBs in human livers and mouse models were positive for this conformation. Cross ß-sheet structure of MDBs is a constant feature at all stages of their development. Furthermore, the spectral analysis of bound LCOs demonstrated that MDBs in ASH, NASH and HCC have similar molecular structures, underlining the conformationally well-defined nature of MDBs.

More detailed analysis of the individual MDB components showed that the cross ß-sheet structure can be attributed to keratin in MDBs, which is in line with the absence of cross ß-sheet structure in IHBs containing p62 and ubiquitin but lacking keratin. The binding of LCOs to MDBs could also be reproduced *in vitro* by co-transfection of *Krt8, ubiquitin* and *p62* (Stumptner *et al.*, 2007). Interestingly, LCOs bound to K8 even in the absence of p62 as observed in cells transfected with *Krt8* only. Comparison of conformational properties of K8 and K18 in transfected cells further revealed that K8 instantaneously acquired cross ß-sheet structure when it accumulated as cytoplasmic aggregates. In contrast to K8, overexpressed K18 did not spontaneously acquire cross ß-sheet structure. Binding of LCOs to K18 aggregates was observed only after application of additional oxidative stress to transfected cells. These different conformational properties of K8 and K18 could have major biological implications in the context of MDB formation. Previous studies demonstrated that *krt8*$^{-/-}$ mice do not develop MDBs

after DDC-feeding.(Nakamichi *et al.*, 2005) In contrast, *krt18*$^{-/-}$ mice develop MDBs more rapidly than wild-type mice after DDC-feeding, and even spontaneously at high age (Haybaeck et al., unpublished) (Nakamichi *et al.*, 2005). Therefore the different abilities of *krt8*$^{-/-}$ and *krt18*$^{-/-}$ mice to form MDBs could, at least in part, be attributed to the preference of K8 to acquire cross ß-sheet structure.

To investigate whether the different properties of K8 and K18 are intrinsic features of the polypeptides or are mediated by post-translational modifications like transamidation and phosphorylation or if they are a consequence of interaction with other cellular proteins, we have purified K8 and K18 from normal mouse liver and analyzed their individual conformation by circular dichroism. Isolated K8, at least under the experimental conditions applied, and showed less α-helical structure than K18. Since both polypeptides were isolated from normal mouse liver, this difference is an endogenous property of normal keratins and cannot be attributed to alterations by post-translational modification due to toxic stress conditions or differences in the interaction of keratins with other cellular proteins, such as heat shock proteins. Hence, the instantaneous acquisition of cross ß-sheet structure by K8 when not assembled into IF (as is the situation in hepatocytes with imbalance of *Krt8* and *Krt18* expression or in cells transfected only with *Krt8* or in isolated K8 polypeptides), might explain the essential role of keratin in MDB formation. ß-sheets are "sticky" and spontaneously bind to each other to form filamentous protein aggregates. The preferred acquisition of cross ß-sheet structure by K8 might also explain why no other cellular proteins besides keratin, p62 and stress proteins are major MDB components.

CHAPTER 3 part II

Influence of autophagy/Microtubule Light Chain 3 on p62 and misfolded K8/18

Introduction

There are three systems for protein degradation used by all eukaryotic cells: the 1) ubiquitin-proteasome system 2) calcium dependent proteolysis and 3) the lysosome. The proteasomal pathway targets selective degradation of short lived and abnormal/misfolded proteins by labeling them with Lys-48-linked polyubiquitin chains. The lysosomal degradation occurs through extracellular and plasma membrane proteins transferred by endocytosis and cytoplasmic components delivered by autophagy. Autophagy has been categorized in 3 major ways depending upon differing in the delivery route of cytoplasmic material. These catagories include macroautophagy (hereafter called autophagy), microautophagy, and chaperone-mediated autophagy (Bjorkoy *et al.*, 2005; Pankiv *et al.*, 2007). Macroautophagy is regarded as the central pathway. Macroautophagy involves the seggregation of a region of the cytoplasm within a double membrane-bounded autophagosome. There, then undergoes a maturation process followed by including fusion events with endosomes and/or lysosomes. Then autophagosomes form the structures referred to as amphisomes and autolysosomes (Bjorkoy *et al.*, 2005; Pankiv *et al.*, 2007). Autophagy is regarded to be largly a nonselective, bulk degradation pathway which is responsible for degradation of the majority of the long lived proteins. Human p62/sequestosome-1 protein interacts with both LC3, the mammalian homologue of yeast Atg8, and ubiquitin. It is hypothesized that p62 binds to polyubiquitinated keratins which are destined to undergo autophagic degradation. LC3 binds to p62 and mediates this autophagic degradation. It was also hypothesized that misfolded K8 cannot activate apoptosis or autophagy by itself. Ubiquitin though interacts with LC3 may need p62 to carry the cargo of misfolded proteins to autophagic degradation. Recent studies in the past have demonstrated that the PB1 and LIR domain of p62 are involved in the regulation of interactions with LC3 (Bjorkoy *et al.*, 2005; Pankiv *et al.*, 2007). Nevertheless, how the specific stretches of amino acids (SH_2 domain and ZIP domain which together constitutes PB1domain) govern this interaction has not been investigated. In addition the function of phosphorylation sites in PB1 and other domains may be crucial in governing this interaction. Therefore in this section the focus is on how LC3 influences these interactions.

Results

3.9.Role of p62 in autophagy

3.9.1. Misfolded keratins themselves, alone cannot induce autophagic response through LC3

To investigate if misfolded keratins themselves are capable to induce the autophagy, K8 was co-transfected with GFP-LC3 and analyzed for co-localization. K8 did not co-localize with LC3 (Figure 18A). K18 also did not show any pattern of even a limited co-localization with LC3 (data not shown). These data suggests that K8/K18 alone is not capable of directly inducing an autophagic response.

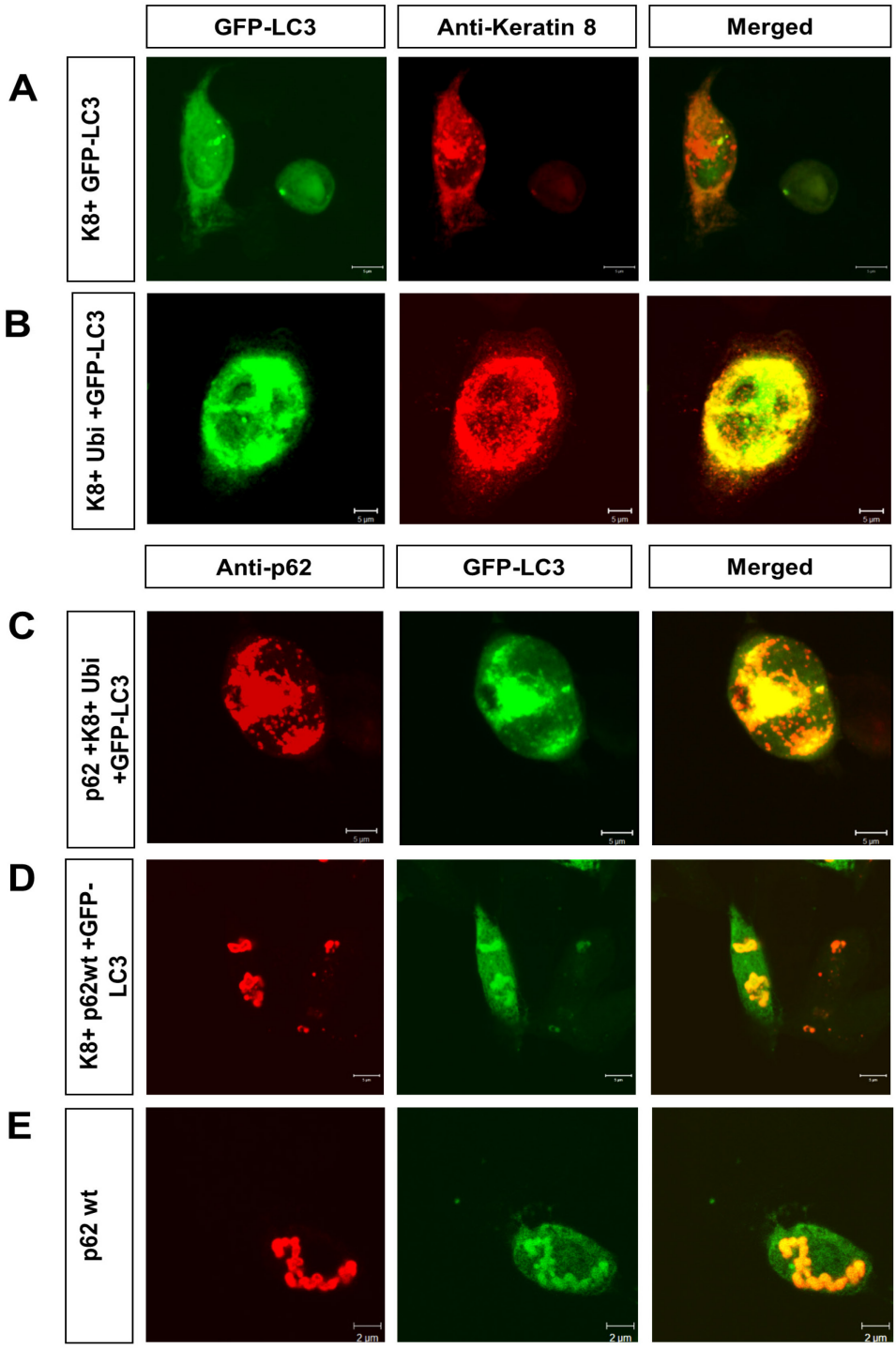


Figure 18: **Association of LC3 with ubiquitin and p62 but not with K8** (*A*) CHO-K1 cells co-transfected with *Krt8* and *GFP-LC3*, stained with anti-K8 (red) show no co-localization. Scale – 5µm (*B*) CHO-K1 cells co-transfected with *Krt8*, *Ubiquitin* and *GFP-LC3*, stained with anti-K8 (red) show profound co-localization indicating ubiquitinated K8 might interact with LC3. Scale – 5µm (*C*) CHO-K1 cells co-transfected with *p62wt, Krt8*, *Ubiquitin (in vitro MDBs)* and *GFP-LC3*, stained with anti-p62 (red) show co-localization. Scale – 5µm (*D*) CHO-K1 cells co-transfected with *Krt8*, *p62wt* and *GFP-LC3*, stained with anti-p62 (red) show co-localization. Scale – 5µm (*E*) CHO-K1 cells co-transfected with *p62wt* and *GFP-LC3* stained with anti-p62 (red) display profound co-localization with GFP-LC3. Scale – 2 µm.

3.9.2. Ubiquitinated misfolded K8/18 co-localize with LC3

To address the question if ubiquitinated misfolded K8 is able to interact with LC3, ubiquitin along with K8 and LC3 was co-transfected and analyzed for co-localization. 'ubiquitinated' K8/K18 was able to interact with LC3 (Figure 18B). To investigate the role of p62 in interaction with LC3, p62 along with K8 and LC3 was co-transfected and analyzed for co-localization. A co-localization was observed in case of p62 and misfolded K8/K18 with LC3 (Figure 18C).

3.9.3. p62 interacts with LC3/ATG 8

To look into the proposed involvement of p62-LC3 interaction in the chronic liver disorders, molecular basis of p62-LC3 interaction was focused. In our experiments of p62 with LC3, p62 aggregates showed profound co-localization with LC3. p62 also showed profound co-localization with LC3 in the presence of K8 and/or ubiquitin (Figure 18C, D). This highlights the significance of p62.

3.9.4. Molecular basis of p62-LC3 interaction

To look into the role of phosphorylation sites and other domains involved in this interaction, deletion constructs and phospho-mutants (p62S24A and p62S152A) of p62 were co-transfected with GFP-LC3 and were analyzed for profound co-localization. p62S24A showed only a limited co-localization with GFP-LC3 whereas p62S152A did not show any change in co-localization pattern as compared to p62wt (Figure 18D, 20A, B). p62ΔSH$_2$ and p62ΔUBA profoundly co-localized with GFP-LC3 whereas p62ΔZIP showed only a limited co-localization (Figure 20C, D, E). This data suggests that phosphorylation site S24 may participate to define the interaction pattern not only with kinases but also with other interaction partners. In addition it can be reasoned that the PKCζ interacting region is involved in regulating the interaction with LC3 along with the LIR domain. This can be speculated because it was previously reported that deletion of LIR and PB1 domain disrupted the interaction of p62 with LC3. Therefore when the PKCζ interacting region is deleted with the help of the LIR domain p62 is still able to bind to LC3. Thus interaction is limited but not completely prevented.

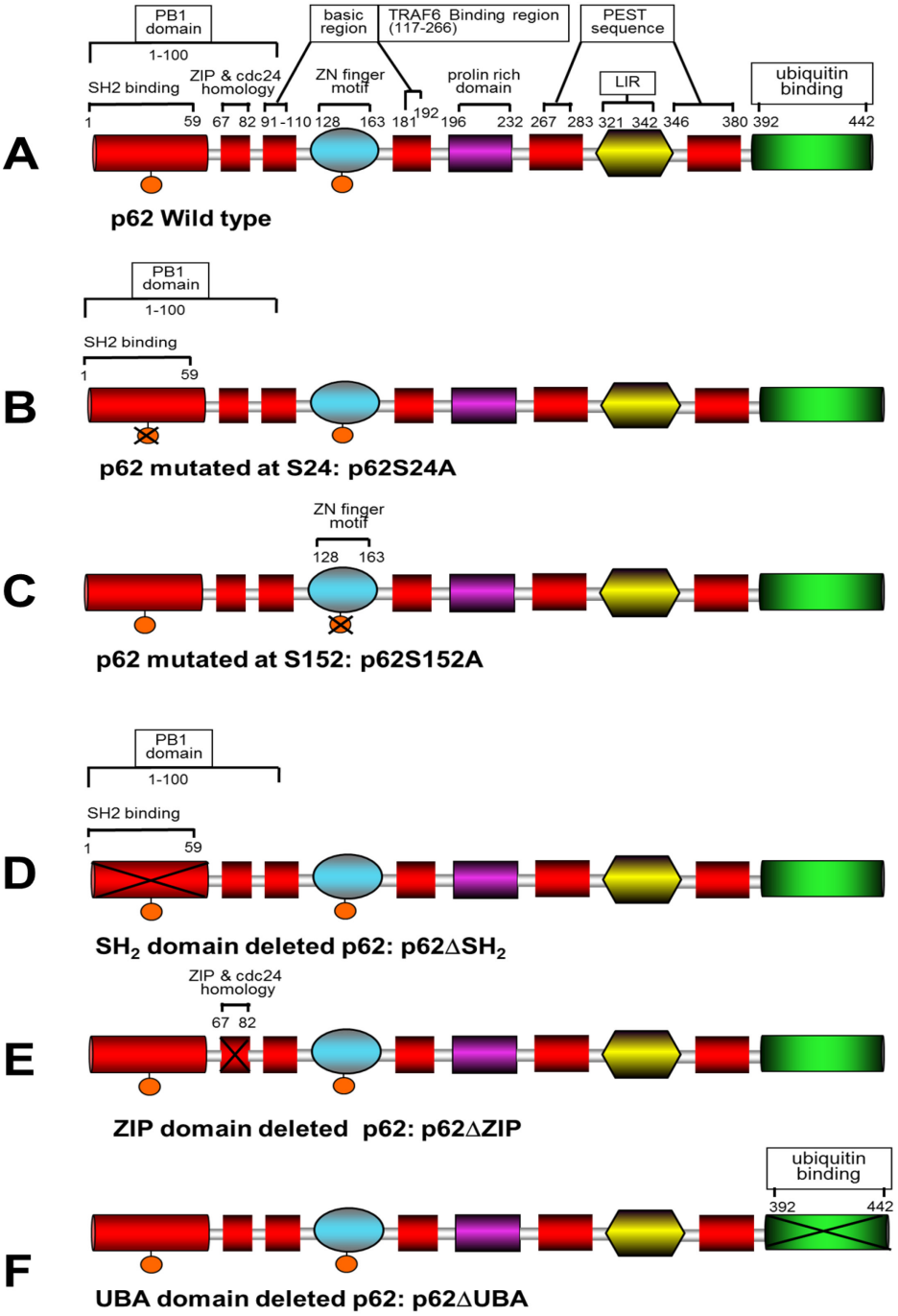


Figure 19: schematic representation of the multidomain adaptor p62wt. (*A*) Domain organization of p62wt (*B*) Scheme: p62 mutated at S24 (*C*) Scheme: p62 mutated at S152 (*D*) Scheme: SH_2 domain deleted p62 (*E*) Scheme: ZIP domain deleted p62 (*F*) Scheme: UBA domain deleted p62

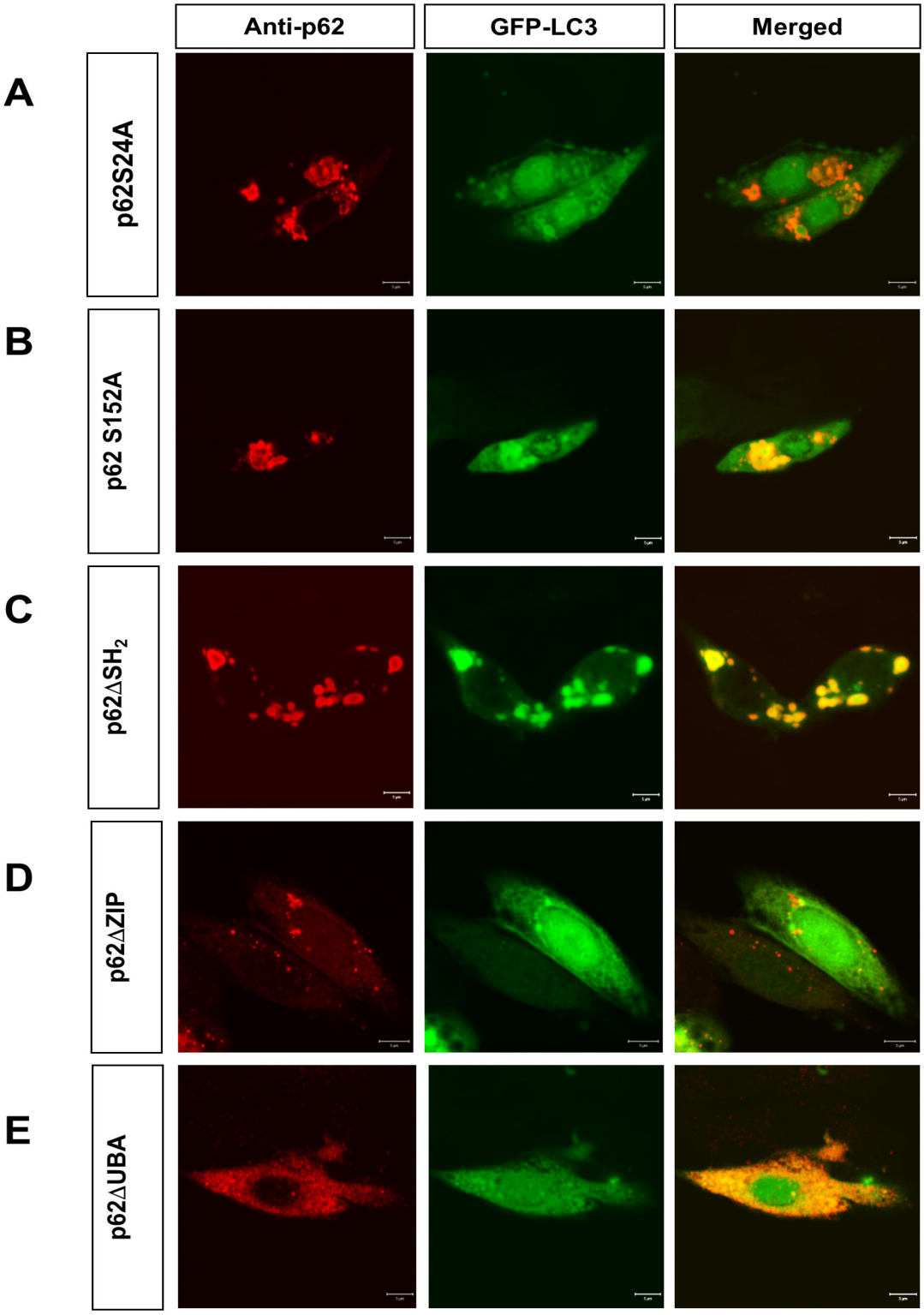


Figure 20: ***In vitro*** **analysis of phosphorylation sites and domains of p62 involved in interaction with LC3**: (*A*) CHO-K1 cells co-transfected with *p62S24A* and *GFP-LC3* stained with anti-p62 (red) showed a limited /in part co-localization. (*B*) CHO-K1 cells co-transfected with *p62S152A* and *GFP-LC3*, stained with anti-p62 (red) showed profound co-localization which indicates possibly phosphorylation S152 may not govern this interaction. (*C*) CHO-K1 cells co-transfected with *p62ΔSH*$_2$ and *GFP-LC3*, stained with anti-p62 (red) shows profound co-localization indicating no involvement of

SH_2 domain of p62 in regulating the interaction. (*D*) CHO-K1 cells co-transfected with *p62ΔZIP* and *GFP-LC3*, stained with anti-p62 (red) shows limited co-localization indicating possible involvement of ZIP domain of p62 due to partial disruption in the interaction. (*E*) CHO-K1 cells co-transfected with *p62ΔUBA* and *GFP-LC3* stained with anti-p62 (red) show profound co-localization. Scale – 5 µm.

3.10. Misfolded keratins themselves do not trigger apoptosis

To understand if not autophagy whether misfolded keratins trigger apoptosis, the presence of apoptosis therefore was determined for caspase 3 and propidium iodide (PI). GFP-K8 and GFP-K18 were co-transfected in CHO-K1 cells and post-transfection 16-18 hours analyzed for PI by flow cytometry. The results were then compared with a non-transfected control and only vector pEGFP-C1 transfected cells. The results demonstrated the absence of PI uptake denoted lack of apoptosis in un-transfected cells whereas a Sub G1 peak indicating lower levels of apoptosis was observed in case empty pEGFP-C1 transfected CHO-K1 cells (Figure 22A, B and C). This indicates transfection can also induce cellular damage that triggers lower levels of apoptosis. Hk8dsred was then transfected and analyzed after post transfection 16 to 18 hours for the presence of cleaved caspase 3 however when compared to even a non-transfected control, no significant apoptosis was evident (Figure 22A-D). Presence of apoptosis was also measured using TUNEL assay and Annexin V in CFP-K8 and CFP-K18 transfected CHO-K1 cells however there was no evidence of apoptosis compared to controls (data not shown). This data suggests that the misfolded keratins themselves did not activate apoptosis.

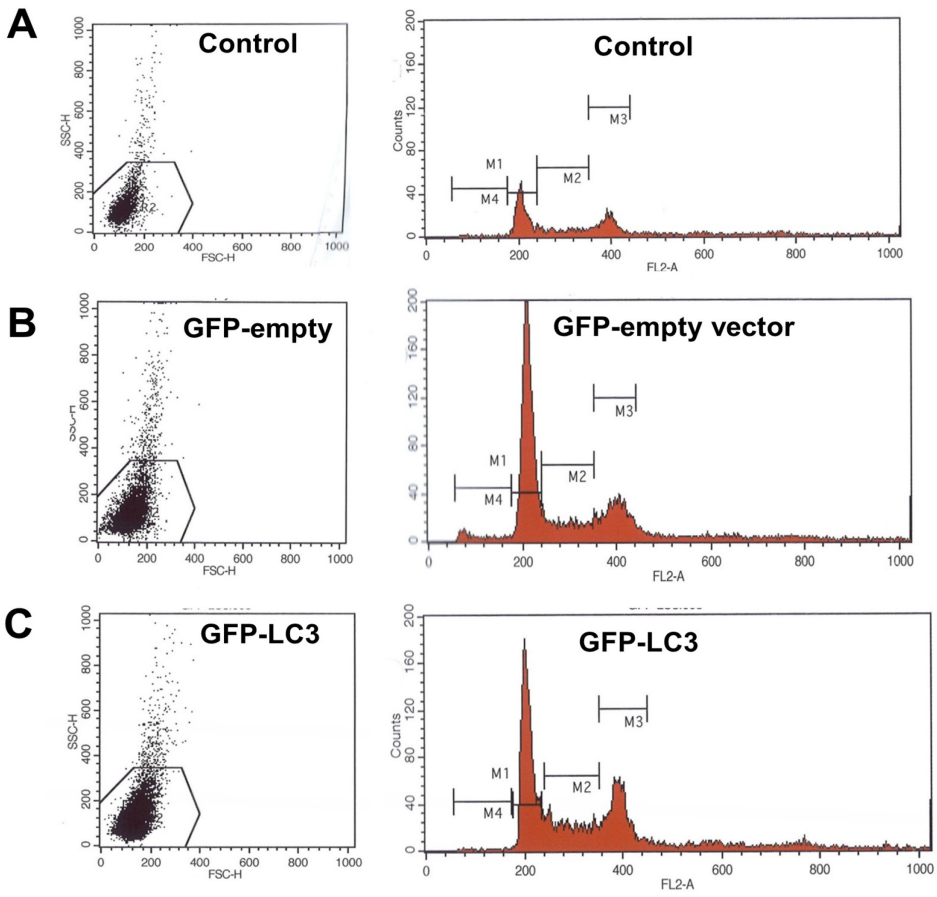


Figure 21: **GFP-LC3 overexpression induces cell death but not by apoptosis**: (*A*) FACS analysis of CHO-K1 cells transfected with only *pCDNA4mychis* vector and labelled with PI showed no induction of apoptosis. (*B*) CHO-K1 cells transfected with *pEGFP-N1* vector showed trivial elevation of apoptosis (*C*) CHO-K1 cells transfected with *GFP-LC3* showed no elevation of apoptosis when compared to controls. For numerical analysis three independent experiments were performed.

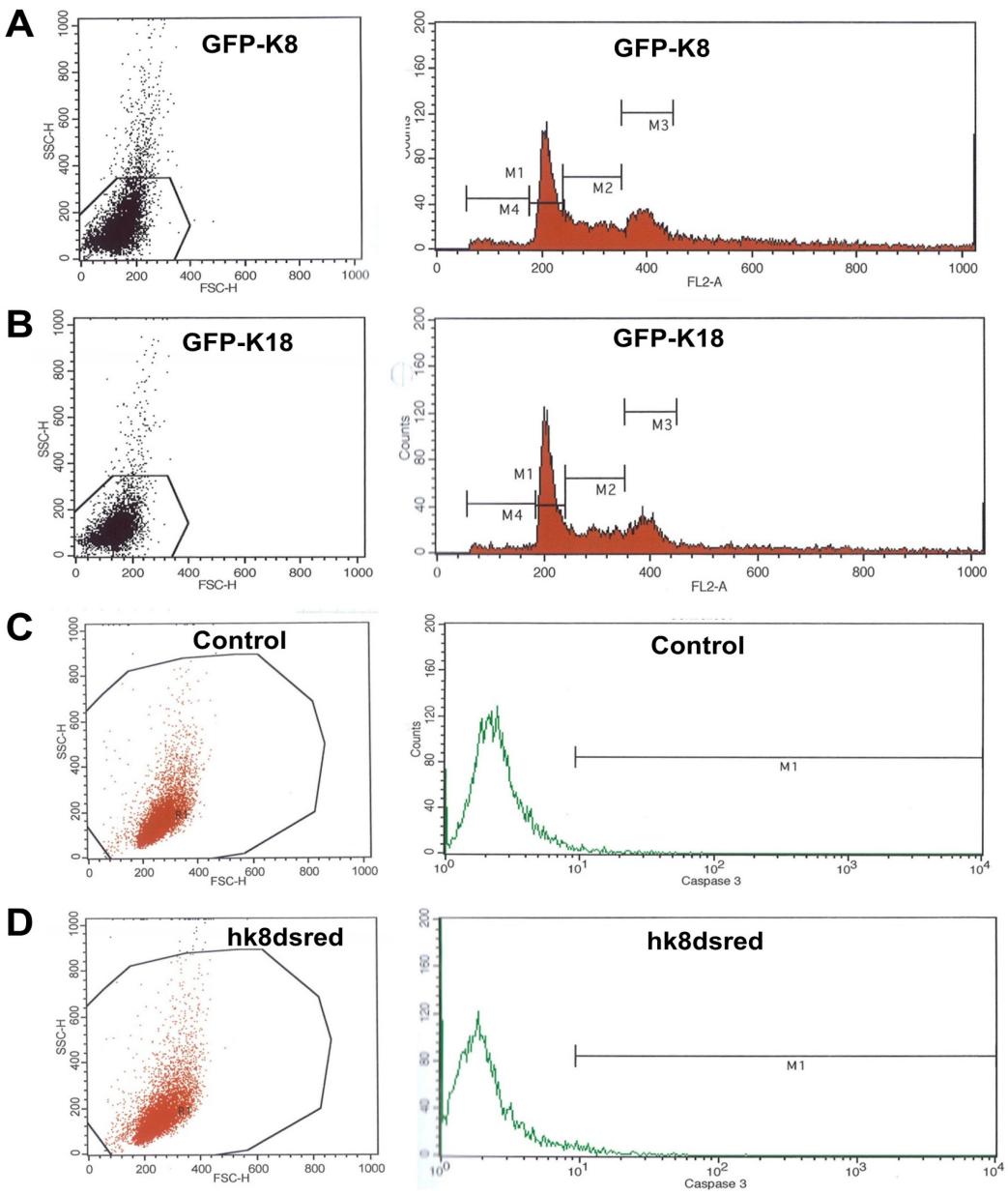


Figure 22: Keratin 8 and 18 alone do not induce apoptosis: (*A*) FACS analysis of CHO-K1 cells transfected with *GFP-Krt8* and labelled with PI showed no induction of apoptosis. (*B*) CHO-K1 cells transfected with *GFP-Krt18* and labelled with PI shows no elevation of apoptosis. (*C*) CHO-K1cells transfected with pdsred2N1 vector and labelled with caspase3 showed no elevation of caspase 3. For numerical analysis three independent experiments were performed. (*D*) CHO-K1 cells transfected with hk8dsred2N1 and labelled with caspase3 show no induction of caspase 3.

3.11. Live cell imaging and dynamics of hk8 aggregates, p62 and LC3 Dynamics of hk8dsred

Live cell imaging of hk8dsred2N1 facilitated the understanding of the dynamics of keratin 8 in misfolded state, as a function of time. As the cells survived in the initial 18-20 hours' time period, it can be hypothesized that keratin aggregates may not be toxic

initially. These aggregates might acquire toxicity with time and increased deposition at the same location in cytosol. It was a clear observation that these aggregates were not static; shuttling of the aggregates from one end to the other within cytosolic compartments was another indication for continuous transportation of the aggregates. This video file termed as hk8dsred is available on
http://www.medunigraz.at/pathologie/images/content/file/p62/new/

Video 3B: hk8dsred: Real time imaging of transiently transfected CHO-K1 cells with hk8dsRed2N1 in red channel; Accumulation of K8-positive inclusions can be observed over the period of 24-48 hours.

3.12. Independent dynamics of GFP-LC3 and GFP-p62

Live cell imaging of over expressed GFP-LC3 in CHO-K1 cells displayed earlier cell death (within 12 hours post transfection) by autophagy. Overexpression of GFP-LC3 in CHO-K1 cells did not activate apoptosis (Figure 21C). As proposed, live cell imaging with only GFP-p62 did not show any sign of apoptotic cell death in 6-8 hours of post-transfection. p62 molecules displayed strict cytosolic distribution pattern whereas GFP-LC3 showed cytosolic and nuclear translocation. These video files termed GFP-LC3, GFP-p62 are available on
http://www.medunigraz.at/pathologie/images/content/file/p62/new/

Video3A/3Aii: GFP-LC3: Real time imaging of transiently transfected CHO-K1 cells with GFP-LC3 in green channel; Accumulation of GFP-LC3 can be observed over the period of 24-48 hours.

Video 3E: GFP-p62: Real time imaging of transiently transfected CHO-K1 cells with GFP-p62 in green channel; Accumulation of GFP-p62 can be observed over the period of 24-48 hours. http://www.medunigraz.at/pathologie/images/content/file/p62/new/

3.13. Influence of GFP-LC3 and p62 on hk8dsred aggregates

To look into the turnover of the aggregates GFP-LC3 and p62 were co-transfected along with hk8dsred. It provided some insights into transportation and aggregation dynamics of the proteins involved. K8 and p62 were confined to the cytosol whereas GFP-LC3 translocated in cytosol as well as in the nucleus. These preliminary experiments provided weaker evidence that p62 may influence the stability of the aggregates when compared to a situation where p62 is not co-transfected along with GFP-LC3 and hk8dsred.

http://www.medunigraz.at/pathologie/images/content/file/p62/new/

Video 3C: GFP-LC3+hk8dsred

Real time imaging of transiently transfected CHO-K1 cells with GFP-LC3 (green channel), p62wt along with hk8dsRed2N1 in red channel; Accumulation of K8-positive inclusions can be observed over the period of 24 hours. The video is displayed as 2 frames per second. http://www.medunigraz.at/pathologie/images/content/file/p62/new/

Video 3D: GFP-LC3+ p62wt+ hk8dsred

Real time imaging of transiently transfected CHO-K1 cells with GFP-LC3 (green channel), p62wt along with hk8dsRed2N1 in red channel; Accumulation and partial elimination of K8-positive inclusions can be observed over the period of 24 hours. The video is displayed as 2 frames per second.
http://www.medunigraz.at/pathologie/images/content/file/p62/new/

Discussion

Protein degradation by basal constitutive autophagy is one of the key cellular processes to avoid accumulation of polyubiquitinated protein aggregates and to maintain cellular homeostasis. Imbalance in protein homeostasis and dysregulation of autophagy is linked to development of chronic degenerative pathologies. The polyubiquitin-binding protein p62/SQSTM1 is found in cellular inclusion bodies together with polyubiquitinated and cytosolic keratin aggregates that accumulate in various chronic, toxic, and degenerative diseases. Here data demonstrated a direct interaction between p62 and the autophagic effector proteins LC3 (Fig. 18D). The interaction between p62 and LC3 is mediated by a N-terminal PB1 domain and deletion of the SH_2 domain enhances the interaction with LC3 and deletion of the ZIP domains weakens the interaction. The data also demonstrated that phosphorylation sites in PB1 domain may additionally contribute to regulate the interaction with LC3. Phosphorylation site S24 might be involved to regulate the interaction of p62 with LC3 as p62S24A fails to show a prominent co-localization indicating weakening of interaction with LC3 whereas S152 showed no difference with interaction with LC3 compared to p62wt (Fig 20A, B).

The double tag strategy was used to demonstrate that the interaction between p62 and LC3 that may affect the stability of the p62-positive bodies containing polyubiquitinated K8, by autophagy. The data also demonstrates that misfolded keratins cannot activate apoptosis by themselves whereas ubiquitin though interacts with LC3 may not be adequate for degradation of K8 aggregates by autophagy. Over-expression

of GFP-LC3 leads to initiation of autophagic cascades and therefore leads to digestion of plasma membrane and ultimately cellular death. Live -cell imaging of K8 in CHO-k1 cells was performed to improve our understanding of the dynamic processes during misfolding of K8. Live cell imaging revealed that keratin aggregates are not static in nature. The cell transports these aggregates within intracellular compartments; however, the aggregates are confined to cytosol whereas GFP-LC3 shows not only cytosolic but also nuclear distribution. Misfolded K8 could not interact with LC3 and therefore ubiquitin and p62 may act as mediators to facilitate the degradation of misfolded K8 aggregates.

CHAPTER 3 part III
Influence of phosphorylation on interaction of p62 and misfolded K8

Introduction

Keratin 8 and 18 are the members of large family of intermediate filament (IF) cytoskeletal proteins, which are expressed in a tissue-specific manner. They are assembled as heteropolymeric cytoplasmic filaments. Other proteins which include neurofilaments, α-internexin, desmin, vimentin, glial filaments, and the nuclear lamins also belong to the IF family. Several human diseases are associated with severe alterations of IFs. One of the most common pathological features of many IF-related diseases is the accumulation of intracytoplasmic inclusions bodies that consists of modified IF proteins, for example in neurodegenerative diseases such as Parkinson's disease, Lewy bodies and amyotrophic lateral sclerosis. Although the pathogenetic mechanisms involved are as not yet clear, posttranslational modifications of IF proteins and p62, such as phosphorylation, limited proteolysis, and cross-linking, may play a major role in MDB and IHB formation. For example, the presence of hyperphosphorylated K8/18 was reported suggesting that K8/18 hyperphosphorylation may play a contributing role in MDB formation (Stumptner *et al.*, 2000). Moreover it was speculated that, the site-specific phosphorylation of K8/18 cytoskeleton and p62 in different stages of MDB induction provides clearly indirect evidence for the involvement of various protein kinases (Stumptner *et al.*, 2000). Therfore this part of the thesis is focused at unraveling the role of various kinases and phosphorylation involved in the MDB and IHB formation. To understand the role of the specific phsophorylation sites identified by mass spectrometry, the phosphorylation sites S24 and S152 were mutated and analyzed for colocalization with various identified and unidentified kinases and also with K8 by overexpressing these constructs in 'liver pathology mimicking cell culture models'.

Results

3.14. Kinases involved in MDB and IHB pathogenesis

3.14.1. Presence of Jun Kinase 1 (JNK1a/ MAPK8) in the aggregates

c-Jun N-terminal kinases (JNKs), were originally designated as the kinases that interact and phosphorylate c-Jun. They belong to the mitogen-activated protein kinase family and are induced upon various stimuli such as heat, and osmotic shock, oxidative stress, cytokines. They also play a crucial role in the cellular apoptosis pathway. Interaction of JNK might occur through a dual phosphorylation of threonine (Thr) and tyrosine (Tyr) residues (Hui *et al.*, 2008). To investigate the role of JNK in the progression of steatohepatitis, presence of JNK was determined through immunohistochemistry on the cryosections from ASH and HCC. As depicted in figure 23A JNK is overexpressed in the nuclei of tumor cells as well as of inflammatory cells like granulocytes, monocytes, macrophages and lymphocytes occurring within the HCC infiltration zone. Even mitotic figures within hepatocytes were highlighted by JNK immunostaining (Figure 23B). IHBs displayed a strong positivity for JNK in addition to the above described inflammatory cells which revealed a heterogenous staining pattern (Figure 23C, D) Moreover, cytoplasmic positivity of JNK1 could be demonstrated in HCC and MDBs (Figure 23E, F).

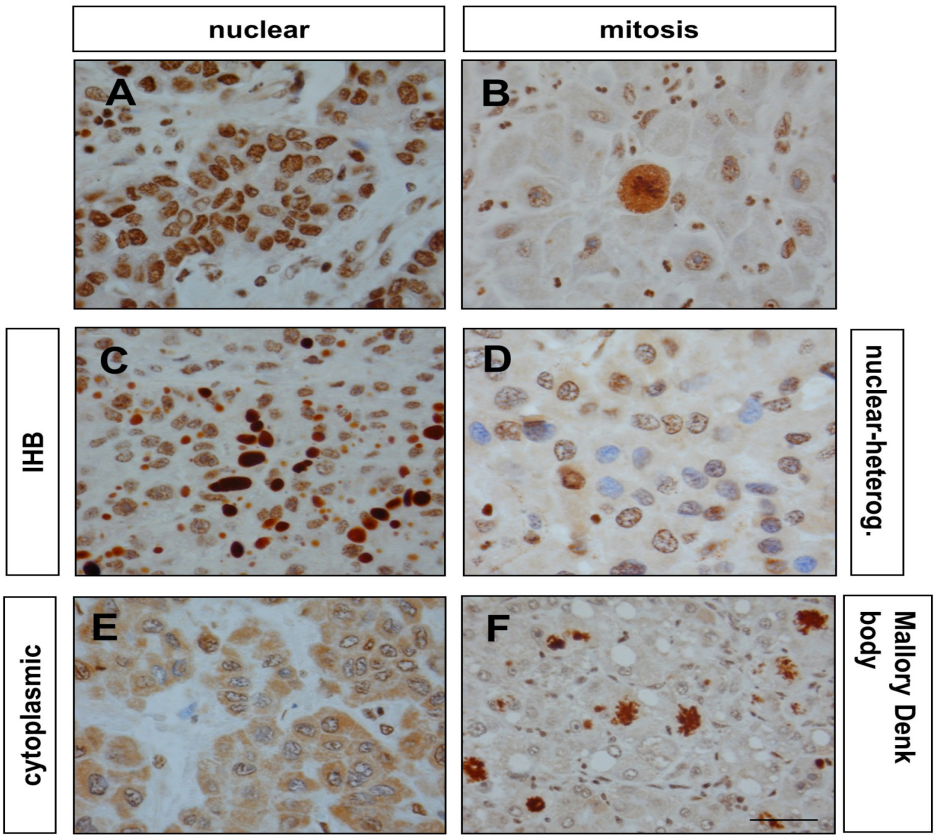


Figure 23: **Presence of JNK1a in various inclusion bodies**: (*A*) Immunohistochemistry showed overexpression of JNK1 in nuclear and inflammatory cells. (*B*) Mitotic figures of hepatocyte showed presence of JNK1 in nucleus. (*C-F*) Presence of JNK1 in cytoplasmic IHBs and MDBs scale – 500 µm

3.14.2. JNK1a associates with MDBs and IHBs 'in vitro'

To translate these findings '*in vitro*', p62, K8 along with GFP- JNK were co-transfected in CHO-K1 cells to generate MDB and IHB like inclusion bodies and analyzed for co-localization with JNK (Figure 24A). 12-14 hours post transfection JNK was activated by 45J UV stress (and after 20 minutes time interval the cells were fixed for further analysis). A profound co-localization was observed which indicated the possible interaction of JNK with p62 or K8 (Figure 24A-C). Granular pattern of JNK was evident from MDB/IHB like aggregates. The presence of JNK in IHBs and MDBs '*in vivo'* can therefore be correlated to '*in vitro*' data.

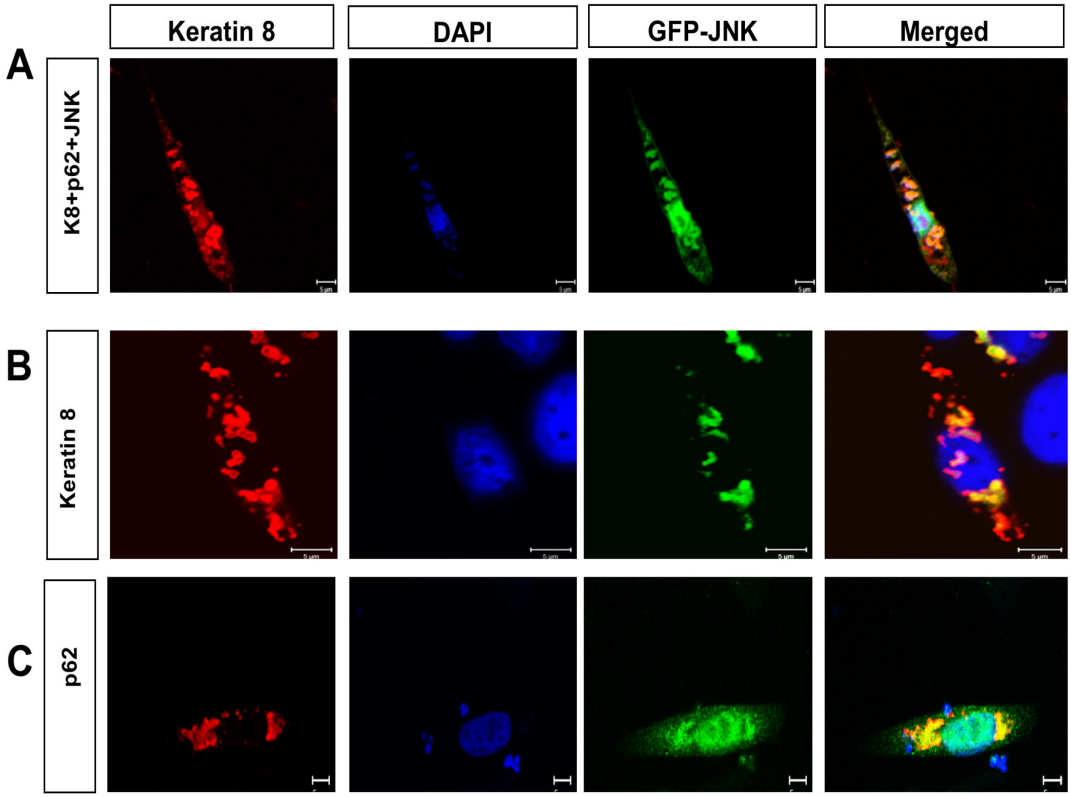


Figure 24: **JNK1a interacts with proteins involved in MDB formation**

Interaction of JNK1a with p62 and K8 in inclusion bodies: (*A*) Immunocytochemistry showed of JNK1a interacts with *in vitro* 'MDBs' when CHO-K1 cells co-transfected with equimolar ratios of human *JNK1, p62* and *Krt8*. (*B*) CHO-K1 cells were co-transfected with equimolar ratios of human *JNK1* and *Krt8*. JNK1a co-localizes with cytoplasmic K8 aggregates. (*C*) CHO-K1 cells co-transfected with equimolar ratios of human *JNK1a* and *p62wt*. P62 aggregates stained with anti-p62 (in green) in the cytoplasm co-localize with JNK1a (red). Scale – 5 µm.

3.14.3. JNK1a interacts with K8 and p62

To investigate if JNK interacts with K8, JNK and K8 were co-transfected in CHO-K1 cells in cytoplasm. In line with previous reports (He *et al.*, 2002), JNK showed a profound co-localization with K8. This underlines that keratin 8 is the substrate for JNK (Figure 24B).

To define another specific interaction partner, p62 and JNK were co-transfected and analyzed for co-localization (Figure 24C). From the co-localization analysis, it appears that JNK interacts with p62, and p62 might be another substrate of JNK (Figure 24C).

3.14.4. Predicted phosphorylation sites of p62

In order to predict the phosphorylation sites of p62 involved in interaction with JNK and aPKC, the amino acid sequence was subjected to phosphorylation site prediction program. Netphos 2.0 found several serine and threonine phosphorylation sites with

high prediction score (0.5 to 0.9) in the functional domains of p62 shown in table 5 and 6.

Table 5: Predicted sites for serine phosphorylation by JNK and aPKC.

Position	Score	p62 domain	Sequence
24	0.995	SH_2/PB1	IRRFSFCCS
28	0.721	SH_2/PB1	SFCCSPEPE
78	0.962	ZIP/PB1	LVAFSSDEE
79	0.928	ZIP/PB1	VAFSSDEEL
152	0.942	ZZ	YDLCSVCEG
180	0.765	TRAF6	SEGFSHSRW
207	0.939	TRAF6 & Proline rich domain	PGNWSPRPP
224	0.713	TRAF6 & Proline rich domain	PTAESASGP
226	0.950	TRAF6 & Proline rich domain	AESASGPSE
229	0.897	TRAF6 & Proline rich domain	ASGPSEDPS
233	0.706	TRAF6	SEDPSVNFL
243	0.669	TRAF6	NVGESVAAA
272	0.997	PEST	LTPVSPESS
275	0.968	PEST	VSPESSSTE
276	0.982	PEST	SPESSSTEE
277	0.997	PEST	PESSSTEEK
282	0.948	PEST	TEEKSSSQP
283	0.928	PEST	EEKSSSQPS
284	0.945	PEST	EKSSSQPSS
287	0.988	PEST	SSQPSSCCS
288	0.892	PEST	SQPSSCCSD
318	0.956	PEST	IALESEGRP
332	0.991	PEST/LIR	SDNCSGGDD
342	0.954	PEST/LIR	WTHLSSKEV
343	0.547	PEST	THLSSKEVD
349	0.988	PEST	EVDPSTGEL
361	0.575	PEST	QMPESEGPS
365	0.983	PEST	SEGPSSLDP
366	0.698	PEST	EGPSSLDPS
370	0.991	PEST	SLDPSQEGP

Table 6: Threonine Prediction.

269	0.986	SH_2/PB1	RSRLTPVSP

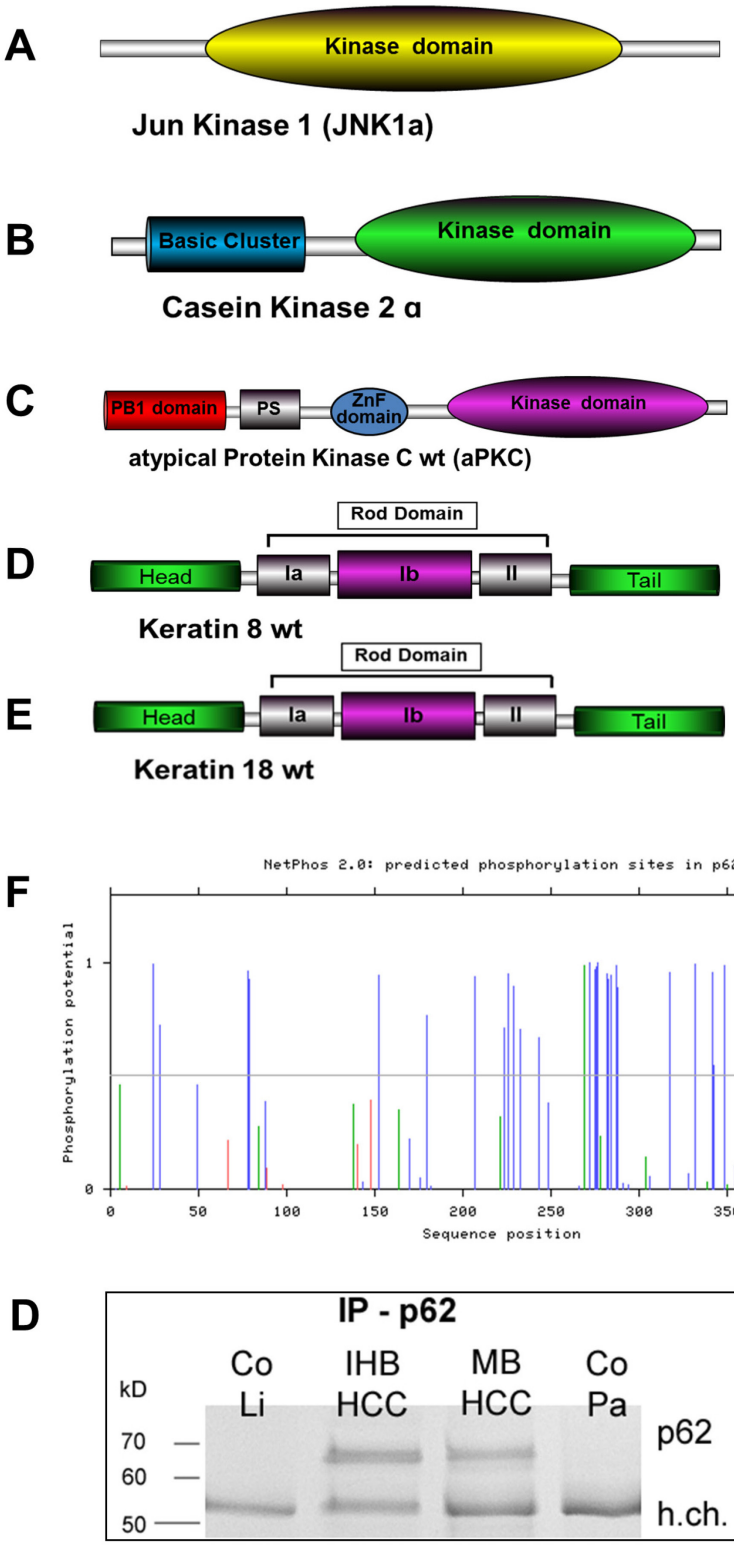


Figure 25: Isolation of p62 from HCC livers and schematic representation of domains of kinases and keratins (*A*) Domain organization of N terminal JNK1a (*B*) Scheme: PKCζ showing N terminal PB1 domain and C terminal catalytic domain (*C*) Scheme: CK2α showing N terminal basic cluster and C terminal catalytic domain (*D*), (*E*) Scheme: K8/18 showing similar domain organization (*F*) Distribution of active Serine and Threonine phosphorylation sites across the p62 amino acid sequence predicted by Netphos (*G*) p62 was pulled down from isolated IHBs and MDBs from

human HCC liver. Lane 1 showed p62 (~65KD) isolated from IHBs. Lane 2 showed heavy chains (~50kd) pulled down along with p62 (~65KD) from MDBs and IHBs.

3.14.5. Determination of phosphorylation sites by Mass-spectrometry

p62 from MDBs as well as IHBs was isolated from human HCC tissue sample (Figure 25D) and was subjected to mass spectrometric analysis to identify phosphorylation sites of p62. The phosphorylation sites identified by mass-spectrometry are displayed in table 7.

Table 7: Phosphorylation sites identified by mass spectrometry

Peptide No	Phosphorylated amino acid	P62 domain	Sequence	Sample
1	S24	SH2, PB1	SFCCSPEPEAEAE	IHB-HCC
2	S152	ZZ-finger TRAF6	CSVCPDYDLCSVCEGK	MB-HCC
3	T269	PEST	SRLTPVSPESSSTEEK	MB-, IHB-HCC
4	S272	PEST	LTPVSPESSSTEEK	MB-, IHB-HCC
5	T269, S272	PEST	SRLTPVSPESSSTEEK	IHB-HCC
6	S361, S365/366	PEST	QMPESEGPSSLDPSQE GPTGL	IHB-HCC
7	S365	PEST	QMPESEGPSSLD	IHB-HCC
8	S366	PEST	QMPESEGPSSLDPSQE GPTGL	MB-HCC
9	S370	PEST	SLQMPESEGPSSLDPSQ EGPTGL	IHB-HCC

(Acknowledgement: - Karl Metchler, Institute of Molecular Pathology, Vienna)

3.14.6. Site directed mutation at key phosphorylation sites S24 and S152 of p62

In order to investigate the role of phosphorylation sites in determination of cellular distribution and interaction with JNK and other known kinases, S24 and S152 were individually replaced by alanine.

3.14.7. Interaction studies with JNK 1a/ MAPK-8: Molecular basis of p62- JNK1a interaction

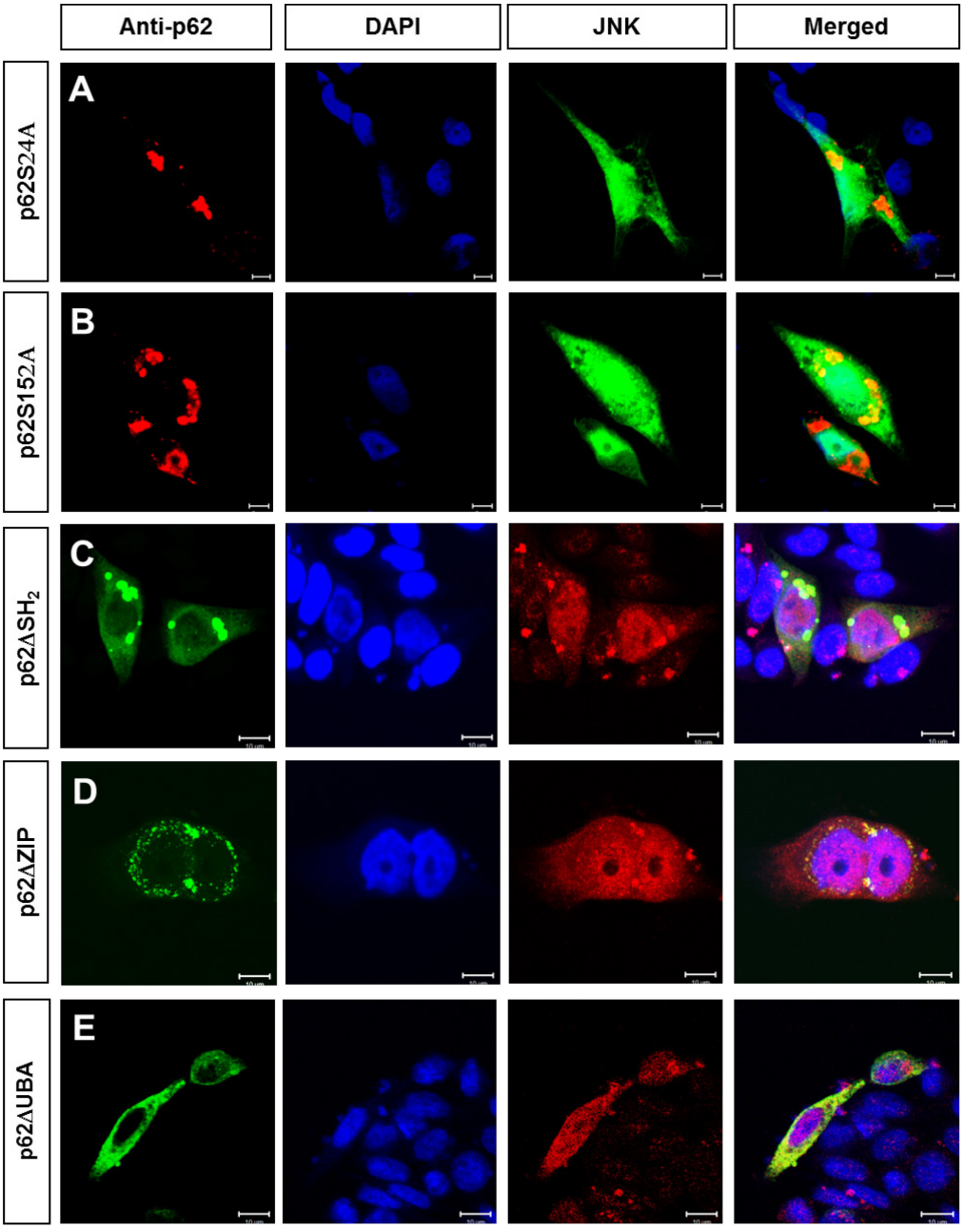


Figure 26: **In vitro analysis of domains of p62 involved in interaction with JNK1a**: (*A*) CHO-K1 cells co-transfected with *p62S24A* and *JNK1a* stained with anti-p62 (red) show co-localization (*B*) CHO-K1 cells co-transfected with *p62S152A* and *JNK1a*, stained with anti-p62 (red) show profound co-localization (*C*) CHO-K1 cells co-transfected with *p62ΔSH*$_2$ and *JNK*, stained with anti-p62 (green) and anti JNK1a (red) shows either no or limited co-localization. (*D*) CHO-K1 cells co-transfected with *p62ΔZIP* and *JNK1a*, stained with anti-p62 (green) and anti JNK1a (red) show co-localization (*E*) CHO-K1 cells co-transfected with *p62ΔUBA*and *JNK1a* stained with anti-p62 (green) and anti JNK1a (red) depicts no co-localization. Scale – 5 µm.

To map the corresponding domains of p62 required for interaction with JNK1, the deletion constructs were co-transfected along with JNK1a and analyzed for co-localization (Figure 26). Figure 19A-F shows domain organization of various p62 wt as well as deletion and phosphorylation constructs. Figure 25A-C shows domain organization of various interacting kinases of p62. In these preliminary experiments with fluorescence microscopy, compared to interaction with p62wt, p62S24A or p62S152A did not inhibit the interaction with JNK (Figure 26A, B). p62ΔSH$_2$ showed limited co-localization with JNK1a suggesting that SH$_2$ domain may be important in regulating the interaction with JNK1a (Figure 26C). Deletion of SH$_2$ domain weakened the interaction. p62ΔZIP showed co-localization with JNK1a indicating that ZIP domain may not be important in regulating the interaction with JNK1a whereas p62ΔUBA completely abolished the interaction with JNK1a proposing importance of UBA domain in facilitating this interaction (Figure 26D, E).

3.14.8. JNK1 overexpression induces cell death.

To investigate the dynamics of JNK1, GFP-JNK was overexpressed in CHO-K1 cells. A moderate rise in apoptosis was observed (Figure 27A-C).

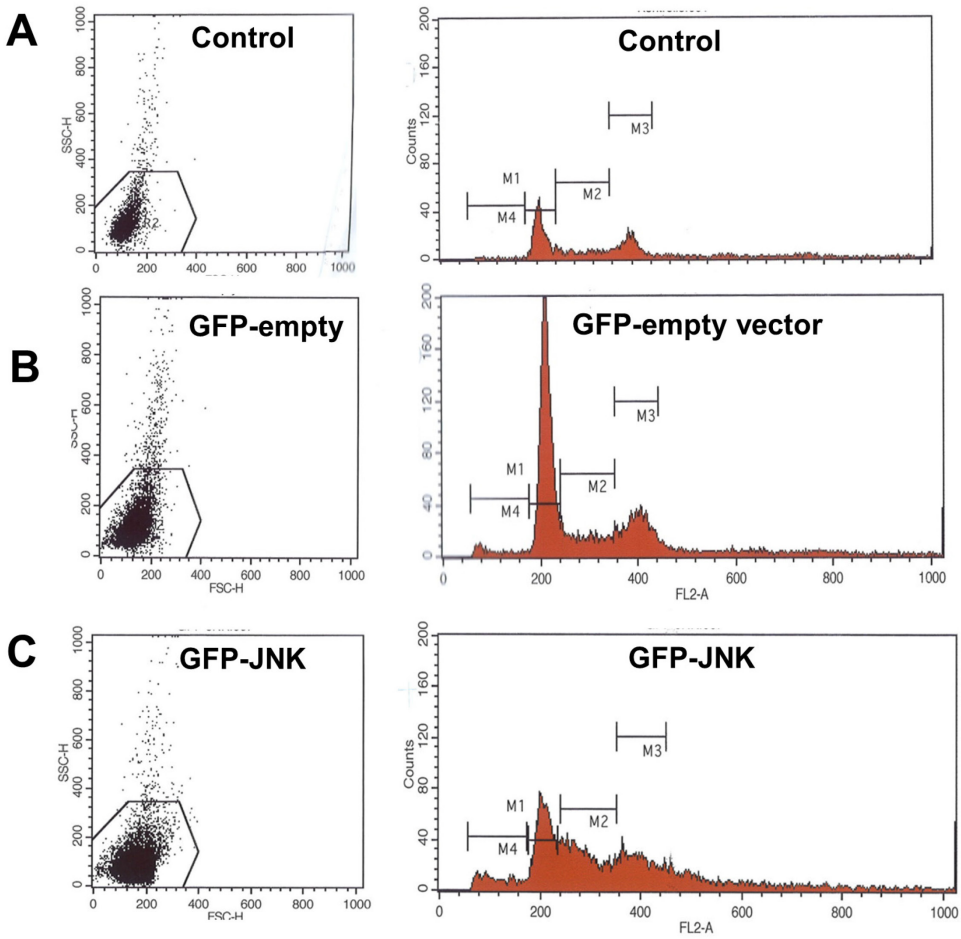


Figure 27: **JNK1a overexpression induces moderate levels of apoptosis**: (*A*) Facs analysis of CHO-K1 cells transfected with only *pCDNA4mychis* vector and labelled with PI shows no induction of apoptosis. (*B*) CHO-K1 cells transfected with *pEGFP-N1* vector shows trivial elevation of apoptosis indicating GFP tag also may exert little toxicity upon overexpression. (*C*) CHO-K1 cells transfected with *GFP- JNK1a* depicts moderate levels of apoptosis when compared to controls. For numerical analysis three independent experiments were performed.

3.15. Interaction studies with PKCζ

3.15.1. p62 interacts with PKCζ

Atypical protein kinase C (PKC) is a family of kinases that are involved in regulating the function of proteins through the phosphorylation of serine and threonine amino acid residues on these proteins. PKCs are often induced by signals such as oxidative stress or increase in the intracellular diacylglycerol or Ca^{2+} concentration (Soh *et al.*, 1999), (Soh *et al.*, 2003). Hence PKCs were reported to play crucial roles in several signal transduction cascades. (Kazi *et al.*, 2007)

As reported previously p62 showed profound co-localization with PKCζ (Lamark *et al.*, 2003) (Figure 28). PKCζ displayed diffused nuclear distribution whereas p62wt exhibited more reticulate distribution often confined to cytosol.

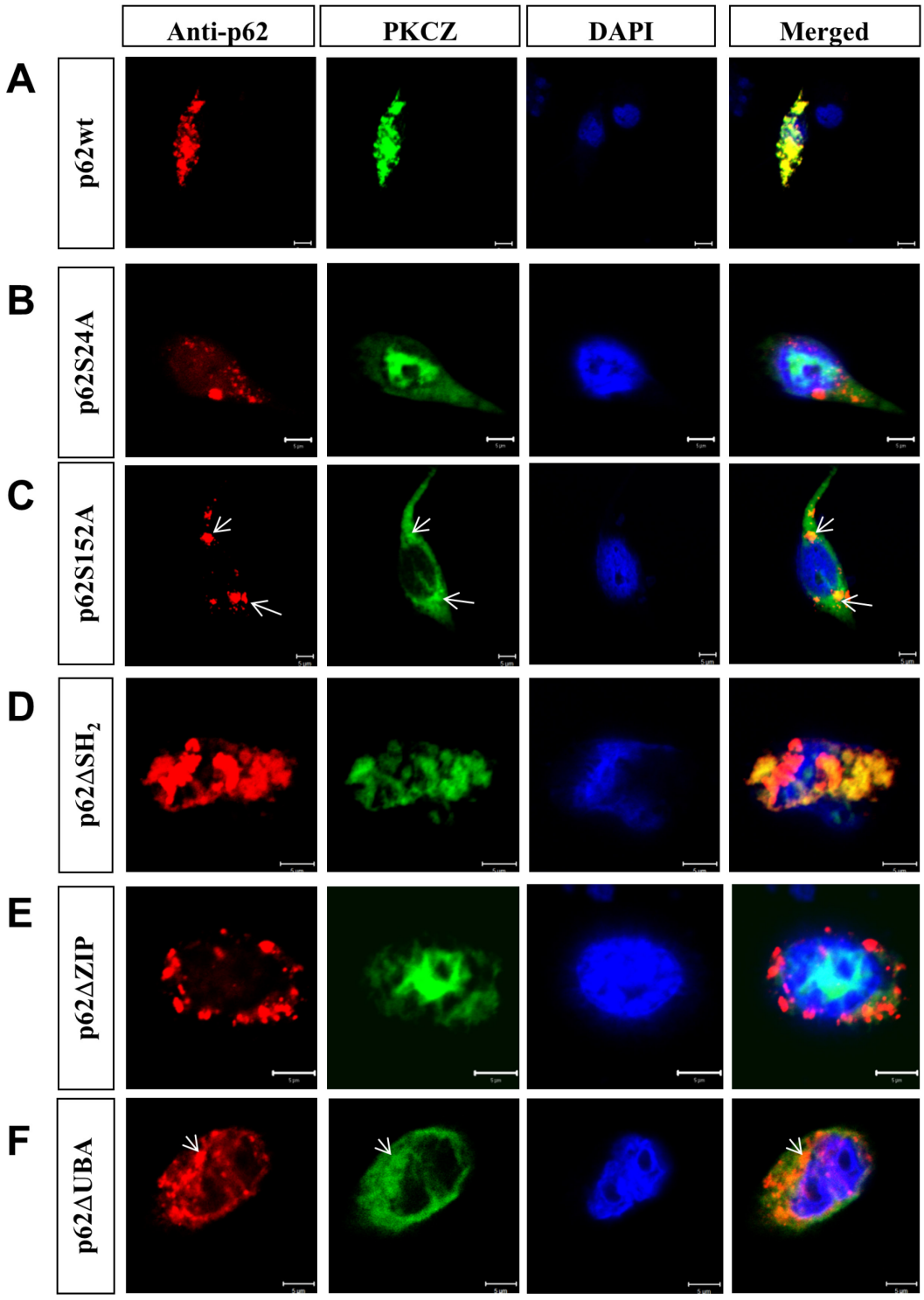


Figure 28: PKCζ interacts with p62: (*A*) CHO-K1 cells co-transfected with equimolar ratios of *p62wt* and *GFP-PKCζ* stained with anti-p62 (red) showed a co-localization. (*B*) CHO-K1 cells co-transfected with *p62S24A* and *GFP-PKCζ* stained with anti-p62 (red) showed a no co-localization. (*C*) CHO-K1 cells co-transfected with *p62S152A* and *GFP-PKCζ*, stained with anti-p62 (red) show limited co-localization (indicated by white arrow). (*D*) CHO-K1 cells co-transfected with *p62ΔSH$_2$* and *GFP-PKCζ*, stained with anti-p62 (red) and anti CK2α (green) showed profound co-localization. (*E*) CHO-K1 cells co-transfected with *p62ΔZIP* and *GFP-PKCζ* stained with anti-p62 (red) showed no co-localization.

(*F*) CHO-K1 cells co-transfected with *p62ΔUBA* and *GFP-PKCζ,* stained with anti-p62 (red) showed only certain structures of p62 co-localized with *GFP-PKCζ* (denoted by white arrow). All scale bars – 5 μm.

3.15.2. Molecular basis of p62-PKCζ interaction

The PB1 domain mediated interaction with p62-PKCζ is well characterized although how the phosphorylation sites and the corresponding domains of p62 regulate the interaction at molecular level is not known. Therefore the deletion constructs and phospho-site mutants (p62S24A, p62S152A) were co-transfected along with PKCζ and analyzed for co-localization. In contrast to p62wt and p62S152, p62S24A showed either limited co-localization or no co-localization. This indicated S24 plays essential role in regulating the interaction with PKCζ (Figure 28A, B and C). p62ΔSH$_2$ and p62ΔUBA co-localized with PKCζ suggesting that SH$_2$ and UBA domain may not be important in regulating the interaction with PKCζ (Figure 28D, E and F).

3.15.3. Interaction studies of p62 with CK2α and molecular basis of p62-CK2α interaction

Previously it was shown that p62 is phosphorylated by CK2α '*in-vitro*' (Yanagawa *et al.*, 1997) however how do phosphorylation sites and the corresponding domains of p62 regulate the interaction at molecular level is not clear till date. Therefore the deletion constructs and phospho-site mutants were co-transfected along with CK2α and analyzed for co-localization. In contrast to p62wt, p62S24A and p62S152 showed either a limited co-localization or no co-localization (Figure 29A, B and C). This indicated S24 and S152 play an indispensible role in regulating the interaction with PKCζ. (Figure 29B, C). p62ΔSH$_2$ and p62ΔZIP co-localized with CK2α suggesting that SH$_2$ and ZIP domain may not be crucial in regulating the interaction with CK2α (Figure 29D, E) whereas in contrast p62ΔUBA did not co-localize with CK2α (Figure 29D, F). There data indicate that presence of UBA domain is mandatory for interaction with CK2α Interestingly, interaction of CK2α with p62 suggests more complex mechanism of signal transduction in the context with MDB and IHB formation.

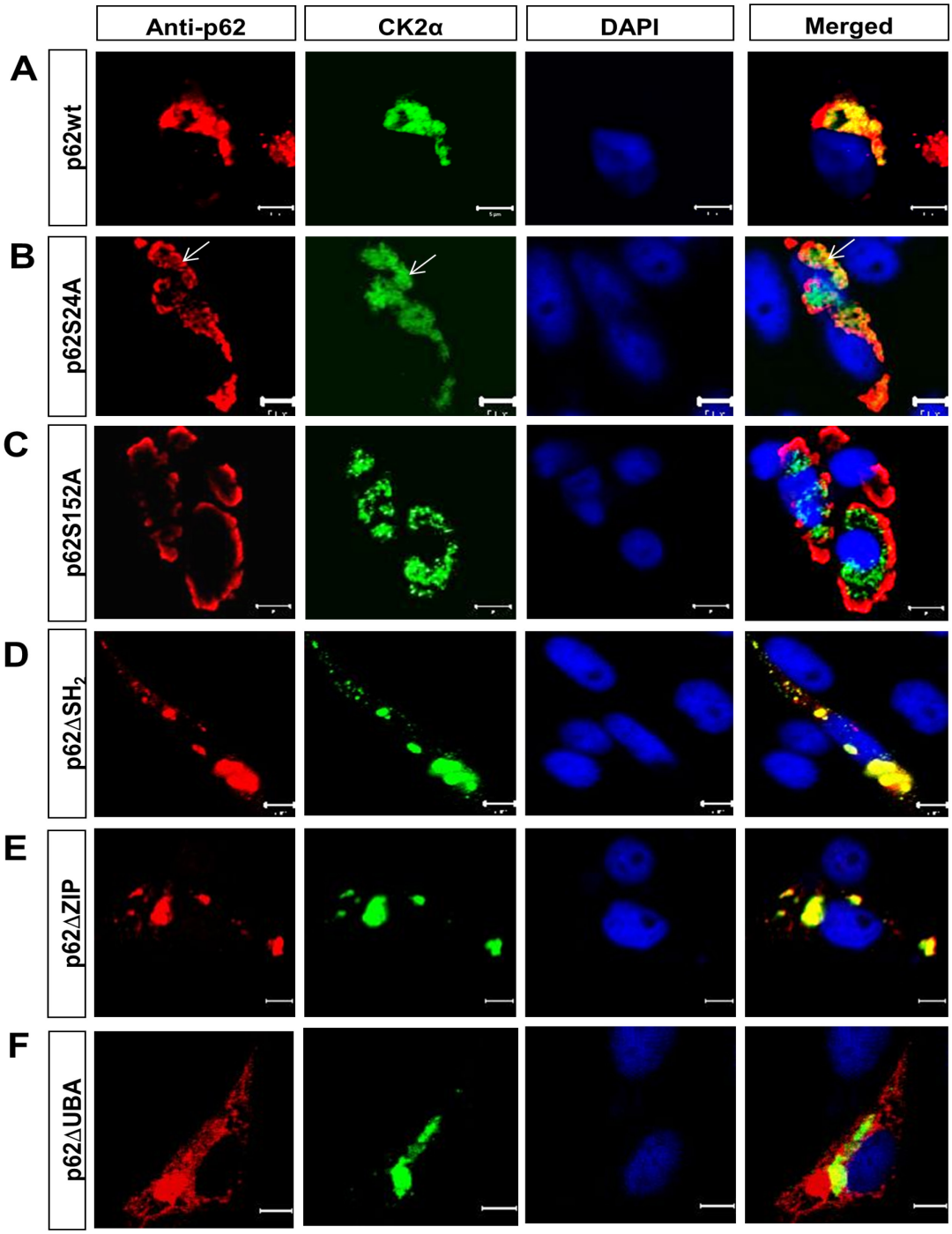


Figure 29: CK2α interacts with p62: (*A*) CHO-K1 cells co-transfected with equimolar ratios of *p62wt* and *CK2a* stained with anti-p62 (red) and anti CK2α (green) showed a profound co-localization which indicates p62 interacts with CK2α. (*B*) CHO-K1 cells co-transfected with *p62S24A* and *CK2a*, stained with anti-p62 (red) and anti CK2α (green) showed a limited co-localization denoted by white arrow. (*C*) CHO-K1 cells co-transfected with *p62S152A* and CK2α stained with anti-p62 (red) and anti CK2α (green) showed no co-localization. (*D*) CHO-K1 cells co-transfected with $p62\Delta SH_2$ and CK2α, stained with anti-p62 (red) and anti CK2α (green) showed profound co-localization. (*E*) CHO-K1 cells co-transfected with *p62ΔZIP* and CK2α, stained with anti-p62 (red) and anti CK2α (green) showed co-localization. (*F*) CHO-K1 cells co-transfected with *p62ΔUBA* and CK2α stained with anti-p62 (red) and anti CK2α (green) depicts very little or lack of co-localization. Scale – 5 µm.

3.15.4. Dynamics of CK2 alpha by live cell imaging

Subcellular dynamics of CK2-α and their transient interaction pattern are the hallmarks of the signal transduction. Live cell imaging of the GFP-CK2α facilitated the understanding of dynamics with the function of time. In addition, live cell imaging allowed real time visualization of GFP-CK2α molecules in CHO-K1 cells. GFP-CK2 showed both cytosolic and nuclear distribution. Therefore it can be concluded that CK2-α molecules might shuttle between the nucleus and the cytosolic compartments. However, post transfection 4-6 hours, overexpression of CK2-α did not induce any early cell death. The video is displayed as 2 frames per seconds

http://www.medunigraz.at/pathologie/images/content/file/p62/new/

Video 4A: GFP-CK2a: Real time imaging of transiently transfected CHO-K1 cells with *GFP-CK2a* (green channel); Accumulation of CK2α molecules can be observed over the period of 24hours

Discussion

The hyperphosphorylation of cytokeratins was demonstrated to be involved in the cellular response to toxic stress (Stumptner *et al.*, 2000) Based on the current studies it does not appear to be a mere phenomenon due to a general deregulation of protein phosphorylation in the course of cellular damage. The data demonstrated association of K8 phosphorylation with a JNK might link to hepatotoxic injury through upregulation of carcinogenic and apoptotic pathways. The data also demonstrated association of p62 phosphorylation with a JNK, PKC and CK2α towards involvement of multiple pathways of cellular signalling. The key phosphorylation site S24 and S152 showed diverse response towards interaction with kinases. Selective interaction of these phosphorylation sites highlights their importance. Interaction of p62 with PKC or interaction of misfolded K8 as well as MDBs with JNK indicates possible of upregulation of inflamatory and apoptotic pathways. Additionally disruption of co-localization with various kinases by p62 deletion mutants highlights the importance of various domains of p62 in mediating the interaction. JNK1, PKCζ and CK2α are the key players in various signalling pathways and carcinogenesis and therefore these interactions are indicators of more complex cellular regulation in steatohepatitis and HCC. Although the immunofluorescence studies show clearly interaction of JNK1, PKCζ and CK2α with p62 and K8, immunoprecipitation studies are required to establish these observations. The mechanism through which stress-induced K8 and p62 hyperphosphorylation protects against certain types of liver injury remains mysterious. The influence of phosphorylation on interaction of p62 with K8 indicates the involvement of its role in MDB and IHB pathogenesis. It would be interesting to speculate the roles of phosphorylation sites in regulating the p62+K8 interaction. It is not well understood whether a phosphorylation site or domains of p62 might also contribute to not only to cellular distribution and regulating this interaction but also conformational alterations. Therefore if the phosphorylation site mutation creates different ultracellular distribution or different ultrastructure and conformation it may provide the key evidence of functional role of phosphorylation site. It would be interesting whether ubiquitination is mandatory for peculiar ultrastructure observed in MDB and IHB pathogenesis and how do the phosphorylation sites regulate the interaction of the interaction of p62 with ubiquitinated keratins.

CHAPTER 3 part IV

Influence of structural domains of p62 and ubiquitination on interaction with misfolded K8 and ultrastructure of MDBs

Introduction:

Steatohepatitis and other liver diseases are characterized by presence of cytoplasmic protein aggregates namely Mallory-Denk bodies (MDBs) and Intracellular Hyaline Bodies (IHBs). Sequestosome 1/p62, ubiquitin, Keratin 8 (K8) and Keratin 18 (K18) are the major constituents of MDBs. p62 is an adaptor protein that consists of a number of functional domains. p62 has a characteristic Phox and Bem I (PB1) domain (AA 1-100) at its N terminus.(Moscat *et al.*, 2006). The PB1 domain also can be subdivided into other structural motifs, which were earlier designated as SH_2 domain (AA 1-50) and ZIP (PKC-ζ interacting region).

p62 also contains a Zinc finger domain (ZZ), Microtubule light chain binding protein (LC3) Interacting Region LIR (Ichimura *et al.*, 2008) and a classical polyubiquitin binding domain (UBA) at its C-terminal end. Earlier it was reported that PB1 domain is required for polymerization of p62 (Moscat *et al.*, 2006) but it was not clear that SH_2, ZIP and UBA domains might regulate aggregation property of p62. These domains also may correspond to typical ultrastructure of p62 that can be correlated to *in vivo* MDBs. It is still not yet clear whether interaction of p62 with K8 is facilitated by 1) structural domains of p62 2) ubiquitination or 3) phosphorylation. The role of additional oxidative stress in facilitating or inhibiting the interaction of p62 with K8 in presence and absence of additional ubiquitin also needs to be explored. Luminescent conjugated oligothiophenes (LCOs) have a flexible thiophene backbone and were previously described as fluorescent ligands for cross β sheet conformation Here we also used LCOs to investigate conformational changes in the molecular structure of p62 phospho-mutants (p62S24A, p62S152A) and deletion mutants *in vitro* cellular models to investigate the functional consequences of individual phosphorylation sites and structural domains of p62. This section of the thesis also demonstrates how particular domains of p62 regulate ultrastructure and aggregation property as well as interaction pattern with K8/18. Oxidative stress is one of the important central players in MDB and IHB pathogenesis. It also remains unclear whether under additional oxidative stress p62 co-localizes with K8/18 without additional ubiquitin. Oxidative stress may also interfere with interaction pattern of the components involved in MDBs and IHBs. In this section of results these questions are addressed.

3.16. Role of functional domains and phosphorylation sites in governing ultrastructure and morphology of the aggregates

3.16.1. Role of phosphorylation sites in governing cellular distribution of p62

The schematic representation of p62wt and phosho-mutants p62S24A, p62S152A is displayed in figure 30A, B, C. Compared to p62wt P62S152A did not show any difference in cellular distribution whereas p62S24A, when overexpressed alone, showed prominent diffused distribution over reticulate pattern of distribution (Figure 30E, F) and (Figure 30A, B, C).

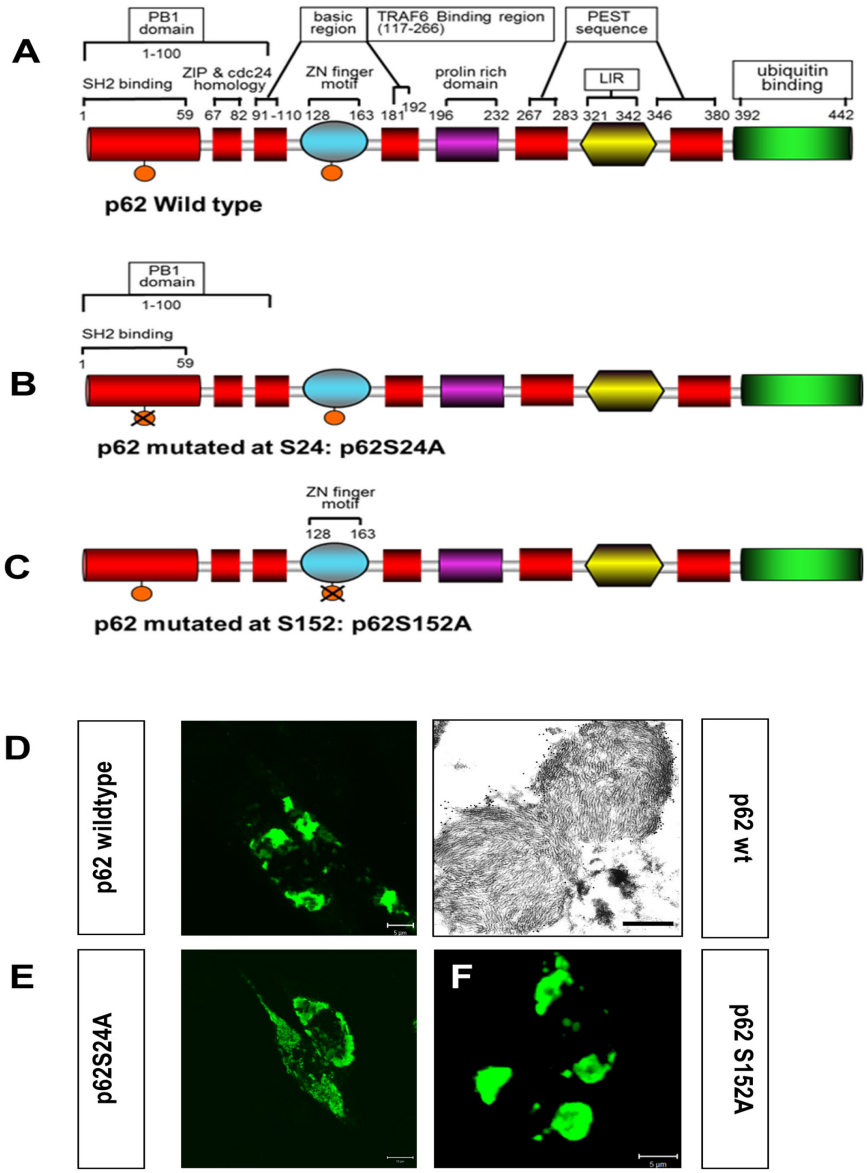


Figure 30: Scheme of multidomain adaptor p62wt, its ultrastructural distribution.

(A) Scheme: domain organization of p62wt (B) Schematic orientation of phosphomutant p62S24A where S24 in PB1 domain is mutated. (C) Schematic orientation of phosphomutant p62S152A where S152 in Zinc finger domain is mutated (D) CHO-K1 cells transfected with *p62wt* and stained with anti-p62 shows

typical reticulate pattern of aggregation. Immunoelectron microscopy shows filamentous ultrastructure of p62. Scale 500 nm (E) CHO-K1 cells transfected with phosphomutant *p62S24A* that shows diffused distribution compared to p62wt shown in *D*. (F) CHO-K1 cells transfected with phosphomutant p62S152A that shows reticulate distribution of aggregates similar to p62wt shown in *D*.

3.16.2. Functional significance of p62 domains in determination of ultrastructure and cellular distribution

To investigate how a particular domain of p62 determines its ultrastructure and cellular distribution, a series of deletion mutants were constructed. (Figure 31 A, B, C). These deletion constructs were then transfected in CHO-K1 cells. The distribution of p62 deletion mutants were then analyzed in comparison to p62 wt. It was observed that deletion of SH_2 domain (or partial deletion of PB1 domain) [amino acids 1-59] leads particularly to a globular IHB like pattern and irregularly shaped MDB like distribution. (Figure 31D) However these both types of aggregates were confined to the cytosol. At this point it is important to note that aggregation property of p62 is not lost even after the deletion of amino acids 1-59. Electron microscopic examination revealed granular amorphous dense appearance which resembles type III MDBs. Interestingly SH_2 deleted p62 lost its filamentous ultrastructure compared to p62wt (Figure 30D, 31D). This leads to further conclusion that filamentous structure of p62 is governed by N terminal SH_2 domain. Deletion of ZIP domain (PKCζ interacting region/ amino acids 67-82) showed irregularly shaped smaller aggregates but IHB or MDB-like distribution pattern was absent. These aggregates were also confined to cytosol. It can also be stated that the aggregation property of p62 was partially lost (Figure 31E, 32E). UBA domain deleted p62 (amino acids 392-442) showed nuclear diffused pattern of distribution in CHO-K1 cells. p62ΔUBA abolished type II MDB like pattern (Figure 31F, 32F). Electron microscopic characterization of p62ΔUBA had shown electron dense granular pattern (Stumptner *et al.*, 2007). This demonstrated that UBA domain also contributes in maintaining the typical filamentous ultrastructure of p62. Aggregation property of p62 was abrogated by UBA deleted p62. This indicated that the typical reticulate pattern of wild type p62 was governed not only by N-terminal SH_2/PB1 domain but also by C-terminal UBA domain.

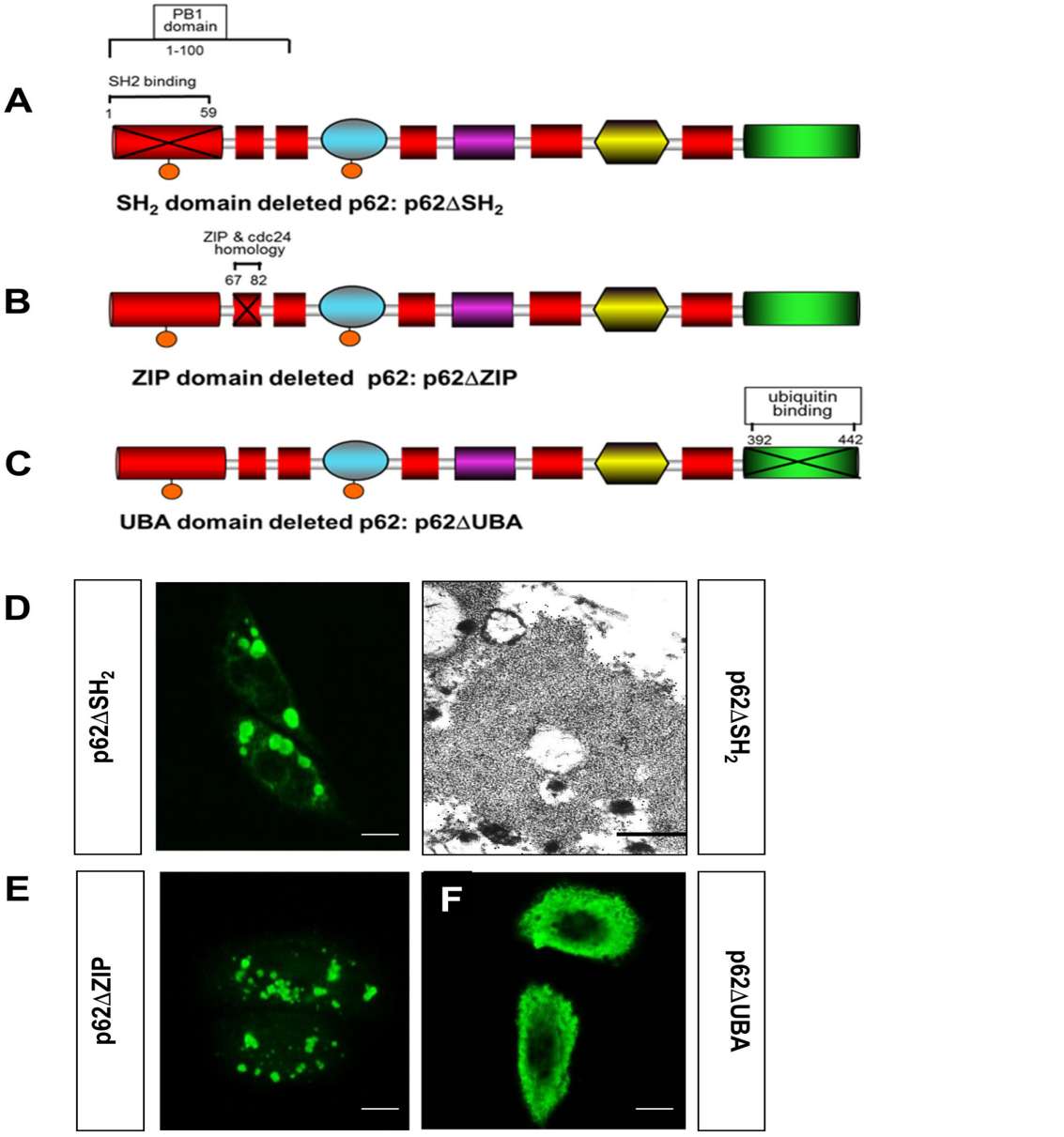


Figure 31: Schematic representation of deletion constructs of p62 and their influence on cellular distribution patterns.

(A) Scheme: domain organization of p62ΔSH$_2$ (amino acid 1-59 deleted) (B) Schematic orientation of p62ΔZIP (amino acids 67-82 deleted). (C) Schematic orientation of p62ΔUBA (amino acids 392-442 deleted) (D) CHO-K1 cells transfected with *p62ΔSH$_2$* and stained with anti-p62 shows circular IHB like aggregation indicating aggregation property is not lost after deletion of amino acid 1-59. Immunoelectron microscopy shows loss of filamentous but IHB like ultrastructure of p62. Scale 500 nm (E) CHO-K1 cells transfected with *p62ΔZIP* that shows irregular shaped aggregates. (F) CHO-K1 cells transfected with *p62ΔUBA* that shows diffused distribution and loss of typical aggregation property. All Scale bars 5µm

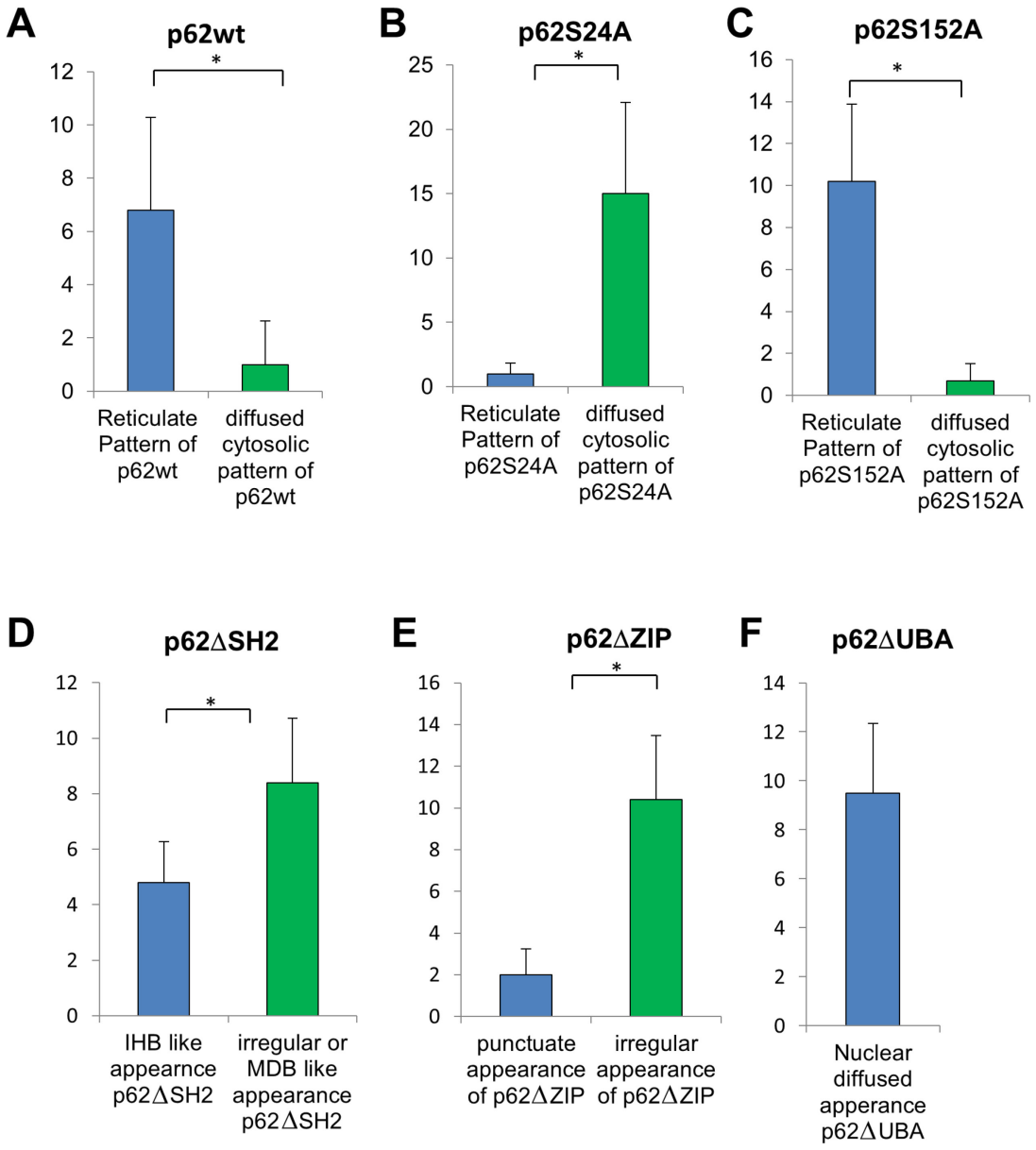


Figure 32: Influence of phosphorylation sites and domains on cellular distribution patterns of p62. (A) CHO-K1 cells transfected with *p62wt* shows typical reticulate pattern of aggregation dominant over diffused distribution. (B) CHO-K1 cells transfected with phosphomutant *p62S24A* that shows diffused distribution dominant over reticulate pattern compared to p62wt shown in *A*. This indicates influence of phosphorylation site S24 in determining structural distribution patterns. (C) CHO-K1 cells transfected with phosphomutant p62S152A that shows reticulate distribution of aggregates similar to p62wt shown in *A*. (D) CHO-K1 cells transfected with $p62\Delta SH_2$ display circular IHB like aggregates as well as irregular MDB like irregular shaped aggregates. (E) CHO-K1 cells transfected with *p62ΔZIP* shows irregular shaped aggregates but also displays punctuate distribution. (F) CHO-K1 cells transfected with *p62ΔUBA* exhibits only prominent diffused nuclear distribution. Data are expressed as the mean of the ratio of fluorescent bodies detected in at least 10-20 cells from 10 random microscopic fields of 3 independent experiments ± SD. *P<0.05; compared to controls, using unpaired T test. Transfection efficiency of the CHO-K1 cells was between 45 to 60 %.

3.16.3. Impact of p62 domains and phosphorylation sites in determining cellular distribution patterns of p62 with K8

In order to determine the role of phosphorylation sites and peculiar domains of p62 in interaction with K8/K18, the deletion constructs and phospho-site mutants were co transfected with K8 and K18 individually but without additional ubiquitin. In case of K18 data is not shown to avoid redundancy. P62wt did not co-localize with K8 or K18 (Figure 33A). Interestingly, the prominent diffused pattern of p62S24A was suppressed when co-transfected with K8 or K18 and reticulate pattern was more eminent (Figure 33B). Similar observations were also noticed in case of keratin 8 aggregates where diffuse dispersion, due to keratin monomers, was not much prominent over its reticulate cytosolic distribution (Figure 34B). Therefore it can be concluded that some of the phosphorylation sites may be capable of governing the cellular distribution patterns. In contrast to p62S24A and K8/K18, p62S152 showed reticulate distribution similar to p62wt when co-transfected along with K8/K18 (Figure 33C). P62wt and K8/K18 showed reticulate pattern of distribution without profound co-localization (in the absence of additional ubiquitin) whereas p62ΔSH$_2$ distinctly co-localized with K8/K18 even without the presence of additional ubiquitin (Figure 33D). This clearly indicates that the SH$_2$ domain is involved in the regulation of ubiquitin mediated interaction with K8/K18. The cellular distribution of p62ΔSH$_2$+K8 was confined to cytosol and showed typical IHB and irregular shaped MDB like pattern. Compared to interaction with p62wt+K8, it can be concluded that these two proteins definitely governed and influenced the distribution of each other. Electron microscopic examination of p62ΔSH$_2$+K8 disclosed IHB and type III MDB like granular amorphous ultrastructure (Figure 37A, C) p62ΔZIP+K8 showed irregularly shaped aggregates and limited co-localization with K8 or K18 (Figure 33E, 34E). In line with previous observations, p62ΔUBA+K8 did not show any co-localization and disclosed only electron dense granular amorphous type III MDB like ultrastructure (Figure 33F, 34F). This highlighted importance of UBA domain in governing not only the interaction with K8/18 but also defining a peculiar ultrastructure.

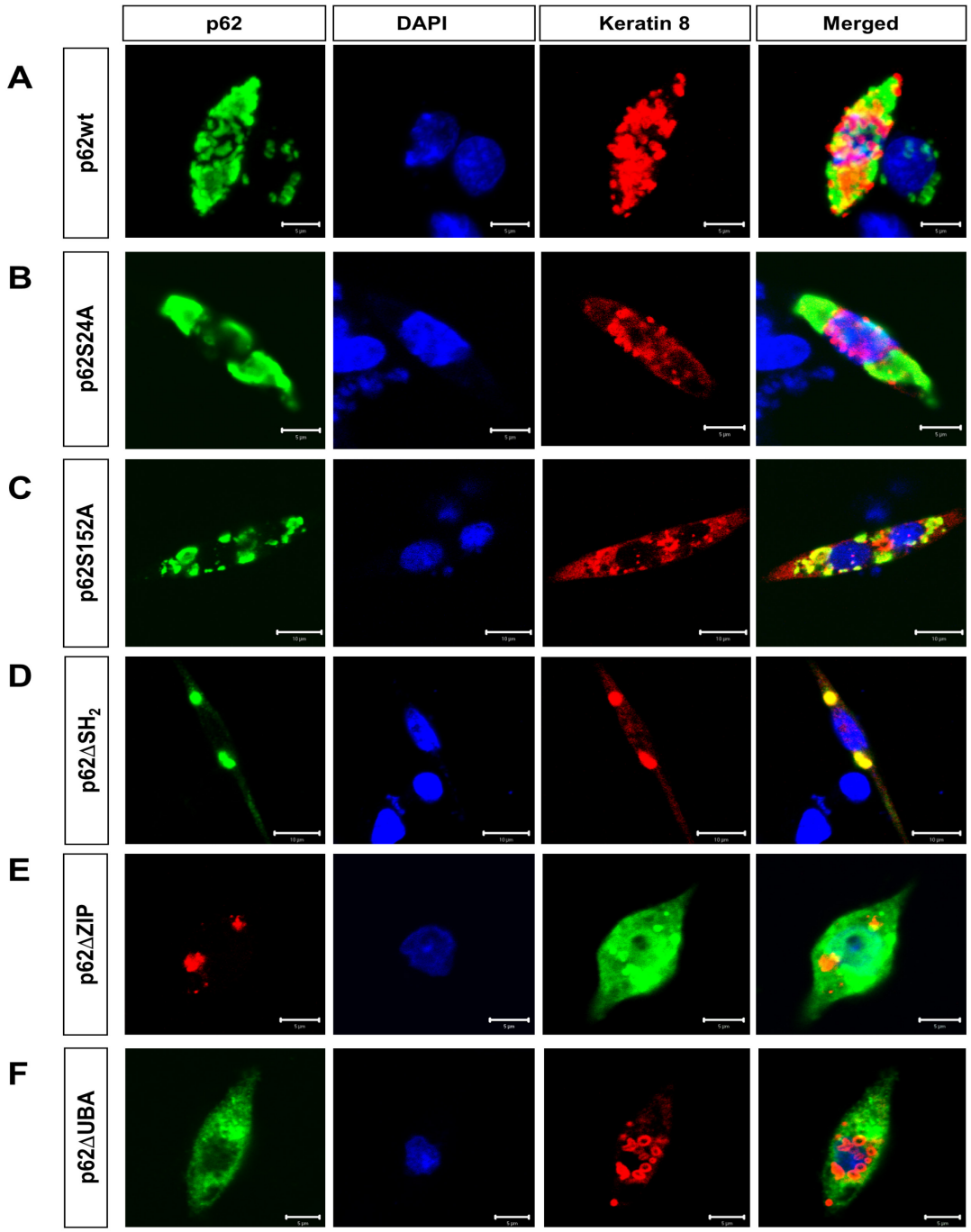


Figure 33: **SH_2 and ZIP domain of p62 are involved the regulating the interaction with K8** :(*A*) CHO-K1 cells co-transfected with *p62wt* and *Krt8*, stained with anti-p62(green) and anti-K8 (red) show a no co-localization. (*B*) CHO-K1 cells co-transfected with *p62S24A* and *Krt8*, stained with anti-p62 (green) and anti-K8 (red) show no co-localization. (*C*) CHO-K1cells co-transfected with *p62S152A* and *Krt8* stained with anti-p62 (green) and anti-K8 (red) show no co-localization (*D*) CHO-K1 cells co-transfected with *p62ΔSH*$_2$ and *Krt8*, stained with anti-p62 (green) and anti-K8 (red) show profound co-localization. (*E*) CHO-K1 cells co-transfected with *p62ΔZIP* and *Krt8*, stained with anti-p62 (green) and anti-K8 (red) exhibit a limited co-localization. (*F*) CHO-K1 cells co-transfected with *p62ΔUBA* and *Krt8* stained with anti-p62 (red) and anti-K8 depicts no co-localization. Scale – 5 µm.

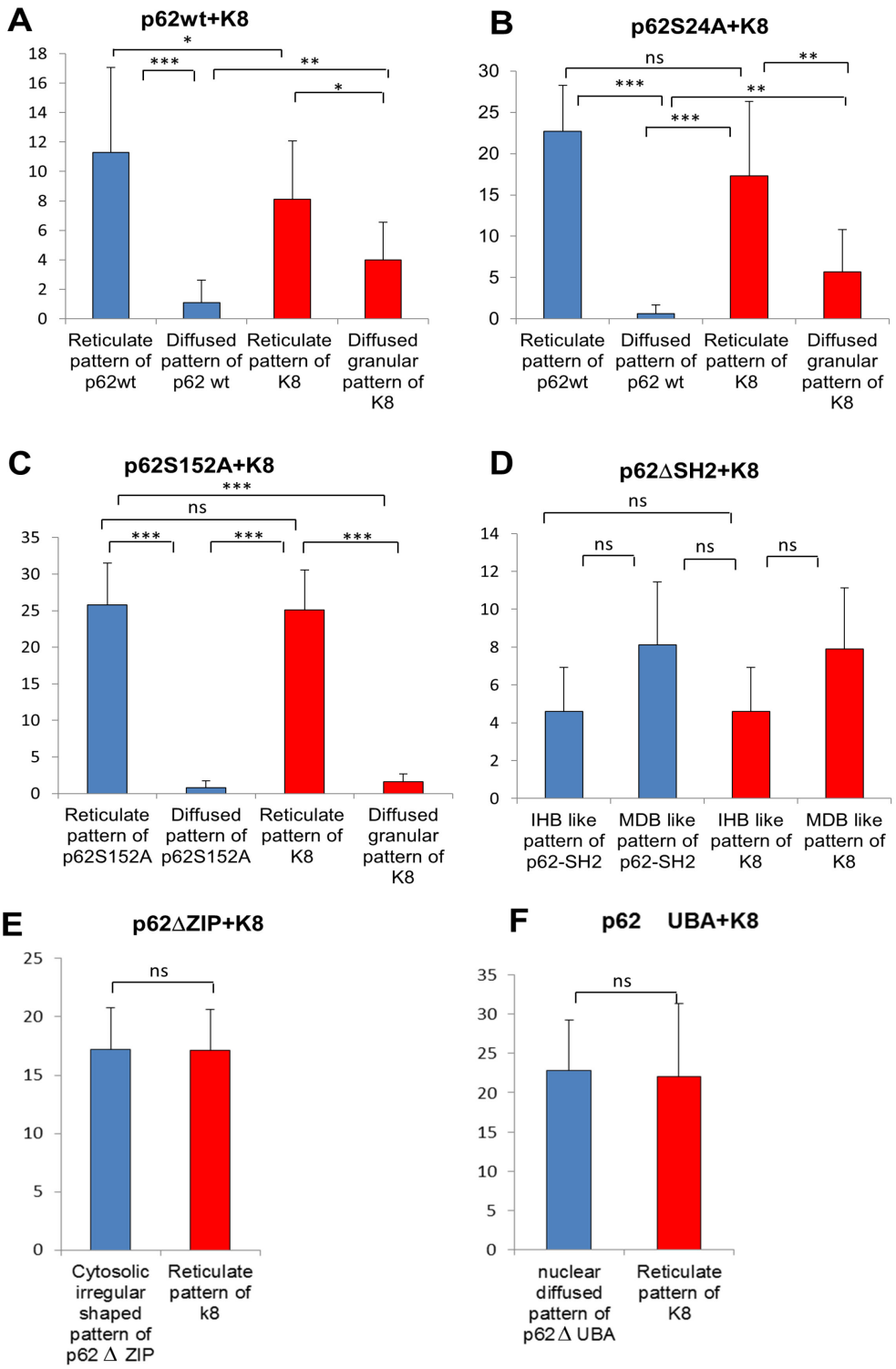


Figure 34: Influence of K8 and p62 mutants on cellular morphology of the aggregates. (*A*) CHO-K1 cells transfected with *p62wt and Krt8* show typical prominent reticulate patterns of aggregates dominant over diffused distribution. (*B*) CHO-K1 cells transfected with *p62S24A and Krt8* show typical prominent reticulate patterns of aggregates dominant over diffused distribution. (*C*) CHO-K1 cells transfected with p62S152A *and Krt8* show similar pattern of aggregation as shown on *A* and *B*. (*D*) CHO-K1 cells transfected with *p62ΔSH*$_2$ *and Krt8* display circular IHB like aggregates as well as irregular MDB like irregular shaped aggregates. (*E*) CHO-K1 cells transfected with *p62ΔZIP and*

Krt8 exhibit irregular shaped aggregates of p62 but typical reticulate pattern of K8 is retained. (F) CHO-K1 cells transfected with *p62ΔUBA and Krt8* expose only prominent diffused nuclear distribution whereas K8 display typical reticulate pattern of aggregation. This designates there is no influence of p62ΔZIP and K8 on cellular distribution of each other. Data are expressed as the mean of the ratio of fluorescent bodies detected in at least 10-20 cells from 10 random microscopic fields of 3 independent experiments ± SD. *P<0.05, **P<0.01,***P<0.001; compared to controls, using one-way ANOVA followed by Bonferroni's multiple comparison test. Transfection efficiency of the CHO-K1 cells was between 45 to 60 %.

3.16.4. Influence of ubiquitin on the interaction with p62 with K8

To investigate how the presence of additional ubiquitin influences the interaction of p62 with K8/K18 and whether phosphorylation sites and domains of p62 have a role to play, the deletion constructs and phospho-site mutants p62S24A and p62S152A were co transfected along with K8/K18 and ubiquitin. P62wt co-localizated with K8 in the presence of ubiquitin (Figure 35A). Due to additional ubiquitin, p62 and K8 always showed homogenous distribution (Figure 36A). The diffused distribution p62wt and p62S24A was suppressed in the presence of ubiquitin. Only diffused distribution of p62S24A is displayed in (Figure 35B, 36B). Also, p62S152A did not show any difference in cellular distribution when compared to p62wt (Figure 35C, 36C). This can lead to a conclusion that selected phosphorylation sites S24 and S152 may not be crucial in regulating the interaction of ubiquitinated keratins with p62. SH_2 deleted p62 showed co-localization with K8 in presence of additional ubiquitin (Figure 35D). However the IHB like and MDB like homogenous distribution of p62ΔSH_2 and K8 was a constant observation (Figure 35D, 36D) Therefore presence or absence of ubiquitin does not seem to influence the interaction of p62ΔSH_2 and K8. Electron micrographic analysis denoted the loss of filamentous ultrastructure observed in case of p62ΔSH_2 when compared to p62wt; surrounded by granular, amorphous, electron dense irregular shaped ultrastructure K8 that resembled type II MDBs (Figure 37C). In contrast, ZIP deleted p62 showed profound co-localization with K8 in the presence of ubiquitin (Figure 35E). It can be speculated that that K8 was ubiquitinated to which ZIP deleted p62 could bind through its UBA domain. This data indicates that the ZIP domain may be 'accessory' but may not be 'mandatory' in facilitating the interaction of p62. In presence of additional ubiquitin p62ΔZIP displayed similar cytosolic diffused dispersion whereas reticulate pattern of K8 was also consistent (Figure 36E). In line with previous observations, p62ΔUBA abolished interaction with misfolded keratins in the presence of additional ubiquitin (Figure 35F). As far as distribution analysis is

concerned there was two distinct patterns were observed 1) nuclear diffused pattern attributed to p62ΔUBA and 2) typical reticulate pattern that belongs to K8

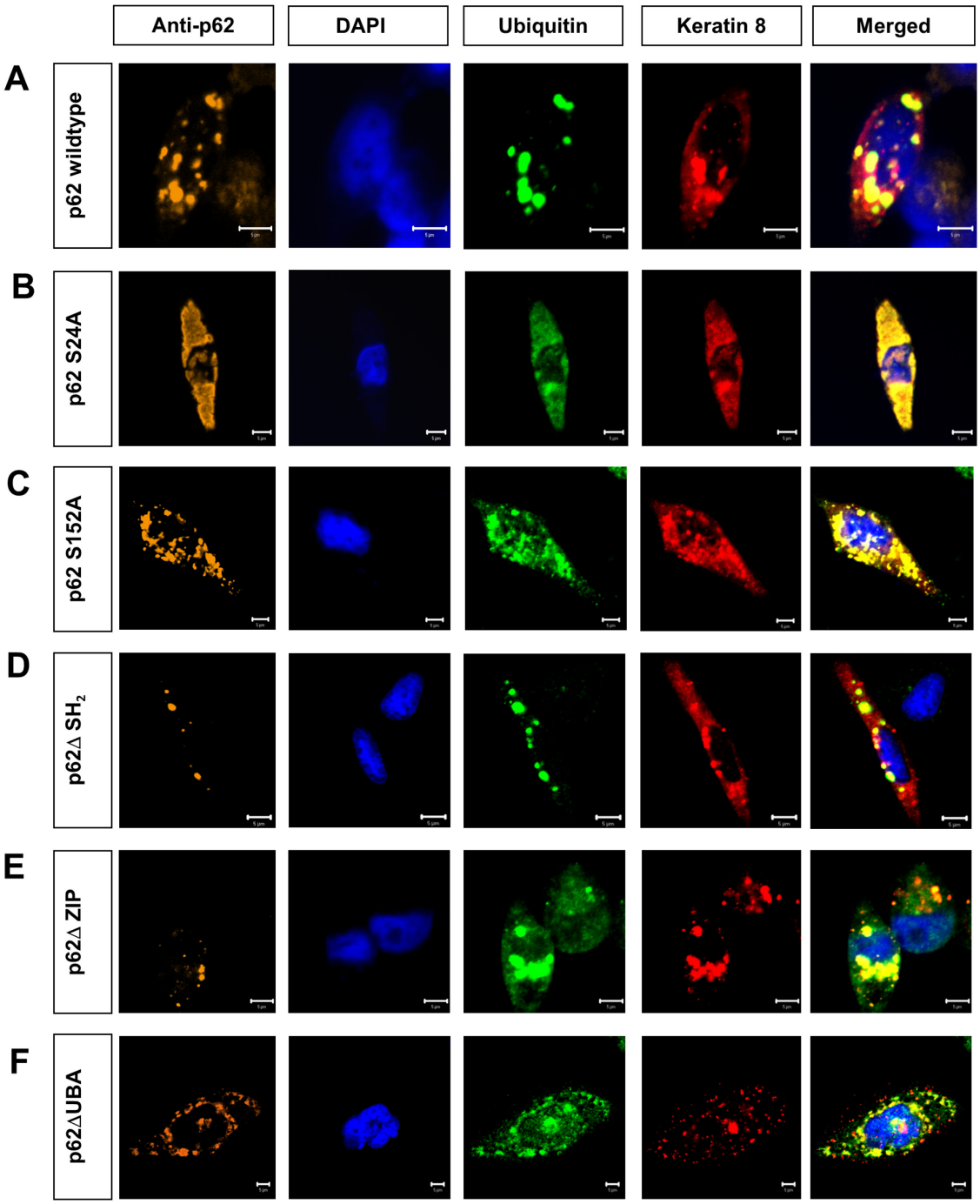


Figure 35: **Influence of ubiquitin on the interaction on p62 with K8; ubiquitin distributes itself according to p62** (*A*) CHO-K1 cells co-transfected with *p62wt, Ubi* and *Krt8*, stained with anti-p62(amber), Ubi (green) and anti-K8 (red) show a co-localization. Typical reticulate pattern of p62, Ubi and K8 are visible. Presence of ubiquitin appears to be mandatory to facilitate colocalization. (*B*) CHO-K1 cells co-transfected with *p62S24A, Ubi* and *Krt8*; show co-localization. (*C*) CHO-K1cells co-transfected with *p62S152A, Ubi* and *Krt8* stained with anti-p62 (amber) and anti-K8 (red) show co-localization in presence of ubiquitin (green) (*D*) CHO-K1 cells co-transfected with

p62ΔSH$_2$, Ubi and *Krt8*, exhibit profound co-localization (*E*) CHO-K1 cells co-transfected with *p62ΔZIP, Ubi* and *Krt8*, display a limited co-localization.. (*F*) CHO-K1 cells co-transfected with *p62ΔUBA, Ubi* and *Krt8* depicts no co-localization. (red). All scale bars – 5 µm.

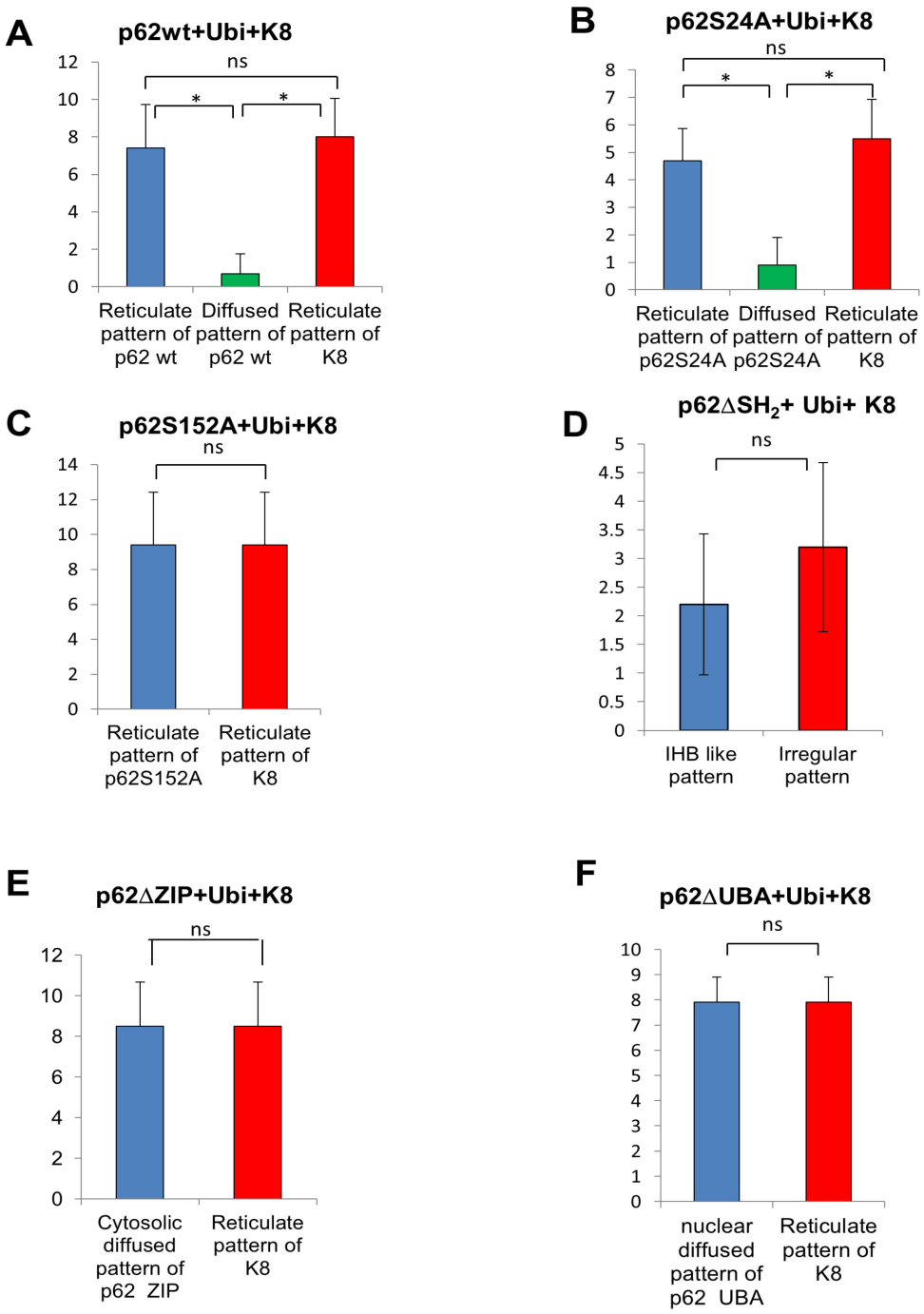


Figure 36: Influence of ubiquitin on cellular morphology of the K8 and p62 aggregation. (A) CHO-K1 cells co-transfected with equimolar ratios of human *p62wt, Ubi and Krt8* show typical prominent reticulate patterns of aggregates dominant over diffused distribution. However diffused pattern of K8 is lost due to additional ubiquitin (B) CHO-K1 cells co-transfected with equimolar ratios of *p62S24A, Ubi and Krt8* did not show much difference in distribution patterns compared to p62wt shown in *(A)*. (C) CHO-K1 cells co-transfected with equimolar ratios of human *p62S152A, Ubi*

and Krt8 did not show much difference compared to p62wt (D) CHO-K1 cells co-transfected with equimolar ratios of p62ΔSH$_2$*, Ubi and Krt8* did not exhibit much difference compared to p62wt (shown in *A)* display circular IHB like aggregates as well as irregular MDB like irregular shaped aggregates. (E) CHO-K1 cells co-transfected with equimolar ratios of *p62ΔZIP, Ubi and Krt8* exhibit irregular shaped aggregates of p62 but typical reticulate pattern of K8 is retained. (F) CHO-K1 cells co-transfected with equimolar ratios of *p62ΔUBA, Ubi and Krt8* expose only prominent diffused nuclear distribution whereas K8 display typical reticulate pattern of aggregation. Data are expressed as the mean of the ratio of fluorescent bodies detected in at least 10-20 cells from 10 random microscopic fields of 3 independent experiments ± SD. *P<0.05, **P<0.01, ***P<0.001; compared to controls, using one-way ANOVA followed by Bonferroni's multiple comparison test. Transfection efficiency of the CHO-K1 cells was between 45 to 60 %.

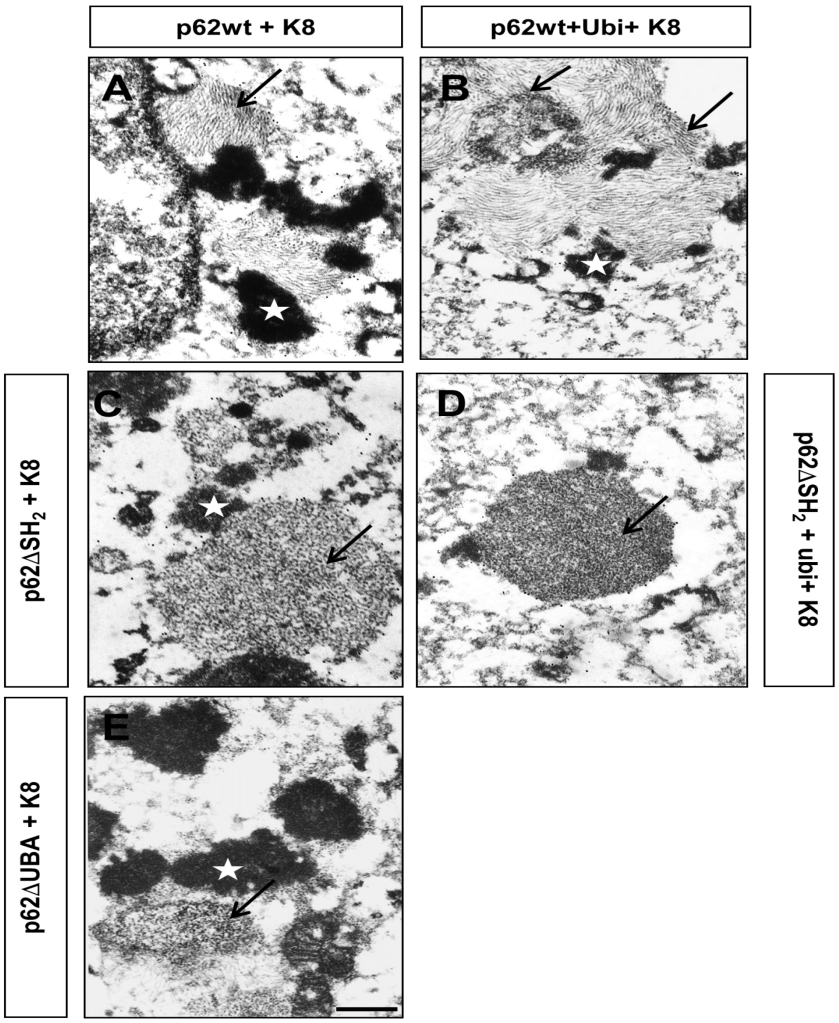


Figure 37: Immunoelectron microscopy of CHO-K1 cells co-transfected with K8, ubiquitin and p62; contribution of the domains of p62 for specific ultrastructure.

Immunoelectron micrographs of p62wt and keratin aggregates in transfected cells stained with anti p62 and K8 antibodies and secondary antibodies linked to 18 nm gold particles. (A) CHO-K1 cells transfected with human *p62wt* and *Krt8*; filamentous ultrastructure of p62 shown by black arrowhead. Granular, densely packed amorphous K8 aggregates that resembles type III MDBs (*asterisk*) (B) CHO-K1 cells transfected with equimolar ratios of *p62wt, Ubi* and *Krt8*; aggregates that resembles type II like MDBs are shown by black arrowheads, granular amorphous K8 aggregates (*asterisk*). (C) CHO-K1 cells transfected with *p62ΔSH2,* and *Krt8*; compared to p62wt loss of filamentous structure that resembles IHB like ultrastructural pattern is shown by black arrow, densely packed amorphous K8 aggregates (*asterisk*). (D) CHO-K1 cells co-transfected with equimolar ratios of *p62ΔSH2, Ubi* and *Krt8*; Additional presence of ubiquitin does not influence IHB like granular ultrastructural pattern of *p62ΔSH2* indicated by black arrow however type II like MDBs are abrogated by *p62ΔSH2*. (E) CHO-K1 cells co-transfected with equimolar ratios of *p62ΔUBA* and *Krt8*; however type II like MDBs are abrogated by *p62ΔUBA* shown by arrow but obtuse, amorphous K8 aggregates (asterisk) continue to exist. Scale bar: 500 nm.

3.16.5. Deletion of SH2 domain induces cross β-sheet structure of p62

To investigate how the domains and phosphorylation sites of p62 configure its structural conformation and the structural basis of selective co-localization of SH_2 domain deleted p62 and K8, LCOs were used to stain p62 mutants. The p62 phospho-mutants and deletion constructs were transfected in the CHO-K1cells and stained with anti p62 antibodies and h-HTAA and/or p-FTAA. p62S24A, p62152A were not stained by LCOs (data not shown). This indicated that phosphorylation sites S24 and S152 do not have an influence on structural orientation of p62 in the context with cross β-sheet conformation. Deletion of UBA and ZIP domain also did not induce cross β-sheet conformation whereas interestingly, deletion of SH_2 domain induces cross β-sheet conformation of p62 (Figure 38A-F). This data indicates that a peculiar structure of protein may also dictate its functional interaction. Therefore it can be predicted that cross β-sheet rich aggregates of p62ΔSH$_2$ and K8 either have an affinity towards each other or the cellular machinery transports these aggregates to a similar location in the cytosol. This may indicate both p62ΔSH$_2$ and K8 acquire cross β-sheet conformation which facilitates the interaction between these two proteins.

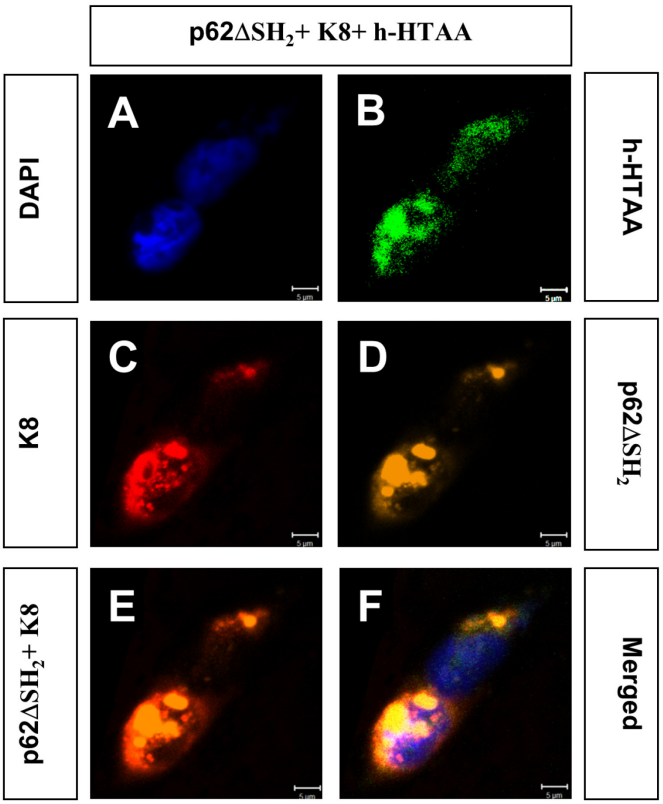


Figure 38: SH_2 domain deleted p62 and K8 acquire cross β-sheet structure. CHO-K1 cells transfected with human *p62ΔSH$_2$*, stained with anti-p62 (amber), K8(red) and h-HTAA (green). (*A*) Nuclear staining by DAPI (*B*) h-HTAA staining (green). (*C*) Keratin 8. (*D*) p62ΔSH$_2$ (amber) IHB like inclusion bodies.(*E*) co-localization of p62ΔSH$_2$ and K8 (*F*) h-HTAA stains both p62ΔSH$_2$ and K8 aggregates. All scale bars: 5 µm.

3.16.6. Additional oxidative stress does not have inhibitory effect on p62, Ubi, K8 interaction

In order to understand the impact of oxidative stress upon interaction of p62 with K8, CHO-k1 cells were co-transfected with p62 and K8 without additional ubiquitin. Cells were stressed using two independent stressors. UV-light and BSO were used as stressors. Under additional oxidative stress p62 did not co-localize with K8 (Figure 39A) indicating the presence of ubiquitin is mandatory for the interaction (Figure 39B). To investigate whether additional oxidative stress inhibits the interaction of p62, ubiquitin K8, CHO-K1 cells were transfected with *p62, ubi* and *Krt 8,* UV-induced stress was generated (Figure 39C, D). Additionally, in the independent experiments cells were also stressed overnight using 100μM and 250 μM BSO before transfection of p62*, ubi* and *krt 8*. Irrespective of additional oxidative stress either by UV or BSO, p62 always showed profound co-localization with K8 only in the presence of ubiquitin (Figure 39E, F).

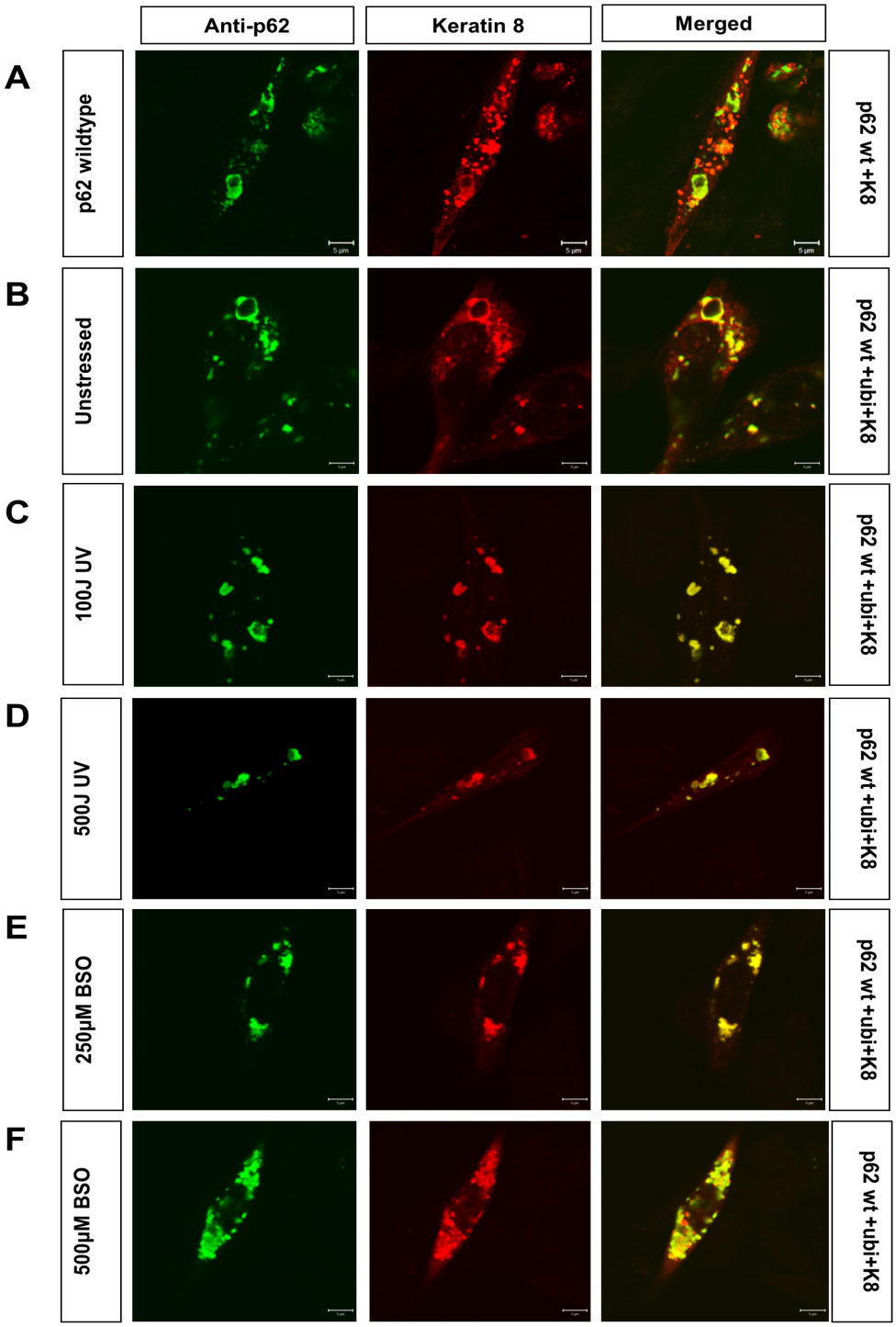


Figure 39: Additional oxidative stress did not inhibit the interaction of p62, ubiquitin, K8*'in vitro'* (A) CHO-K1 cells transfected with equimolar ratios of human *p62 and Krt8* stained with anti-p62 (red) and anti-K8 (red). Absence of co-localization indicated no interaction between p62 and K8. (B) CHO-K1 cells co-transfected with equimolar ratios of *p62*, *ubiquitin* and *Krt8,* and stained with anti-p62 (green), anti-K8 (red). Co-localization of K8 and h-HTAA under unstressed conditions is visible. (*C*) CHO-K1 cells co-transfected with equimolar ratios of *p62*, *ubiquitin* and *Krt8* and stressed with 100J UV, stained with anti-K8 (red) and anti p62 (green) denotes co-localization. (D) CHO-K1 cells co-transfected with equimolar ratios of *p62*, *ubiquitin* and *Krt8* and stressed with 500J

UV, stained with anti-K8 (red) and anti p62 (green) denotes no inhibition in binding of p62wt, ubiquitin and K8. (E) CHO-K1 cells with equimolar ratios of *p62*, *ubiquitin, Krt8* and stressed with 250μM BSO, stained with anti-K8 (red) and anti-p62 (green) show co-localization. (F) (E) CHO-K1 cells with equimolar ratios of *p62*, *ubiquitin, Krt8* and stressed with 500μM BSO, stained with anti-K8 (red) and anti-p62 (green) show even higher stress levels do not inhibit of interaction between p62, ubi and K8. All scale bars: 5 μm.

Discussion

This data shows that interaction of p62 with K8 has ubiquitination as a predominant factor. Additionally structural domains of p62 also regulate aggregation properties of p62 and interaction with misfolded K8. Deletion of SH_2 domain (or PB1 domain partially) leads to loss of filamentous ultrastructure of p62 but resembles IHB like aggregation pattern. Deletion of ZIP domain (or remaining PB1 domain) leads to irregularly shaped aggregates whereas UBA domain deleted p62 shows diffused distribution but only a partial loss of filamentous ultrastructure and lack of interaction with K8.

This '*in vitro*' studies demonstrate that MDBs and IHBs can be induced in tissue culture cells by co transfecting various components of MDBs such as keratin 8 or 18/p62/ubiquitin and p62/ubiquitin, respectively. However chemical composition of MDBs and IHBs associated with diseased human liver might differ. IHBs, are characterized by indistinct fibrillar and granular ultrastructure whereas MDBs were classified into 3 distinguished categories : (a) type 1 is uncommon and composed of bundles of filaments arranged in parallel arrays that closely resembles amyloid fibrils like ultrastructure (b) common and classical type 2, displays closely confined, indiscriminately organized filaments and blurred surface coat; (c) type 3 lacks of fibrillar ultrastructure displays but shows increased electron density and that results granular-amorphous appearance. The current data demonstrates contribution of structural domains of p62 and ubiquitin in defining various types of MDB ultrastructure. The additional oxidative stress may interfere with the components of MDBs but not with their interaction. The oxidative stress generated by BSO or UV did not inhibit the interaction of MDB components. In case of additional oxidative stress p62 still requires presence of additional ubiquitin for covalent binding with misfolded K8. Other reports have shown that oxidative stress is also one of the classical inducers of p62 and therefore it may be one of the key players in progression of the disease.

CHAPTER 4

General Discussion

4. Discussion:

4.1. Structural characterization of the MDBs and predominant components p62 and K8

The cross β-sheet structure of keratin in MDBs resembles that of prion-induced protein aggregates and amyloid-beta fibrils in neurodegenerative diseases, suggesting molecular similarities in these degenerative disorders. In the protein-misfolding diseases mentioned, two principally divergent scenarios might be associated with protein aggregate formation: on the one hand, there is ample literature about the toxicity of amyloid plaques in neurodegenerative disease, suggesting that MDBs may contribute to liver damage (reviewed in Denk et al., 2000; Strnad et al., 2008). Previous studies on the role of ß-sheet-rich proteins in neurodegenerative diseases suggested that not only conformational transition but also their assembly into insoluble β-sheet-rich aggregates might confer toxicity at a certain stage (Nagai et al., 2008). On the other hand, the primary toxicity of non-sequestered proteins with ß-sheet conformation is also well known (Nagai et al., 2008). In this context, MDB formation could be seen as the sequestration of keratin into insoluble, non-toxic aggregates, which will eventually be removed by proteasomal or autophagic pathways (Bardag-Gorce et al., 2005; Bardag-Gorce et al., 2004; Harada et al., 2008; Mathew et al., 2009;). It is currently not possible to distinguish these scenarios.

LCOs also appear as novel inexpensive extension to routinely established immunohistochemical analysis of MDBs. On the one hand LCOs demonstrated good sensitivity since they detected even very small MDBs as shown in figure 3E. On the other hand LCO staining is more specific than p62 staining since p62 is not suitable for distinction of MDBs and IHBs. Therefore, due to the specificity of conformational changes of keratin in MDBs as shown here, LCO binding might serve as a new structural marker for the detection of MDBs and classification of hepatocytic protein aggregates. Furthermore, we demonstrated that LCOs can be readily applied to FFPE tissue sections opening the opportunity for their future application in routine diagnosis of liver and other diseases (Sigurdson et al., 2007, Nilsson et al., 2010). The constant presence of cross ß-sheet structure in MDBs might even become a target for therapy to prevent their accumulation by using cross ß-sheet binding substances as drugs. (*Gastroenterology* Sep; 141(3):1080-1090)

4.2. Multiple facets of interaction of p62 with misfolded K8/18

Aggregation of keratins resemble the amorphous deposits also found in other degenerative diseases such as Alzheimer's disease and amylotrophic lateral sclerosis as well as in prion diseases whereas ultrastructure of p62wt closely resembles to the fibrillar amyloids (Zatloukal et al., 2004b). The organization of typical regular amyloid-type filaments by p62 can be abolished by the presence of additional components, such as keratin and ubiquitin, in support of the fact that mixed or composite amyloids do not exist.

Three types of distinguished MDBs were previously reported : (i) type 1 is uncommon and composed of bundles of filaments with a mean diameter of approximately 14 nm arranged in parallel arrays that closely resembles amyloid fibrils like ultrastructure (ii) common and classical type 2, displays closely confined, indiscriminately organized filaments with a mean diameter of aprox.15 nm and blurred surface coat; (iii) type 3 displays increased electron density and lack of fibrillar ultrastructure resulting to granular-amorphous appearance (Yokoo *et al.*, 1982). The following conditions are responsible for MDB formation *in vivo* and *in vitro* (1) overexpression of p62, ubiquitin and keratins; (2) polyubiquitinated misfolded K8/18 (3) p62 with intact PB1 and UBA domain for binding with ubiquitinated keratin; and (4) Screwed ratio of K8:K18 (Zatloukal *et al.*, 2000).

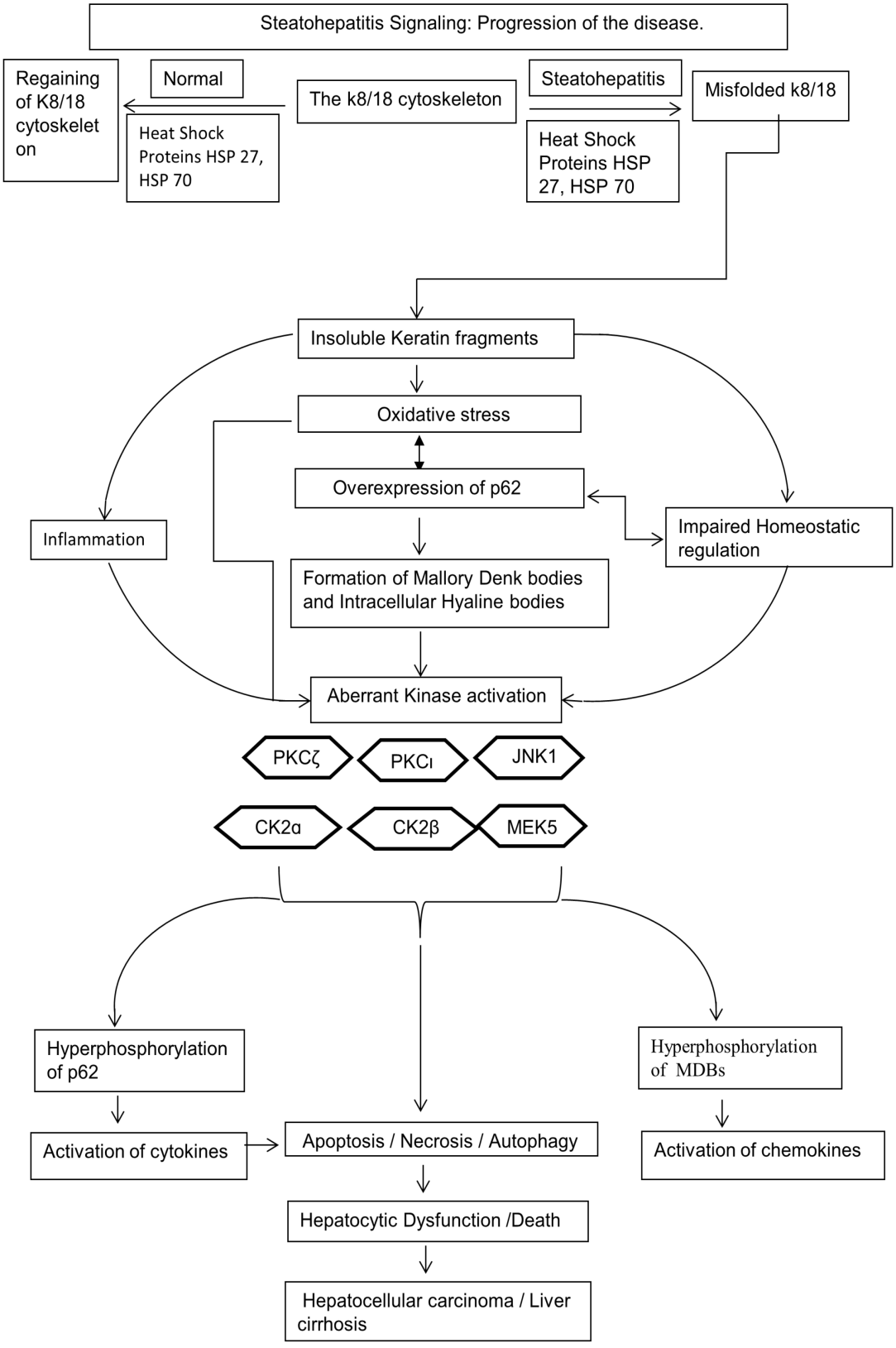
The ultrastructure of MDBs suggests that different domains of p62 and K8/18 along with ubiquitin dictate various patterns of distinct structures. The inability to maintain the keratin 8 to keratin 18 ratio appears to be the result of posttranslational events or keratin turnover (e.g., prohibitory effect of keratin 8 due to hyperphosphorylation on keratin degradation whereas increased keratin 8 stability due to transglutaminase modification as proposed in the recent articles. (Nakamichi et al., 2005, Zatloukal et al., 2000, Zatloukal et al., 1989a). Role of p62 is crucial in maintaining the turnover of the aggregates as revealed by the other recent reports (Duran et al., 2008).

4.3. Ubiquitination and phosphorylation involved in MDB pathogenesis with reference to p62

Molecular pathogenesis of steatohepatitis involves various complex molecular mechanisms. Therefore role of post-translational modifications might be crucial in defining the complex etiology involved in MDB formation. Interaction of ubiquitinated misfolded keratins with kinases such as JNK is also striking. However it needs further

studies and evaluation to establish these findings. It appears that keratin 8 hyperphosphorylation might be the consequence of unregulated kinase interaction. It can be hypothesized that the ability of the keratins to change the conformation from predominantly alpha helical to cross β-sheets may facilitate the keratins to interact with certain kinases which otherwise would not be the case. Therefore prevention of hyperphosphorylation of MDBs and p62 might be another therapeutic strategy that can be aimed at. Accordingly, one can postulate that MDBs are more likely to arise in diseases that result in an imbalance in cellular homeostasis with accumulation of predominantly keratin 8. Moreover, the final formation of inclusion bodies is a complex process, which results due to evasion of cellular rescue mechanisms against aberrant (either unfolded or misfolded) and potentially toxic amyloid like proteins, and requires additional factors, such as oxidative or ER stress, impairment of protein degradation systems. Phosphorylation with known and unknown interaction partners of p62 unravels the role of p62 in various cellular processes. Immunofluorescence and immunoelectron microscopic studies indicate that how the phosphorylation sites regulate not only the interaction pattern but also cellular distribution patterns. The principal findings of this study relate to the mechanism of p62-induced MDB and IHB formation. The data may indicate that (i) posttranslational modification of p62 is involved in MDB pathogenesis. (ii) possibility of either p62-JNK or K8-JNK interaction that may trigger the pathway of apoptosis however further studies are required to establish these results. (iii) functional relevance of the domains involved in regulating various interactions of p62 with its protein partners. (iv) the contribution of structural domains of p62 involved in MDB and in IHB formation (v) ubiquitin as another key player that defines cellular interaction of p62 with K8/18. These data provide mechanistic insight into the cellular mechanism of MDB formation and fate of the cell towards apoptosis/ autophagy and a model relevant to human ASH and NASH. Preliminary experiments demonstrate the involvement of various kinases that might indicate the hyperphosphorylation of p62 and K8/18 cytoskeleton which ultimately may lead progression of disease due to altered signaling cascade. A scheme is proposed showing how phosphorylation may lead to activation of different pathways leading to further cellular consequences. However further studies and additional technologies are required to establish these findings. Recent studies proposed a role for autophagy in removal of diffuse ubiquitinated proteins delivered by p62/sqstm1 (Bjorkoy *et al.*, 2005; Pankiv *et al.*, 2007). The key domains of p62 that appears to regulate the interaction

with other protein partners, may also decide the aggregation property of p62. It is the first evidence that not only UBA domain but also SH_2 (or PB1) domain of p62 as well as ubiquitin play an important role in a co-localization with K8/18. Deletion of SH_2 domain (or partial PB1 domain) retains the ability of p62 to form IHB like inclusion bodies whereas p62-ZIP (PKC-ζ interacting domain) showed limited interaction with ubiquitin and did not allow typical aggregate formation. This indicates that p62wt in IHBs either attains complex quaternary structure in which SH_2 domain is masked or the SH_2 domain becomes inaccessible resulting in IHB like inclusion bodies. Given the fact that only SH_2 deleted p62 acquires cross β-sheet conformation but IHBs that consist of p62wt lack this particular conformation, it can also be stated that molecular structural pattern is unable to explain the pathogenesis involved in IHB formation. However the involvement of ubiquitin and other proteins in inducing p62 to acquire different conformation than cross β-sheet sheets cannot be ruled out. It was further clear that deletion of only SH_2 domain induces cross β-sheet conformation of p62 whereas deletion of ZIP or UBA does not. As K8 also acquires cross β-sheet conformation, it may be proposed that SH_2 deleted p62 and K8/K18 co-localization is an example of interaction resulted due to presence of cross β-sheet conformation. From these data it also can be predicted that proteins that may acquire cross β-sheet conformation also may acquire capability to interact with misfolded K8.



Scheme: Progression of steatohepatitis and HCC due to aberrant phosphorylation

4.4. p62 at the intersection of autophagy and apoptosis

The complex signaling network that determines whether cells proliferate, senesce, or die acquires a remarkable degree of specificity with a relatively smaller number of key signaling proteins. This accuracy is acquired through the multi-domain protein adapters that organize and segregate the signaling cascades. Our studies support the fact that p62 binds the autophagy regulator Atg8/LC3 through a domain termed the LC3-interacting region (LIR). Some of the recent reports as previously mentioned also indicate a clear link between autophagy and p62. The observation that overexpression of not GFP-p62 but GFP-LC3 alone induces a rapid cellular death by digesting the membrane, point out towards probable protective functions of p62. Further studies are required to confirm these findings. Ubiquitin is reported to induce autophagy however the failure of ubiquitin to facilitate the removal of the aggregates itself by autophagy highlights mandatory requirement for p62 (Kim *et al.*, 2008). Our data suggest that p62 associates with polyubiquitinated keratins and its recruitment may require triggering the apoptosis or autophagy. This designates that the p62 containing inclusion bodies are signaling hubs that may determine whether cells avoid apoptosis by triggering the NF-κB pathway, or prefer apoptosis, by activating the caspase-8 and its downstream effector proteins (Jin *et al.*, 2009). It is still not clear if p62 also regulates necrosis in this fashion. According to our observations the misfolded keratins cannot activate autophagy or apoptosis. In addition a recent report also suggests Keap1 interaction with p62 is required to upregulate nrf-2 pathway which is a critical regulator of the cellular defense mechanism against oxidative stress. Therefore it can be stated that p62 appears to be at the central control point which decides the fate of the cells towards a survival or death.

My studies on MDB formation *in vivo* and *in vitro* provide the information of p62 with misfolded K8/18 in the context of human chronic degenerative liver diseases associated with the MDBs. Ubiquitinated p62-containing cellular protein aggregates are characteristic hallmarks of a wide range of chronic degenerative diseases such as Alzheimer's disease, α-1 antitrypsin deficiency, Parkinson's disease, amyotrophic lateral sclerosis, and Huntington's disease and results of my studies, therefore, appear relevant in even a greater context.

5. References

Almstedt K, Nystrom S, Nilsson KP, Hammarstrom P (2009). Amyloid fibrils of human prion protein are spun and woven from morphologically disordered aggregates. *Prion* **3**(4)**:** 224-235.

Aslund A, Sigurdson CJ, Klingstedt T, Grathwohl S, Bolmont T, Dickstein DL*, et al.* (2009). Novel pentameric thiophene derivatives for in vitro and in vivo optical imaging of a plethora of protein aggregates in cerebral amyloidoses. *ACS Chem Biol* **4**(8)**:** 673-684.

Babu JR, Geetha T, Wooten MW (2005). Sequestosome 1/p62 shuttles polyubiquitinated tau for proteasomal degradation. *J Neurochem* **94**(1)**:** 192-203.

Bardag-Gorce F, Francis T, Nan L, Li J, He Lue Y, French BA*, et al.* (2005). Modifications in P62 occur due to proteasome inhibition in alcoholic liver disease. *Life Sci* **77**(20)**:** 2594-2602.

Bardag-Gorce F, Vu J, Nan L, Riley N, Li J, French SW (2004). Proteasome inhibition induces cytokeratin accumulation in vivo. *Experimental and molecular pathology* **76**(2)**:** 83-89.

Baribault H, Penner J, Iozzo RV, Wilson-Heiner M (1994). Colorectal hyperplasia and inflammation in keratin 8-deficient FVB/N mice. *Genes Dev* **8**(24)**:** 2964-2973.

Bence NF, Sampat RM, Kopito RR (2001). Impairment of the ubiquitin-proteasome system by protein aggregation. *Science* **292**(5521)**:** 1552-1555.

Bjorkoy G, Lamark T, Brech A, Outzen H, Perander M, Overvatn A*, et al.* (2005). p62/SQSTM1 forms protein aggregates degraded by autophagy and has a protective effect on huntingtin-induced cell death. *J Cell Biol* **171**(4)**:** 603-614.

Bradford MM (1976). A rapid and sensitive method for the quantitation of microgram quantities of protein utilizing the principle of protein-dye binding. *Anal Biochem* **72:** 248-254.

Brooks DJ (2009). Imaging amyloid in Parkinson's disease dementia and dementia with Lewy bodies with positron emission tomography. *Mov Disord* **24 Suppl 2:** S742-747.

Cadrin M, French SW, Wong PT (1991). Alteration in molecular structure of cytoskeleton proteins in griseofulvin-treated mouse liver: a pressure tuning infrared spectroscopy study. *Exp Mol Pathol* **55**(2)**:** 170-179.

Clavaguera F, Bolmont T, Crowther RA, Abramowski D, Frank S, Probst A*, et al.* (2009). Transmission and spreading of tauopathy in transgenic mouse brain. *Nat Cell Biol* **11**(7)**:** 909-913.

Denk H, Franke WW, Dragosics B, Zeiler I (1981). Pathology of cytoskeleton of liver cells: demonstration of mallory bodies (alcoholic hyalin) in murine and human hepatocytes by immunofluorescence microscopy using antibodies to cytokeratin polypeptides from hepatocytes. *Hepatology* **1**(1)**:** 9-20.

Denk H, Franke WW, Kerjaschki D, Eckerstorfer R (1979). Mallory bodies in experimental animals and man. *Int Rev Exp Pathol* **20:** 77-121.

Denk H, Gschnait F, Wolff K (1975). Hepatocellar hyalin (Mallory bodies) in long term griseofulvin-treated mice: a new experimental model for the study of hyalin formation. *Lab Invest* **32**(6)**:** 773-776.

Denk H, Stumptner C, Fuchsbichler A, Muller T, Farr G, Muller W*, et al.* (2006). Are the Mallory bodies and intracellular hyaline bodies in neoplastic and non-neoplastic hepatocytes related? *J Pathol* **208**(5)**:** 653-661.

Denk H, Stumptner C, Zatloukal K (2000). Mallory bodies revisited. *J Hepatol* **32**(4)**:** 689-702.

Denk H, Zatloukal K, Preisegger K (1989). Ubiquitin--a common denominator in intermediate filament pathology of brain and liver? *Hepatology* **10**(4)**:** 514-515.

Donaldson KM, Li W, Ching KA, Batalov S, Tsai CC, Joazeiro CA (2003). Ubiquitin-mediated sequestration of normal cellular proteins into polyglutamine aggregates. *Proc Natl Acad Sci U S A* **100**(15)**:** 8892-8897.

Downward J (2003). Targeting RAS signalling pathways in cancer therapy. *Nat Rev Cancer* **3**(1)**:** 11-22.

Duncan JS, Gyenis L, Lenehan J, Bretner M, Graves LM, Haystead TA*, et al.* (2008). An unbiased evaluation of CK2 inhibitors by chemoproteomics: characterization of inhibitor effects on CK2 and identification of novel inhibitor targets. *Mol Cell Proteomics* **7**(6)**:** 1077-1088.

Duran A, Linares JF, Galvez AS, Wikenheiser K, Flores JM, Diaz-Meco MT*, et al.* (2008). The signaling adaptor p62 is an important NF-kappaB mediator in tumorigenesis. *Cancer Cell* **13**(4)**:** 343-354.

Franke WW, Denk H, Schmid E, Osborn M, Weber K (1979). Ultrastructural, biochemical, and immunologic characterization of Mallory bodies in livers of griseofulvin-treated mice. Fimbriated rods of filaments containing prekeratin-like polypeptides. *Lab Invest* **40**(2)**:** 207-220.

Greten FR, Eckmann L, Greten TF, Park JM, Li ZW, Egan LJ*, et al.* (2004). IKKbeta links inflammation and tumorigenesis in a mouse model of colitis-associated cancer. *Cell* **118**(3)**:** 285-296.

Harada M, Hanada S, Toivola DM, Ghori N, Omary MB (2008). Autophagy activation by rapamycin eliminates mouse Mallory-Denk bodies and blocks their proteasome inhibitor-mediated formation. *Hepatology* **47**(6)**:** 2026-2035.

Hazan R, Denk H, Franke WW, Lackinger E, Schiller DL (1986). Change of cytokeratin organization during development of Mallory bodies as revealed by a monoclonal antibody. *Lab Invest* **54**(5)**:** 543-553.

He T, Stepulak A, Holmstrom TH, Omary MB, Eriksson JE (2002). The intermediate filament protein keratin 8 is a novel cytoplasmic substrate for c-Jun N-terminal kinase. *J Biol Chem* **277**(13)**:** 10767-10774.

Herland A, Nilsson KP, Olsson JD, Hammarstrom P, Konradsson P, Inganas O (2005). Synthesis of a regioregular zwitterionic conjugated oligoelectrolyte, usable as an optical probe for detection of amyloid fibril formation at acidic pH. *J Am Chem Soc* **127**(7)**:** 2317-2323.

Hoozemans JJ, van Haastert ES, Nijholt DA, Rozemuller AJ, Eikelenboom P, Scheper W (2009). The unfolded protein response is activated in pretangle neurons in Alzheimer's disease hippocampus. *Am J Pathol* **174**(4)**:** 1241-1251.

Hui L, Zatloukal K, Scheuch H, Stepniak E, Wagner EF (2008). Proliferation of human HCC cells and chemically induced mouse liver cancers requires JNK1-dependent p21 downregulation. *J Clin Invest* **118**(12)**:** 3943-3953.

Huiyuan Li FR SS, Bitan PMaG (2009). Amyloids and Protein Aggregation Analytical Methods Meyers RA, ed. Encyclopedia of Analytical Chemisty R.A Meyers (Ed.) :john Wiley & Sons Ltd.

Ichimura Y, Kumanomidou T, Sou YS, Mizushima T, Ezaki J, Ueno T*, et al.* (2008). Structural basis for sorting mechanism of p62 in selective autophagy. *J Biol Chem* **283**(33)**:** 22847-22857.

Jain A, Lamark T, Sjottem E, Larsen KB, Awuh JA, Overvatn A*, et al.* (2010). p62/SQSTM1 is a target gene for transcription factor NRF2 and creates a positive feedback loop by inducing antioxidant response element-driven gene transcription. *J Biol Chem* **285**(29)**:** 22576-22591.

Janig E, Stumptner C, Fuchsbichler A, Denk H, Zatloukal K (2005). Interaction of stress proteins with misfolded keratins. *Eur J Cell Biol* **84**(2-3)**:** 329-339.

Jin Z, Li Y, Pitti R, Lawrence D, Pham VC, Lill JR*, et al.* (2009). Cullin3-based polyubiquitination and p62-dependent aggregation of caspase-8 mediate extrinsic apoptosis signaling. *Cell* **137**(4)**:** 721-735.

Kachi K, Wong PT, French SW (1993). Molecular structural changes in Mallory body proteins in human and mouse livers: an infrared spectroscopy study. *Experimental and molecular pathology* **59**(3)**:** 197-210.

Kazi JU, Soh JW (2007). Isoform-specific translocation of PKC isoforms in NIH3T3 cells by TPA. *Biochem Biophys Res Commun* **364**(2)**:** 231-237.

Kim JY, Ozato K (2009). The sequestosome 1/p62 attenuates cytokine gene expression in activated macrophages by inhibiting IFN regulatory factor 8 and TNF receptor-associated factor 6/NF-kappaB activity. *J Immunol* **182**(4)**:** 2131-2140.

Kim PK, Hailey DW, Mullen RT, Lippincott-Schwartz J (2008). Ubiquitin signals autophagic degradation of cytosolic proteins and peroxisomes. *Proc Natl Acad Sci U S A* **105**(52)**:** 20567-20574.

Komatsu M, Kurokawa H, Waguri S, Taguchi K, Kobayashi A, Ichimura Y*, et al.* (2010). The selective autophagy substrate p62 activates the stress responsive transcription factor Nrf2 through inactivation of Keap1. *Nat Cell Biol* **12**(3)**:** 213-223.

Komatsu M, Waguri S, Koike M, Sou YS, Ueno T, Hara T*, et al.* (2007). Homeostatic levels of p62 control cytoplasmic inclusion body formation in autophagy-deficient mice. *Cell* **131**(6)**:** 1149-1163.

Kopito RR, Sitia R (2000). Aggresomes and Russell bodies. Symptoms of cellular indigestion? *EMBO Rep* **1**(3)**:** 225-231.

Lamark T, Perander M, Outzen H, Kristiansen K, Overvatn A, Michaelsen E*, et al.* (2003). Interaction codes within the family of mammalian Phox and Bem1p domain-containing proteins. *J Biol Chem* **278**(36)**:** 34568-34581.

Lau A, Wang XJ, Zhao F, Villeneuve NF, Wu T, Jiang T*, et al.* (2010). A noncanonical mechanism of Nrf2 activation by autophagy deficiency: direct interaction between Keap1 and p62. *Mol Cell Biol* **30**(13)**:** 3275-3285.

Maeda S, Kamata H, Luo JL, Leffert H, Karin M (2005). IKKbeta couples hepatocyte death to cytokine-driven compensatory proliferation that promotes chemical hepatocarcinogenesis. *Cell* **121**(7)**:** 977-990.

Magin TM (1998). Lessons from keratin transgenic and knockout mice. *Subcell Biochem* **31:** 141-172.

Mahajan V, Klingstedt T, Simon R, Nilsson KP, Thueringer A, Kashofer K*, et al.* (2011). Cross beta-sheet conformation of keratin 8 is a specific feature of Mallory-Denk bodies compared to other hepatocyte inclusions. *Gastroenterology*. in press.

Mallory F (1911). Cirrhosis of the liver. Five different types of lesions from which itmay arise. *Bul. Johns Hopkins Hosp* (22)**:** 69–75.

Mathew R, Karp CM, Beaudoin B, Vuong N, Chen G, Chen HY*, et al.* (2009). Autophagy suppresses tumorigenesis through elimination of p62. *Cell* **137**(6)**:** 1062-1075.

Moscat J, Diaz-Meco MT (2009). p62 at the crossroads of autophagy, apoptosis, and cancer. *Cell* **137**(6)**:** 1001-1004.

Moscat J, Diaz-Meco MT, Albert A, Campuzano S (2006). Cell signaling and function organized by PB1 domain interactions. *Mol Cell* **23**(5)**:** 631-640.

Nagai Y, Popiel HA (2008). Conformational changes and aggregation of expanded polyglutamine proteins as therapeutic targets of the polyglutamine diseases: exposed beta-sheet hypothesis. *Curr Pharm Des* **14**(30)**:** 3267-3279.

Nakamichi I, Toivola DM, Strnad P, Michie SA, Oshima RG, Baribault H*, et al.* (2005). Keratin 8 overexpression promotes mouse Mallory body formation. *J Cell Biol* **171**(6)**:** 931-937.

Nilsson KP (2009). Small organic probes as amyloid specific ligands--past and recent molecular scaffolds. *FEBS Lett* **583**(16)**:** 2593-2599.

Nilsson KP, Aslund A, Berg I, Nystrom S, Konradsson P, Herland A*, et al.* (2007). Imaging distinct conformational states of amyloid-beta fibrils in Alzheimer's disease using novel luminescent probes. *ACS Chem Biol* **2**(8)**:** 553-560.

Nilsson KP, Ikenberg K, Aslund A, Fransson S, Konradsson P, Rocken C*, et al.* (2010). Structural typing of systemic amyloidoses by luminescent-conjugated polymer spectroscopy. *Am J Pathol* **176**(2)**:** 563-574.

Nilsson KP, Rydberg J, Baltzer L, Inganas O (2004). Twisting macromolecular chains: self-assembly of a chiral supermolecule from nonchiral polythiophene polyanions and random-coil synthetic peptides. *Proc Natl Acad Sci U S A* **101**(31)**:** 11197-11202.

Omary MB (2009). "IF-pathies": a broad spectrum of intermediate filament-associated diseases. *J Clin Invest* **119**(7)**:** 1756-1762.

Pankiv S, Clausen TH, Lamark T, Brech A, Bruun JA, Outzen H*, et al.* (2007). p62/SQSTM1 binds directly to Atg8/LC3 to facilitate degradation of ubiquitinated protein aggregates by autophagy. *J Biol Chem* **282**(33)**:** 24131-24145.

Park I, Chung J, Walsh CT, Yun Y, Strominger JL, Shin J (1995). Phosphotyrosine-independent binding of a 62-kDa protein to the src homology 2 (SH2) domain of p56lck and its regulation by phosphorylation of Ser-59 in the lck unique N-terminal region. *Proc Natl Acad Sci U S A* **92**(26)**:** 12338-12342.

Rusten TE, Stenmark H (2010). p62, an autophagy hero or culprit? *Nat Cell Biol* **12**(3)**:** 207-209.

Sanz L, Diaz-Meco MT, Nakano H, Moscat J (2000). The atypical PKC-interacting protein p62 channels NF-kappaB activation by the IL-1-TRAF6 pathway. *EMBO J* **19**(7)**:** 1576-1586.

Sanz L, Sanchez P, Lallena MJ, Diaz-Meco MT, Moscat J (1999). The interaction of p62 with RIP links the atypical PKCs to NF-kappaB activation. *EMBO J* **18**(11)**:** 3044-3053.

Seidel K, Brunt ER, de Vos RA, Dijk F, van der Want HJ, Rub U*, et al.* (2009). The p62 antibody reveals various cytoplasmic protein aggregates in spinocerebellar ataxia type 6. *Clin Neuropathol* **28**(5)**:** 344-349.

Sigurdson CJ, Nilsson KP, Hornemann S, Manco G, Polymenidou M, Schwarz P*, et al.* (2007). Prion strain discrimination using luminescent conjugated polymers. *Nat Methods* **4**(12)**:** 1023-1030.

Soh JW, Lee EH, Prywes R, Weinstein IB (1999). Novel roles of specific isoforms of protein kinase C in activation of the c-fos serum response element. *Mol Cell Biol* **19**(2)**:** 1313-1324.

Soh JW, Weinstein IB (2003). Roles of specific isoforms of protein kinase C in the transcriptional control of cyclin D1 and related genes. *J Biol Chem* **278**(36)**:** 34709-34716.

Strnad P, Stumptner C, Zatloukal K, Denk H (2008a). Intermediate filament cytoskeleton of the liver in health and disease. *Histochem Cell Biol* **129**(6)**:** 735-749.

Strnad P, Tao GZ, So P, Lau K, Schilling J, Wei Y*, et al.* (2008b). "Toxic memory" via chaperone modification is a potential mechanism for rapid Mallory-Denk body reinduction. *Hepatology* **48**(3)**:** 931-942.

Stumptner C, Fuchsbichler A, Heid H, Zatloukal K, Denk H (2002). Mallory body--a disease-associated type of sequestosome. *Hepatology* **35**(5)**:** 1053-1062.

Stumptner C, Fuchsbichler A, Lehner M, Zatloukal K, Denk H (2001). Sequence of events in the assembly of Mallory body components in mouse liver: clues to the pathogenesis and significance of Mallory body formation. *Journal of hepatology* **34**(5)**:** 665-675.

Stumptner C, Fuchsbichler A, Zatloukal K, Denk H (2007). In vitro production of Mallory bodies and intracellular hyaline bodies: the central role of sequestosome 1/p62. *Hepatology* **46**(3)**:** 851-860.

Stumptner C, Heid H, Fuchsbichler A, Hauser H, Mischinger HJ, Zatloukal K*, et al.* (1999). Analysis of intracytoplasmic hyaline bodies in a hepatocellular carcinoma. Demonstration of p62 as major constituent. *Am J Pathol* **154**(6)**:** 1701-1710.

Tapia JC, Torres VA, Rodriguez DA, Leyton L, Quest AF (2006). Casein kinase 2 (CK2) increases survivin expression via enhanced beta-catenin-T cell factor/lymphoid enhancer binding factor-dependent transcription. *Proc Natl Acad Sci U S A* **103**(41)**:** 15079-15084.

Theis-Febvre N, Martel V, Laudet B, Souchier C, Grunwald D, Cochet C*, et al.* (2005). Highlighting protein kinase CK2 movement in living cells. *Mol Cell Biochem* **274**(1-2)**:** 15-22.

Toivola DM, Strnad P, Habtezion A, Omary MB (2010). Intermediate filaments take the heat as stress proteins. *Trends Cell Biol* **20**(2)**:** 79-91.

Tokuriki N, Tawfik DS (2009). Protein dynamism and evolvability. *Science* **324**(5924)**:** 203-207.

Tyedmers J, Mogk A, Bukau B (2010). Cellular strategies for controlling protein aggregation. *Nat Rev Mol Cell Biol* **11**(11)**:** 777-788.

Wilson MI, Gill DJ, Perisic O, Quinn MT, Williams RL (2003). PB1 domain-mediated heterodimerization in NADPH oxidase and signaling complexes of atypical protein kinase C with Par6 and p62. *Mol Cell* **12**(1)**:** 39-50.

Wu D, Cederbaum AI (2009). Oxidative stress and alcoholic liver disease. *Semin Liver Dis* **29**(2)**:** 141-154.

Yanagawa T, Yuki K, Yoshida H, Bannai S, Ishii T (1997). Phosphorylation of A170 stress protein by casein kinase II-like activity in macrophages. *Biochem Biophys Res Commun* **241**(1)**:** 157-163.

Yokoo H, Harwood TR, Racker D, Arak S (1982). Experimental production of Mallory bodies in mice by diet containing 3,5-diethoxycarbonyl-1,4-dihydrocollidine. *Gastroenterology* **83**(1 Pt 1)**:** 109-113.

Zatloukal K, Denk H, Lackinger E, Rainer I (1989a). Hepatocellular cytokeratins as substrates of transglutaminases. *Lab Invest* **61**(6)**:** 603-608.

Zatloukal K, Denk H, Lackinger E, Rainer I (1989b). Hepatocellular cytokeratins as substrates of transglutaminases. *Laboratory investigation; a journal of technical methods and pathology* **61**(6)**:** 603-608.

Zatloukal K, French SW, Stumptner C, Strnad P, Harada M, Toivola DM*, et al.* (2007). From Mallory to Mallory-Denk bodies: what, how and why? *Exp Cell Res* **313**(10)**:** 2033-2049.

Zatloukal K, Spurej G, Rainer I, Lackinger E, Denk H (1990). Fate of Mallory body-containing hepatocytes: disappearance of Mallory bodies and restoration of the hepatocytic intermediate filament cytoskeleton after drug withdrawal in the griseofulvin-treated mouse. *Hepatology* **11**(4)**:** 652-661.

Zatloukal K, Stumptner C, Fuchsbichler A, Fickert P, Lackner C, Trauner M*, et al.* (2004a). The keratin cytoskeleton in liver diseases. *J Pathol* **204**(4)**:** 367-376.

Zatloukal K, Stumptner C, Fuchsbichler A, Heid H, Schnoelzer M, Kenner L*, et al.* (2002). p62 Is a common component of cytoplasmic inclusions in protein aggregation diseases. *Am J Pathol* **160**(1)**:** 255-263.

Zatloukal K, Stumptner C, Fuchsbichler A, Janig E, Denk H (2004b). Intermediate filament protein inclusions. *Methods Cell Biol* **78:** 205-228.

Zatloukal K, Stumptner C, Lehner M, Denk H, Baribault H, Eshkind LG*, et al.* (2000). Cytokeratin 8 protects from hepatotoxicity, and its ratio to cytokeratin 18 determines the ability of hepatocytes to form Mallory bodies. *Am J Pathol* **156**(4)**:** 1263-1274.

Zheng Q, Li J, Wang X (2009). Interplay between the ubiquitin-proteasome system and autophagy in proteinopathies. *Int J Physiol Pathophysiol Pharmacol* **1**(2)**:** 127-142.